Proceedings of the

5th Oxford Tidal Energy Workshop

21-22 March 2016, Oxford, UK

Proceedings of the 5th Oxford Tidal Energy Workshop (OTE 2016)

21-22 March 2016, Oxford, UK

Monday 21st March

Session 1: Basin Modelling

11:10 *Power Potential of Tidal Fences in the Bristol Channel*
Guy Houlsby (University of Oxford) 4

11:35 *Observations of Waves at Tidal-stream Energy Sites*
Matt Lewis (Bangor University) 6

12:00 *Numerical Modelling of Two-scale Flow Dynamics*
Paul Bonar (University of Edinburgh) 8

Poster Presentations (1)

12:25 *Examining the Limitation of Depth Averaged Models for Assessing the Interaction of Tidal Energy Extraction and Tidal Flow*
Alice Goward Brown (Bangor University) 10

12:30 *Coupling of BEM-CFD and Coastal Area Models for Assessment of Tidal Stream Turbine Impacts at Regional Scales*
Matt Edmunds (Swansea University) 12

Session 2: Wake characteristics and turbulence (1)

14:00 *Fast optimization of tidal stream turbine positions for power generation in small arrays with low blockage based on superposition of self-similar far-wake velocity deficit profiles*
Peter Stansby (University of Manchester) 14

14:25 *Wake Characteristics of a Scaled Tidal Rotor with Monopile Support Structure for Co-located Wind and Tidal Farms*
David Lande-Sudall (University of Manchester) 16

14:50 *Tidal Turbine Wake Analysis using Vessel- and Seabed-mounted ADCPs*
James McNaughton (GE Renewables) 18

Poster Presentations (2)

15:15 *Impacts of Various Floating Platforms on FOWT System*
Yuanchuan Liu (University of Strathclyde) 20

15:20 *RANS-VOF Modelling of Floating Tidal Streams Systems*
Edward Ransley (Plymouth University) 22

15:25 *Evaluating Passive Structural Control of Tidal Turbines*
Song Fu (University of Strathclyde) 24

Session 3: Turbine Design and Performance (1)

16:00 *Unsteady Tidal Turbine Blade Loading; an Analytical Approach*
Gabriel Scarlett (University of Edinburgh) 26

16:25 *Unsteady Hydrodynamics of Flexible Submerged Foils*
Ignazio Maria Viola (University of Edinburgh) 28

16:50 *Harvesting Energy from a Flexible Flapping Membrane in a Uniform Flow*
Qing Xiao (University of Strathclyde) 30

Tuesday 22nd March

Session 4: Turbine Design and Performance (2)

9:25 *Adjustable Camber for Extended Fatigue Life*
Anna Young (University of Cambridge) 32

9:50 *Tidal Turbine Blade Design from a Fatigue Point of View*
Vesna Jaksic (University College, Cork) 34

10:15 *Performance and Interaction of Short Fences of Tidal Turbines*
Richard Willden (University of Oxford) 36

Session 5: Wake characteristics and turbulence (2)

11:10 *Tidal Turbine Wake Simulation using a High-order Weakly-compressible Cartesian Finite Volume Solver*
Baptiste Elie (EC Nantes) 38

11:35 *A Comparison of Synthetic Turbulence Generation Methods*
Michael Togneri (Swansea University) 40

12:00 *Impact of the Free Surface Proximity on the Performance of a Single Tidal Stream Turbine: A Vortex Filament Approach*
Georgios Deskos (Imperial College) 42

Poster Presentations (3)

12:25 *A BEMT Model for a High Solidity, Hubless and Ducted Tidal Stream Turbine*
Steve Allsop (IDCORE) 44

12:30 *Tidal Turbine Wake Asymmetry due to Wake-Seabed Interactions*
Lada Murdoch (CFD People Ltd.) 46

Session 6: Turbine Design and Performance (3)

14:00 *Experimental Study of the Boundary Conditions on an Undulating Membrane Tidal Energy Converter*
Martin Träsch (ADEME) 48

14:25 *Unsteady Load Relief of an Axial Flow Tidal Turbine in Sheared Flow by Individual Pitch Control*
Jianxin Hu (University of Oxford) 50

14:50 *Large-Eddy Simulation of Tidal Turbines Using the Immersed Boundary Method*
Pablo Ouro (Cardiff University) 52

Workshop Organisers:

Richard H. J. Willden	(Chairman)	University of Oxford
Christopher R. Vogel	(Co-Chairman)	University of Oxford

Scientific Committee Members:

T. A. A. Adcock	(University of Oxford)	P. K. Stansby	(University of Manchester)
G. T. Houlsby	(University of Oxford)	C. Stock-Williams	(E.On)
I. Masters	(Swansea University)	C. R. Vogel	(University of Oxford)
T. Nishino	(Cranfield University)	R. H. J. Willden	(University of Oxford)
T. Stallard	(University of Manchester)		

Sponsor:

Oxford Martin School (University of Oxford)

Power Potential of Tidal Fences in the Bristol Channel

Guy T. Houlsby*
Department of Engineering Science, University of Oxford, UK

Sena Serhadlıoğlu
DNV GL, Izmir, Turkey (formerly Department of Engineering Science, University of Oxford, UK)

Summary: Numerical calculations have been made of the power that could be delivered by tidal fences at a number of locations in the Bristol Channel. The calculations use DG-ADCIRC, coupled with modelling of the performance of a THAWT device using performance characteristics derived from a combination of model tests and analyses. Optimal positioning of a fence is considered.

Introduction

The successful future deployment of tidal stream turbines will rely on the accurate modelling of their performance and the optimising of their layout. Several studies [1-3], have revealed that turbines will most efficiently be deployed in the form of a permeable fence aligned across the flow, and not in a series configuration. The THAWT device [4] is well suited to this geometry, and in addition is able to deliver relatively high blockage which further enhances its performance.

Methods

This work extends the study by Serhadlıoğlu [1], using the DG-ADCIRC to solve the shallow water equations for a model of tidal flows in a region extending from the Bristol Channel to the edge of the continental shelf. The model was carefully calibrated against both elevation and velocity data. The principal difference for this study lies in the way the interactions between tidal turbines and the flow was modelled. For this study the performance characteristics are based on the data summarised in [3]. The extracted power and thrust curves for a 0.5m model THAWT device were fitted by a series of piecewise curves, expressing C_P and C_T as functions of tip speed ratio λ, Froude number Fr and blockage ratio B. However, the performance characteristics of a small scale turbine are inferior to that of a full scale device because it operates at much lower Reynolds number Re. Numerical results from [4] were therefore used to adjust the dimensionless performance coefficients to account for an appropriate Re for a full scale (e.g. 10m diameter) device. An iterative process was necessary in this adjustment because of the coupled effects of Fr and Re. The net effect was to increase C_P significantly and C_T slightly.

Results

Analyses were carried out simulating the M2 and S2 tides, both for the locations identified in [1] and for four new positions of a tidal fence, see Fig. 1. Of these locations the best performing was found to be the BCL3 location identified in [1], which was predicted to deliver an average of 91.2MW from a 14.4km fence of 10m diameter THAWT turbines, if the maximum available power could be extracted at any given time. Peak power production was 383.4MW (26.6MW/km), and the capacity factor 24%. However, it would be uneconomic to size generators in order to extract the peak power, so calculations were also carried out in which power capping was used. In these analyses it was assumed, when more power was available than the capped value, that the tip speed ratio would be reduced to achieve the capped power. The corresponding thrust was calculated, which is smaller than the thrust if the uncapped power is extracted, and this in turn reduces the effect on the overall flow.

Table 1 summarises the results for the BCL3 fence with various capping and other options. If power is capped at 15.625MW/km (59% of the peak power), then the average power drops to 82MW, 90% of the uncapped average power, and a capacity factor of 36%. On the other hand, increasing the turbine diameter to 12.5m (without capping), increases the power to 125MW (capacity factor 24%). Note that the proportional increase in power is greater than the proportional increase in swept area, because the higher blockage ratio makes the turbines more effective. Introducing capping allows 112MW average to be generated at a capacity factor of 37%.

The BCL3 site crosses a deep shipping channel, and if this is excluded from the array the uncapped power drops from 91.2MW to 82.7MW. Alternatively, if the turbine size is adjusted to suit the varying bathymetry at the site, it can be increased to 111.9MW, although clearly this depends on the specific distribution of sizes. The uncapped power output is in each case at a capacity factor of about 24%.

* Corresponding author.
Email address: guy.houlsby@eng.ox.ac.uk

Finally, the two arrays BCL3 and BCL0 were considered, acting in series upstream and downstream of each other. The power available is 166.3MW (capacity factor 24%), significantly less than twice the power available from BCL3 alone, indicating the inefficiency of locating turbines in a series configuration.

Conclusions

A pilot study has been carried out examining the power output of THAWT turbines forming fences across the Bristol Channel, and indicators are given of the most effective way to deploy the turbines..

Acknowledgements:

This work was funded by a Shell Springboard prize awarded to Kepler Energy Limited.

References:

[1] Serhadlıoğlu, S. (2014). *Tidal stream resource assessment of the Anglesey Skerries and Bristol Channel*, D.Phil. Thesis, University of Oxford.

[2] Adcock, T.A.A., Draper, S., Houlsby, G.T., Borthwick, A.G.L. and Serhadlıoğlu, S. (2013). The available power from tidal stream turbines in the Pentland Firth, *Proc. Roy. Soc. A*, 469(2157), doi:10.1098/rspa.2013.0072

[3] Serhadlıoğlu, S., Adcock, T.A.A., Houlsby, G.T., Draper, S. and Borthwick, A.G.L. (2013). Tidal stream energy resource assessment of the Anglesey Skerries, *Int. J. Marine Energy*, 3-4, pp e98-e111, doi:10.1016/j.ijome.2013.11.014

[4] McAdam, R., Houlsby, G.T. and Oldfield, M.L.G. (2013). Experimental measurements of the hydrodynamic performance and structural loading of the Transverse Horizontal Axis Water Turbine: Part 3, *Renewable Energy*, 59, pp 82-91, doi:10.1016/j.renene.2013.03.012

[5] Stringer, R.M., Hillis, A.J. and Zang, J. (2016). Numerical investigation of laboratory tested cross-flow turbines and Reynolds number scaling, *Renewable Energy*, 85, pp 1316-1327, doi:10.1016/j.renene.2015.07.081

Table 1: Performance of different turbine and generator installations at BCL3 site

Array	Average depth (m)	Turbine diameter (m)	Average blockage ratio *B*	Fence length (km)	Capping Power	Average power (MW)
BCL3	26.8	10	0.37	14.4	None	91.2
BCL3	26.8	10	0.37	14.4	15.625 MW/km	82
BCL3	26.8	12.5	0.47	14.4	None	125
BCL3	26.8	12.5	0.47	14.4	20.83 MW/km	112
BCL3, 1.2km gap	25.3	10	0.40	13.2	None	82.7
BCL3	26.8	10, 12.5, 15	Varies	14.4	None	111.9
BCL3 + BCL0	27.5	10	0.36	29	None	166.3

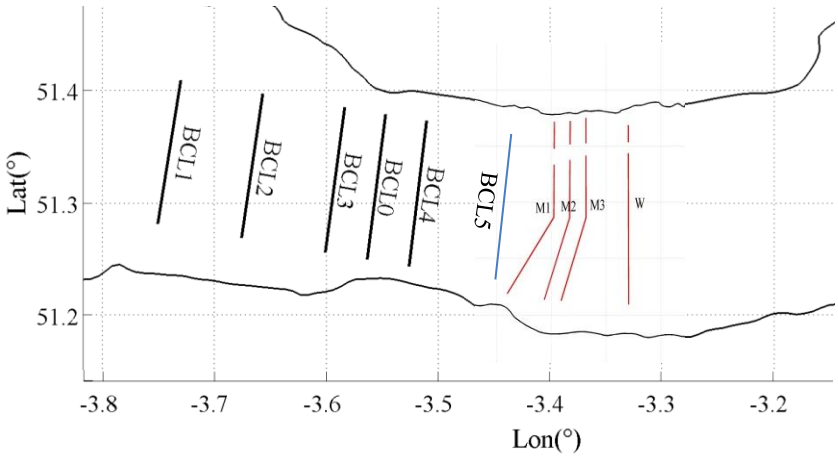

Fig. 1. Locations of tidal fences.

Observations of waves at tidal-stream energy sites

Matt Lewis*, Simon Neill, Peter Robins
School of Ocean Sciences, Bangor University, UK

Summary: The effect of waves on the tidal-stream energy resource were investigated using a dynamically coupled wave-tide oceanographic model (COAWST), and observations of currents and waves at potential sites around the Isle of Anglesey, UK. Evidence is presented for waves reducing tidal current speeds, and hence the available resource, however the relationship appears complex. Furthermore, waves were observed to frequently (92%) be propagating at an angle oblique to the tidal current direction, and this wave-current misalignment may significantly affect turbine resilience and performance. Therefore, further realistic oceanographic condition research is needed in both turbine-scale (design) and basin-scale (resource) studies, with the challenges associated with waves at tidal-stream energy needing to be overcome for the industry to reach its full potential.

Introduction

Very few potential tidal-stream energy sites have a quiescent wave climate [1]. If tidal-stream energy is to make meaningful contributions to government emission targets and provide the UK with a high tech economy, wave resilient turbine designs will need to be developed. Using data from potential tidal-stream energy sites, we seek to prove the two hypotheses proposed by Lewis et al. [1]; undisturbed tidal-stream power available (averaged over a tidal cycle) reduces by 10% per metre increase of wave height, and wave-tide current misalignment frequently occurs at potential tidal-stream energy sites. For completeness, both hypotheses (see [1]) are explained here:

Surface waves contribute momentum and mass to the mean tidal-flow (Stokes velocities and radiation stresses), significantly altering the apparent bed roughness felt by the tidal flow [2]. Thus, the influence of waves is hypothesised to reduce the undisturbed tidal-stream power available (averaged over a tidal cycle) by 10% per metre increase of wave height [1]. Therefore, resource assessment with depth-averaged "tide-only" hydrodynamic models may over-estimate the available resource. Another major assumption within research into the effect of waves on tidal turbine performance and resilience, is that wave propagation is aligned with the rectilinear tidal flow; with either "waves following" (propagating with the tidal current), or "waves opposing" (propagating against the tidal current). As waves propagate into coastal waters, shallow water processes transform their direction; hence, waves tend to travel perpendicular to the coastline whilst tidal currents run parallel. Tidal current misalignment to the tidal turbine has been shown to increase the loading and failure potential [4]; hence wave – tidal current misalignment is likely to further increase the fatigue and extreme loadings of a tidal turbine.

Methods

The effect of waves upon the tidal current was investigated using a spectral wave buoy (Datawell wave-rider) and a RDI 5-beam 600 KHz ADCP. Both instruments were deployed (53.13ºN 4.73ºW) for a 61 day period (Sept – Nov 2014) at the North Wales Demonstration Zone (NWDZ, see seacams.ac.uk). The instruments were deployed in a 44m deep region where peak spring tidal currents can exceed 2.5 m/s and the spring-tidal range is ~5m [5]. Hourly wave direction and tidal current direction were measured with both instruments, and times of misalignment (angle between the direction of wave propagation and the tidal current direction) were identified. The data from NWDZ was combined with two further field campaigns at additional tidal-stream energy locations around Anglesey (further details in [6]); 53.32ºN 4.79ºW and 53.44ºN 4.30ºW. A moving 25-hour averaging window used to calculate a daily depth-averaged M2 (major semi-diurnal lunar constituent) velocity signal, which can be correlated (Linear regression and Pearson Correlation) to the daily averaged wave climate. Data near the surface (~5m) were removed from analysis to avoid surface effects and we assume this to also remove wind current effects.

Results

Times of wave-current misalignment were identified in the NWDZ ADCP record, as shown in Figure 1. We find 8% of the time (61 days) the observed wave climate direction was inline to the depth-averaged tidal current (with a ±20° tolerance). Although a weak correlation between the M2 depth-averaged tidal current and the daily wave climate was found at NWDZ (R^2 of 1%), stronger linear correlations were found at the other two sites (21% and 29%) with the presence of waves also shown to alter the shape of the velocity profile (see [6]). Hence, the weak linear correlation between wave height and current speed may be because of spatial and temporal variability, or wave-tide interactions (including wave-current misalignment or wind-driven flows), which indicates a

* Corresponding author.
Email address: m.j.lewis@bangor.ac.uk

dynamically coupled modelling approach is required. Finally, comparison between measured significant wave height from the wave buoy and ADCP, shows evidence of bias, which has a positive trend with tidal velocity speed (R^2 of 96% with 0.07 bias for *Hs* ADCP *versus Hs* buoy and a Pearson correlation of 32% for this δHs compared to tidal velocity). Therefore, we believe caution should be exercised when using wave data from the 5-beam ADCPs at high velocity sites.

Conclusions

Analysis from our observations appears to provide evidence for the two theories proposed by Lewis et al. [1]; that waves effect the tidal-stream resource available by slowing the depth-averaged current speed (averaged over a tidal cycle), and wave-tide misalignment frequently occurs at potential tidal-stream energy sites. Whilst uncertainty remains in the ADCP wave climate observations, some evidence suggests waves reduced the available resource (excluding likely extreme condition shut down periods), however this relationship appears complex; for example, future work should also investigate wave direction, wave period and wind-induced currents. The evidence presented here indicates wave-tide misalignment should be considered in turbine-scale studies and dynamically coupled wave-tide models may be required to accurately quantify the technical tidal-stream energy resource and aid researchers in characterizing oceanographic conditions.

Acknowledgements:

MJL and SPN would like to acknowledge the support of the NRN-LCEE Ser Cymru Welsh Government through the research QUOTIENT and thank Marco Piano and Sophie Ward for the data from the WEFO EU Seacams project.

References:

[1] Lewis, M. J., Neill, S. P., Hashemi, M. R., & Reza, M. (2014). Realistic wave conditions and their influence on quantifying the tidal stream energy resource. Applied Energy, 136, 495-508.
[2] Prandle D, Wolf J. Some observations of wave-current interaction, Coastal Engineering 1999; 37: 471 - 485.
[3] Luznik L, Flack KA, Lust EE, Taylor K. The effect of surface waves on the performance characteristics of a model tidal turbine. Renewable Energy 2013; 58: 108-114.
[4] Galloway PW, Myers LE, Bahaj AS. Quantifying wave and yaw effects on a scale tidal stream turbine. Renewable Energy 2014: 63; 297-307.
[5] Lewis, M., Neill, S. P., Robins, P. E., & Hashemi, M. R. (2015). Resource assessment for future generations of tidal-stream energy arrays. Energy, 83, 403-415.
[6] Lewis, M., Neill, S. P., Robins, P. E., & Hashemi, M. R. (2015). Observations of flow characteristics at potential tidal stream energy sites. 11th European Wave and Tidal Energy Conference, Nantes, Sept 2015.

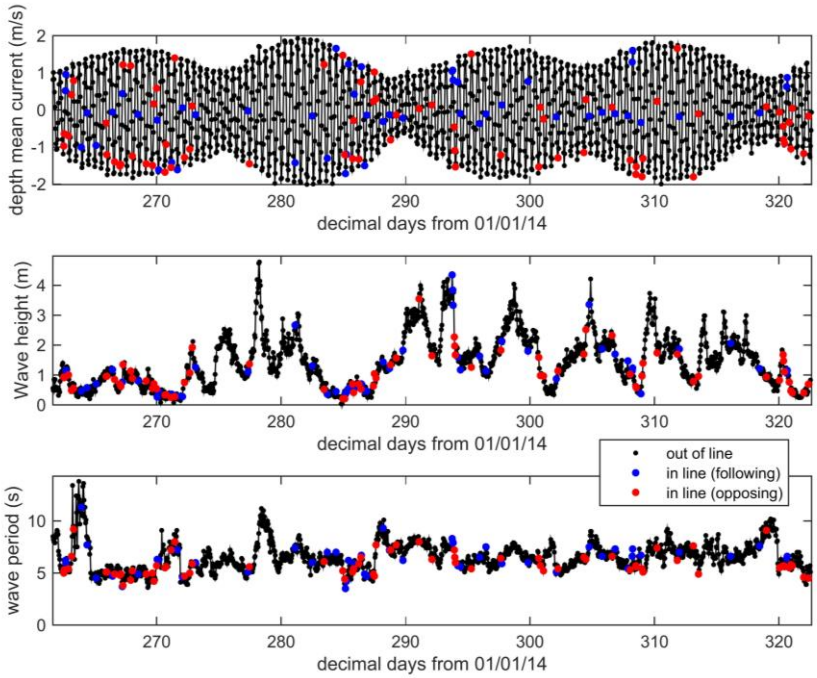

Fig. 1. Wave-tidal current misalignment observed at a potential tidal-stream energy site.

Numerical modelling of two-scale flow dynamics

Paul A. J. Bonar*, Vengatesan Venugopal, Alistair G. L. Borthwick
Institute for Energy Systems, School of Engineering, University of Edinburgh, UK

Thomas A. A. Adcock
Department of Engineering Science, University of Oxford, UK

Summary: Two-scale actuator disc theory is shown to predict qualitatively the performance of a lateral array of tidal turbines in a depth-averaged channel model. The agreement between the numerical and analytical models is improved by extrapolating the numerical results to zero background roughness. Increasing background roughness is shown to reduce the optimal turbine spacing and increase the peak power coefficient of the array.

Introduction

To maximise power output, a tidal turbine array should be designed to sweep the largest permissible fraction of the flow cross-section [1]. Since it would be impractical to fill a cross-section with turbines, developers must consider the variation of power output with array width (array blockage, B_A) and the size and spacing of individual turbines (local blockage, B_L). The two-scale ADT [2] provides a useful description of the basic effects of B_A and B_L on the performance of a lateral array of turbines. Specifically, it predicts an optimal lateral spacing (optimal B_L) to maximise the maximum power coefficient ($C_{PG(max)}$) of the array. Subsequent studies employing three-dimensional RANS simulations [3] and physical experiments [4] have shown this theory to predict qualitatively the power and thrust behaviour of lateral rows of porous discs. The present work shows the theory to predict qualitatively the power performance of a lateral turbine array in a depth-averaged channel model, and investigates the effects of background roughness (C_F) on array performance.

Model

The discontinuous Galerkin version of ADCIRC is used to simulate steady flow through an idealised tidal channel (fig. 1). This flow is driven by a head difference between the flow boundaries, which, following [5], are situated in deep water far upstream and downstream of the channel. Following [6] and [7], turbines are modelled as line discontinuities based on the finite Froude number ADT [8]. This method accounts for local-scale mixing in a sub-grid scale model whilst array-scale mixing is simulated directly by the shallow water equations. For a single row of identical turbine edges, B_A is varied and B_L adjusted to maintain a global blockage (B_G) of 0.1. A constant B_G ensures that, even though the number of edges varies with B_A, this is analogous to varying the lateral spacing between a fixed number of turbines. For each B_L, the edges are tuned to produce $C_{PG(max)}$. In this way, the effect of lateral spacing on $C_{PG(max)}$ is calculated numerically (NM) and compared with the predictions of the theory (AM).

Discussion

In the simple case of fixed B_L and constant inflow, the power extracted by a tidal turbine initially increases with reducing throughflow velocity before decreasing as the applied thrust increasingly diverts flow around the turbine. The optimal thrust may be defined as that produced by the optimal tuning to maximise the useful power output. For two-scale flow, $C_{PG(max)}$ also depends on the balance between local-scale slowing and array-scale choking [2]. As the lateral spacing between turbines is reduced (B_L is increased), $C_{PG(max)}$ initially increases as the decreasing potential for flow diversion around each turbine permits higher optimal thrusts. As B_L is further increased, $C_{PG(max)}$ reduces as the increasing potential for diversion around the entire array necessitates lower optimal thrusts. The value of B_L that maximises $C_{PG(max)}$ is that for which the optimal thrust is maximised.

Fig. 2a shows qualitative agreement between the models, which is improved by extrapolating the numerical results to $C_F = 0$. Contrary to the findings of [3], the results of the NM are lower than those of the AM for low B_L and higher for high B_L. In this case, since the effects of free surface deformation [9] in the NM are expected to have been small, the disparity between the models is thought to be due primarily to two-dimensional flow effects in the NM and the approximate extrapolation of the numerical results to $C_F = 0$. Nevertheless, the present NM provides a suitable basis for qualitative analysis of the effects of C_F on array performance. It is worth noting, however, that due to the low C_F selected, the array mixing length-scale in the NM is not short compared to the channel length (fig. 1), as is assumed in the AM. The significance of this will be considered in future work.

* Corresponding author.
Email address: p.bonar@ed.ac.uk

As reported in [10], for a given B_L, $C_{PG(max)}$ increases with increasing C_F (fig. 2b). This is because, firstly, increasing the resistance of the bypass flow relative to the core flows improves the performance of the turbines, even for a fixed tuning, and secondly, this change in relative resistance increases the optimal thrust, allowing the turbines to be retuned to extract even more power. Further, the amount by which an increase in C_F enhances $C_{PG(max)}$ increases with B_L because, for optimally tuned turbines, the difference between core and bypass velocities increases with B_L, which also means that, after increasing C_F, the additional thrust that can be applied by retuning also increases with B_L. This explains why, for two-scale flow, increasing C_F increases both the peak $C_{PG(max)}$ and the optimal B_L (fig. 2b).

It is important to note, however, that measurement of performance in terms of power coefficient neglects the effect of power extraction on the channel flow rate [1]. In this case, the assumption of constant inflow also conceals the fact that increasing C_F increases frictional dissipation, reducing the amount of power available for extraction.

Acknowledgements:
The authors thank Dr. Takafumi Nishino, Maggie Creed, and anonymous reviewer(s) for their contributions. The first author acknowledges the support of the Energy Technology Partnership and Scotland's Saltire Prize Challenge competitors, who sponsored this research under Scottish Government Grant R43039 (Saltire Studentship).

References:

[1] Vennell, R. (2010). Tuning turbines in a tidal channel. *J. Fluid Mech.* 663, 253-267.
[2] Nishino, T. & Willden, R.H.J. (2012). The efficiency of an array of tidal turbines partially blocking a wide channel. *J. Fluid Mech.* 708, 596-606.
[3] Perez-Campos, E. & Nishino, T. (2015). Numerical validation of the two-scale actuator disc theory for marine turbine arrays. *Proc. 11th EWTEC Conf., Nantes, France.*
[4] Cooke, S.C., Willden, R.H.J., Byrne, B.W., Stallard, T., & Olczak, A. (2015). Experimental investigation of thrust and power on a partial fence array of tidal turbines. *Proc. 11th EWTEC Conf., Nantes, France.*
[5] Adcock, T.A.A., Borthwick, A.G.L., & Houlsby, G.T. (2011). The open boundary problem in tidal basin modelling with energy extraction. *Proc. 9th EWTEC Conf., Southampton, UK.*
[6] Draper, S., Houlsby, G.T., Oldfield, M.L.G., & Borthwick, A.G.L. (2010). Modelling tidal energy extraction in a depth-averaged coastal domain. *IET Renew. Power Gen.* 4 (6), 545-554.
[7] Adcock, T.A.A., Draper, S., Houlsby, G.T., Borthwick, A.G.L., & Serhadlıoğlu, S. (2013). The available power from tidal stream turbines in the Pentland Firth. *Proc. R. Soc. A.* 469: 20130072.
[8] Houlsby, G.T., Draper, S., & Oldfield, M.L.G. (2008). Application of linear momentum actuator disc theory to open channel flow. *Rep. OUEL 2296/08*, Department of Engineering Science, University of Oxford.
[9] Vogel, C.R., Houlsby, G.T., & Willden, R.H.J. (2016). Effect of free surface deformation on the extractable power of a finite width turbine array. *Renew. Energy.* 88, 317-324.
[10] Creed, M.J., Draper, S., Nishino, T., & Borthwick, A.G.L. (2016). Flow through a porous obstruction in a shallow channel. *To be submitted.*

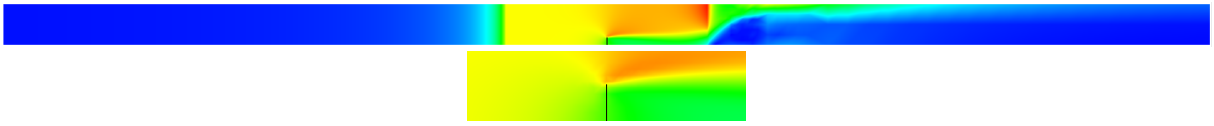

Fig. 1: Plan view of domain showing flow around the turbine array (black line) within the channel. A close-up of the flow around the array is shown below. Contours are of depth-averaged velocity and of arbitrary scale.

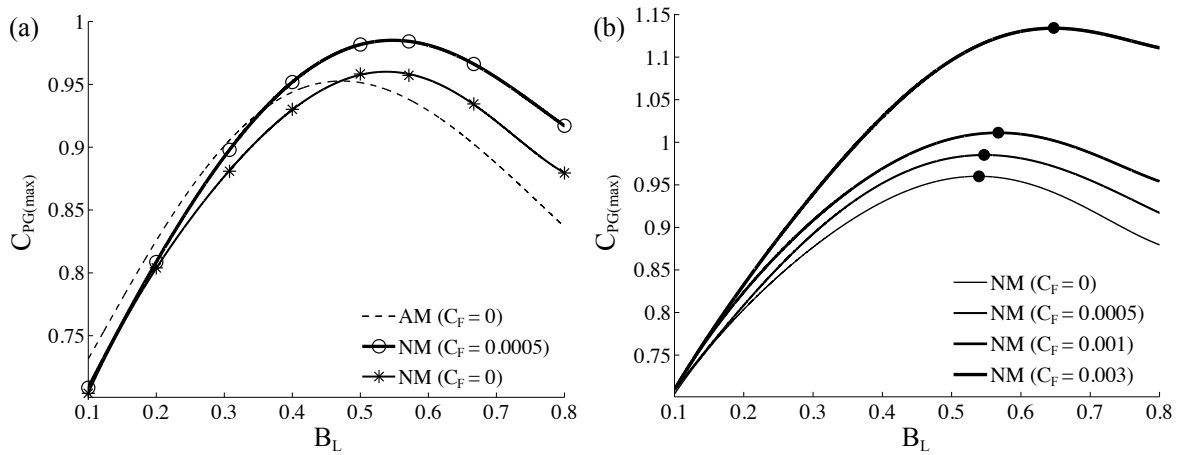

Fig. 2: The effect of lateral spacing (a) and background roughness (b) on $C_{PG(max)}$.

Examining the limitations of depth averaged models for assessing the interaction of tidal energy extraction and tidal flow

Alice Goward Brown*, Simon Neill, Matthew Lewis
School of Ocean Sciences, Bangor University, UK

Summary: Modelling tidal energy extraction poses a multi-scale problem. Technological developments in high performance computing have made 3D modelling of tidal energy extraction feasible in oceanographic resource models. Depth averaged tidal energy extraction leads to a misrepresentation of the velocity profile, which prevents accurate analysis of environmental interactions and resource assessments. Here, an idealised comparison of the two techniques is undertaken. Furthermore, the 3-D method presented here has been successfully applied to a 3D basin-scale hydrodynamic model (ROMS), in-order to examine the hydrodynamic implications of tidal energy extraction.

Introduction

Accurate simulations of tidal stream turbines is a multi-scale challenge [1]. The research question posed ultimately dictates the suitability of different techniques. Previously, depth-averaged models used the actuator disc concept to assess the available power of realistic tidal flows [2, 3]. Tidal energy extraction from depth-integrated models results in a uniform thrust force applied throughout the water column, vertical flow bypass around the device will thus be misrepresented. The increase in turbulence and velocity deficit caused by upstream turbines will impact turbine yield downstream [4]. We hypothesise that beyond 1st generation deployments, the combination of flow speeds, water depth and wave climate, may necessitate three dimensional representation of tidal turbines for accurate resource and impact estimations. Previous comparisons of flume experiments with tidal turbines represented as actuator discs within CFD models have shown similar characteristics between the wake of the experimental and modelled discs [5]. After validation against flume experiments, the actuator disc concept has been applied to 3D ocean circulation models [6]. In order to effectively apply the aforementioned method at a regional scale, tidal energy extraction is implemented as a mid-depth force term. This method is compared with an extraction scenario whereby a uniform thrust force is applied throughout the water column (hereafter referred to as the 2-D method) to examine the implications of disregarding flow bypass above and below turbine arrays. The 3D ROMS (Regional Ocean Modelling System) model has been applied to determine the limitations of using depth-averaged tidal energy extraction techniques when assessing tidal resource characteristics and environmental impacts.

Methods

An idealised channel domain was simulated with a 3-D, free-surface, terrain-following, hydrostatic primitive equation oceanic model (ROMS), typically used for resource assessment [7]. The lateral boundaries were closed and a free slip condition applied. A constant inflow of 2m/s was imposed at the upstream channel boundary. The downstream boundary was clamped for free surface and a reduced physics, Flather condition applied to depth averaged velocities. A radiation condition was used for 3D momentum. A drag coefficient of 0.0025 was imposed at the bed and the model was run until a steady state was achieved, where velocities at the turbine location vary less than 0.01m/s between time steps. The region of tidal energy extraction is represented by a mid-depth force term (Equation (1)). $A_D = \delta x \times \delta y \times T_D$, where δx and δy equal the model resolution in x and y respectively. For 3D tidal extraction, δx and δy equal 100m, the height of the turbine (T_D) is equal to 10m. For the 2-D method, T_D is 30m. The region of tidal energy extraction is in the middle of the channel; the blockage ratio equates to 5%. The amount of energy extracted by the turbine is equal for both cases (Table 1).

$$C_T = \frac{Force}{\frac{1}{2}\rho A_D U_\infty^2} \qquad (1)$$

Results

A comparison of the two methods demonstrates that extracting tidal energy at all water depths fails to reproduce the velocity profile which is characteristic of tidal energy extraction (Figure 1b). The asymmetric profile created

* Corresponding author.
Email address: a.j.gowardbrown@bangor.ac.uk

using a 3D extraction method results from the non-linear interactions between surface waters and the turbines (Figure 1a). For tidal resource estimations, using either the averaged mid-depth 3-D velocities or the whole water column depth averaged velocity to calculate power extraction estimates, results in a 60% discrepancy between estimations, where Power = Force x work done (U_D) (Table 1).

Table 1. Comparison between depth-averaged current velocity and mean mid-depth disc velocity for 2D and 3D extraction scenarios.

	3-D Method: Mean hub height velocity **(**Umid); Depth averaged velocity(**Ubar**)	**2D Method:** Depth averaged velocity(**Ubar**)
T_D	10	30
C_T	0.96	0.32
U_{IN}	2.07m/s; **2m/s**	**2m/s**
U_{OUT}	2.05m/s; **2m/s**	**2m/s**
U_D	1.4m/s; **1.8m/s**	**1.8m/s**
Power	2.4MW; **3MW**	**3MW**

Conclusions

To accurately represent the implication of tidal energy extraction within a regional model, 3D models are required. Depth averaged energy extraction techniques misrepresent the velocity profile, which has consequences for subsequent environmental interactions and resource calculations. 3D tidal energy extraction techniques are becoming more feasible in regional modelling scenarios with advances in high performance computing and more efficient oceanic model parallelisation.

Acknowledgements

The authors would like to thank Fujitsu and HPC Wales for funding this PhD research and providing access and training for high performance computing. Thanks to Thomas Roc and IT Power for their timely release of the turbine patch for the ROMS source code.

References

[1] T. A. Adcock, S. Draper and T. Nishino, "Tidal power generation–A review of hydrodynamic modelling," *Proc. Inst. Mech. Eng. A: J. Power Energy,* pp. 0957650915570349, 2015.

[2] I. Bryden, S. Couch, A. Owen and G. Melville, "Tidal current resource assessment," *Proc. Inst. Mech. Eng. A: J. Power Energy,* vol. 221, pp. 125-135, 2007.

[3] M. Oldfield, S Draper GT Houlsby MLG and A. Borthwick, "Modelling tidal energy extraction in a depth-averaged coastal domain," 2010.

[4] I. G. Bryden, S. I. Couch, A. Owen and G. Melville, "Tidal current resource assessment," *Proc. Inst. Mech. Eng. A: J. Power Energy,* vol. 221, pp. 125-135, MAR 2007, 2007.

[5] M. Harrison, W. Batten, L. Myers and A. Bahaj, "Comparison between CFD simulations and experiments for predicting the far wake of horizontal axis tidal turbines," *Renewable Power Generation, IET,* vol. 4, pp. 613-627, 2010.

[6] T. Roc, D. C. Conley and D. Greaves, "Methodology for tidal turbine representation in ocean circulation model," *Renewable Energy,* vol. 51, pp. 448-464, 2013.

[7] K. M. Thyng and J. J. Riley, "Idealized headland simulation for tidal hydrokinetic turbine siting metrics," in *Oceans 2010,* 2010, pp. 1-6.

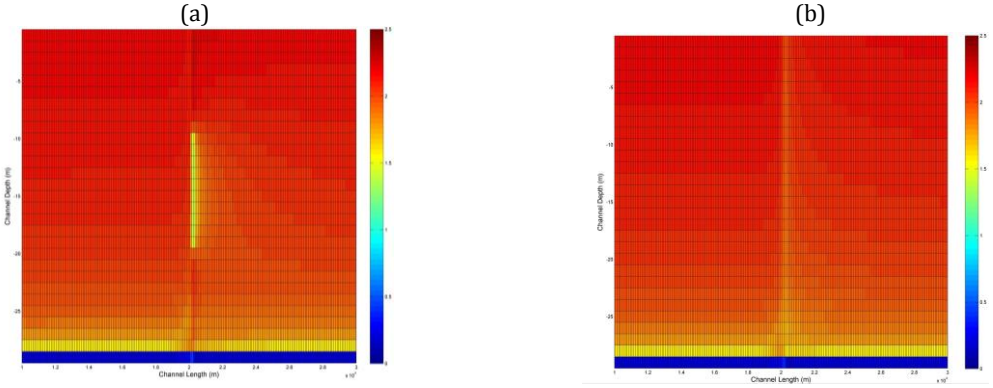

Figure 1. Along channel variation in current velocity (m/s) for the 3-D method (a) and 2-D method (b).

Coupling of BEM-CFD and coastal area models for assessment of tidal stream turbine impacts at regional scales

Iain Fairley, Matt Edmunds*, Alison J Williams, Ian Masters
College of Engineering, Swansea University, UK

Summary: Assessment of the hydrodynamic impacts of tidal stream turbine (TST) arrays relies on numerical simulation of the hydrodynamic regime in the area of interest and a method for turbine implementation. Increasing detail in the representation of the turbine leads to increased computational expense and hence reduces feasible domain size and practicality of transient simulations. Computationally efficient, transient, large scale simulations can be made with coastal area models but accuracy of the turbine representation suffers. This contribution explores the concept of coupling a BEM-CFD simulation of the nearfield array area with a coastal area model of the far field to provide more detailed description of regional scale impact.

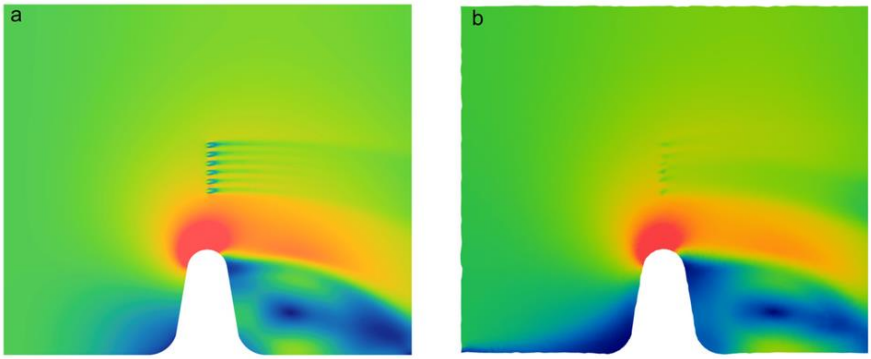

Fig. 1. A comparison between horizontal flow fields for a) the BEM-CFD case and b) the coastal area model. Reproduced from [1]. The colour map is the same for both figures.

Introduction

An important part of any marine energy project is the assessment of hydrodynamic impact. In the near-field wake properties can be explored using a range of CFD techniques. Here we use the BEM-CFD approach [1]. For regional scale assessments, coastal area models that solve the shallow water equations are typically used.

TST's are resolved in the BEM-CFD simulation using Blade Element theory applied to a control volume representing the swept volume of rotor hydrofoils. The control volume averaged computed forces are added to the momentum equation. This results in a time averaged representation of TST interaction with the fluid domain [2]. A major limitation of this approach is computational requirements restricting domain size and complexity.

TSTs in coastal area models are typically included as sub-grid structures using either a local increase in bed resistance or a momentum sink. Actuator disk theory is used to determine appropriate values for both these approaches. Arrays have been implemented both as single entities and as sets of sub-grid turbines.

Figure 1 shows a comparison between horizontal flow fields predicted by the two model types for a 6 turbine fence next to an idealised headland based on [3]. Not only is the nearfield wake different, but differences in the far-field also exist. Two aspects of turbine implementation have been discussed which explain inaccuracies in flow fields predicted by coastal area models [4, 5]. Firstly, many shallow water models do not include the rotor's impact on turbulence: [4] has shown inclusion of a turbulence term improves wake predictions. Secondly, [5] showed that as cell sizes reduce, energy extraction becomes under-represented due to the models assumption that the cell velocity approaches the free-stream velocity.

Here, we look at the potential to improve mid- to far- field impact assessment via a coupling of a coastal area model for the regional simulation with a BEM-CFD model of the array area. A simple test case of a channel is used to demonstrate the concept. The case tested consists of a channel 10km long with a width of 750m. Mean water depths are 30m. A constant hydraulic head of 0.4m drives a current of $3ms^{-1}$ through the channel. We consider the case of three 10m rotors in a fence arrangement. Figure 2 shows a schematic of this test.

* Corresponding author.
Email address: m.edmunds@swansea.ac.uk

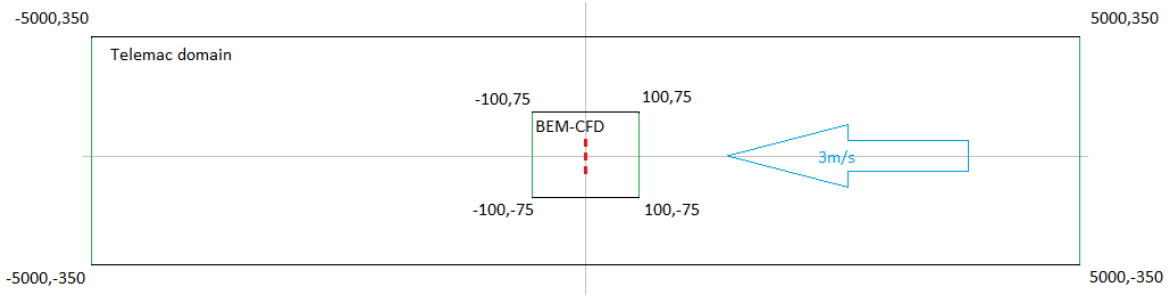

Fig. 2. A schematic showing the test case and the model domains for both the Telemac3D and the OpenFoam (BEM-CFD) model. Red lines indicate the turbine location and green lines open boundaries.

Methods

Two open-source codes are used in this analysis: the coastal area modelling is conducted using Telemac3D and the BEM-CFD using OpenFoam. The BEM-CFD model is used to simulate a fence of three 10m diameter turbines which are deployed in the centre of the channel. Thrust is calculated in the BEM-CFD model based on turbine specific lift and drag. The BEM-CFD domain encapsulates the nearfield around the turbines, covering 200m longitudinally and 150m laterally. Two Telemac3D meshes are used. The first covers the entire channel, this is used to generate inflow conditions for the BEM-CFD model. A second Telemac3D mesh is created coving the same region as the first but with a 'black box' island in the mesh covering the domain of the BEM-CFD mesh. The up- and down-stream sides of this box are specified as open boundaries. Data for these boundaries is obtained from the BEM-CFD simulations and this second Telemac3D mesh used to assess far field turbine impacts. Local and global blockages are implicit in the model coupling. The process used to generate results is as follows:

1. A Telemac3D simulation using the first mesh is run and inflow conditions extracted at the location of the upstream boundary of the OpenFoam model.
2. The OpenFoam model is run with in-flow conditions extracted from the Telemac3D model is step 1.
3. The second Telemac3D model is run with up- and down-stream boundary conditions for the 'black box' extracted from the open foam simulation to assess downstream wakes.

Next steps

The end goal of this work is to provide a comparison between a coastal area model and a coupled BEM-CFD model under realistic conditions. Various tasks need completing:

1. Generate a set of results from the initial test case.
2. Establish a methodology for turbine implantation in Telemac3D for a point of comparison.
3. Assess running Telemac3D in non-hydrostatic mode. The inclusion of dynamic pressure means the CAM and BEM-CFD model are more similar and transfer of boundary conditions between the two may be more suitable. Initial tests suggest running a non-hydrostatic simulation triples computation time.
4. Determine the most efficient way of achieving the inter-model coupling for a transient simulation given differences in computational expense. Currently it is envisaged that a look-up matrix may be appropriate.
5. Test for real-world situation.

Acknowledgements:

This work has been conducted with the support of the EPSRC project Extension of UKCMER Core Research, Industry and International Engagement (EP/M014738/1).

References:

[1] Masters, I., Williams, A., Croft, T.N., Togneri, M., Edmunds, M., Zangiabadi, E., Fairley, I., Karunarathna, H. (2015). "A Comparison of Numerical Modelling Techniques for Tidal Stream Turbine Analysis." Energies **8**(8) 7833-7853

[2] Edmunds M., Williams, A.J., Masters, I., Croft, T.N. (2016) "An Enhanced Disk Averaged CFD Model for the Simulation of Horizontal Axis Tidal Turbines." Under review in Renewable Energy.

[3] Draper, S., Borthwick, A., Houlsby, G. (2013) "Energy potential of a tidal fence deployed near a coastal headland." Philos. Trans. R. Soc. A., **371:** 20120176

[4] Roc, T., Conley, D., Greaves, D. (2013). Methodology of tidal turbine representation in ocean circulation model. Renewable Energy, **51**, 448–464

[5] Kramer, S, Piggot, M., Hill, J., Kregting, L., Pritchard, D., Elsaesser, B. (2014). The modelling of tidal turbine farms using multi-scale, unstructured mesh models. ICOE, Stornoway, UK.

Fast optimisation of tidal stream turbine positions for power generation in small arrays with low blockage based on superposition of self-similar far-wake velocity deficit profiles

Peter Stansby and Tim Stallard
School of Mechanical, Aerospace and Civil Engineering, University of Manchester, Manchester M13 9PL, UK

Far wake velocities of a single horizontal axis three-bladed turbine in shallow flow have been measured previously in the laboratory (Stallard et al 2015) and shown to have self-similar velocity deficit profiles. Wake velocities of arrays of turbines with one, two and three transverse rows have also been measured and simply superimposing the velocity deficits for a single turbine is shown to give accurate prediction of combined wake width and velocity deficit, accounting for variable downstream blockage through volume flux conservation. Array efficiency is defined as the ratio of total power generated to what would be generated by the same turbines in isolation. From prescribed initial turbine positions, generally determined intuitively or by practical considerations, adjusting the turbine positions to increase the power from each turbine, using the chain rule, shows that relatively small movements of 3-4 rotor diameters may increase array efficiency to over 90%.

Fig.1 shows an example of wake velocity prediction for 3 and 4 turbines in a staggered arrangement with 4D longitudinal and 1.5D transverse spacing accounting for blockage .

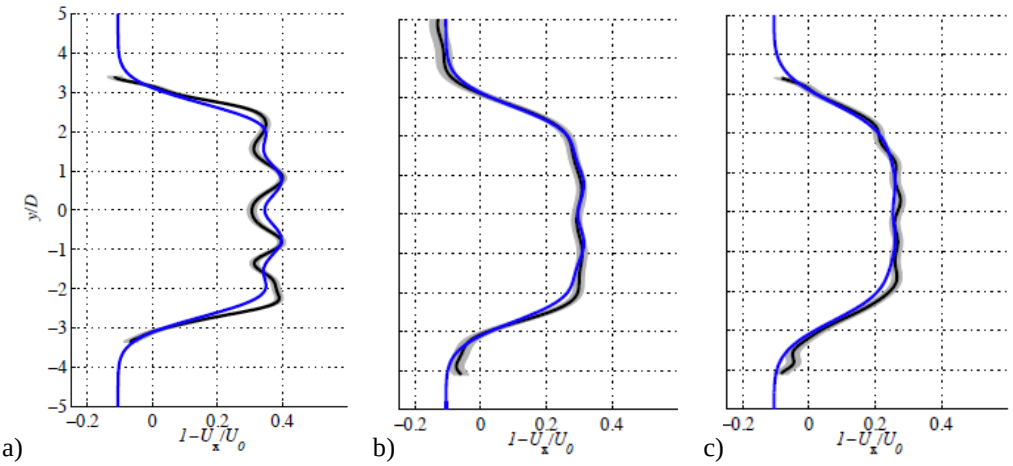

Fig.1 Transverse velocity deficits at a) 8D, b) 10D and c) 12D downstream of front row for two rows of 3 and 4 turbines (upstream and downstream) in staggered arrangement with 4D longitudinal spacing and 1.5D transverse spacing. Superposition model (blue), experiment (black with grey showing variation).

Fig.2 shows optimisation of a 3 row array with 4D longitudinal spacing and 1.5D transverse spacing showing initial and final positions with corresponding array efficiencies of 60% and over 90% respectively. The maximum turbine movement required is 4D and individual turbine efficiencies are also shown.
This work has been published in Stansby and Stallard (2016).

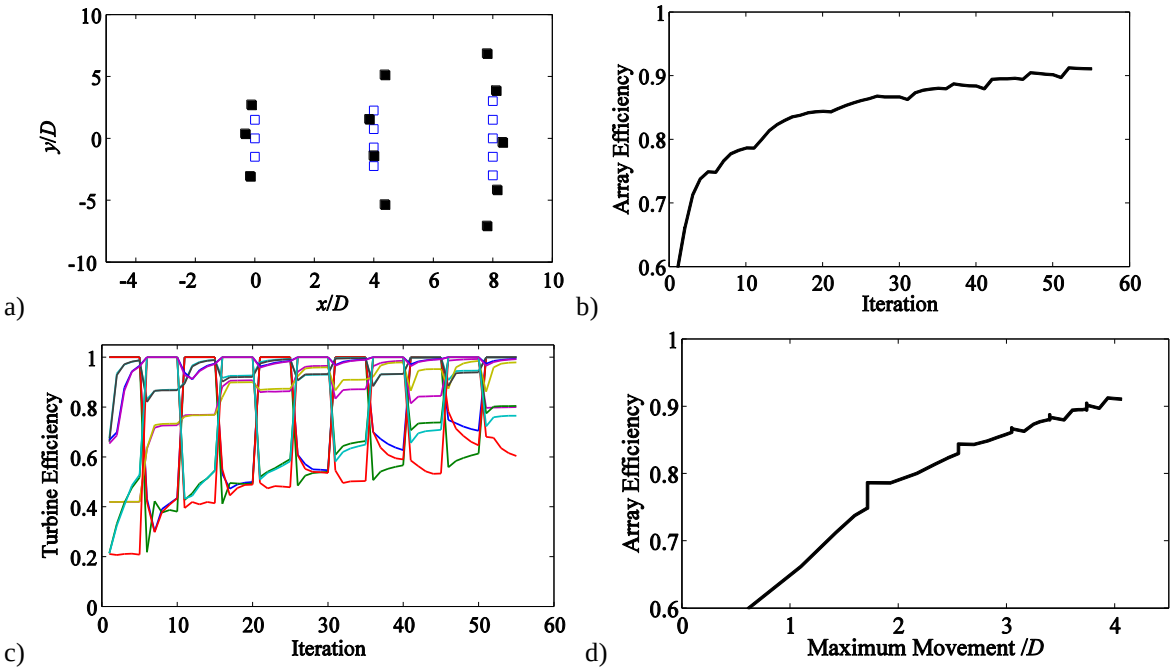

Fig.2 (a) Initial (□) and final positions (■) after 55 iterations of three rows of 3, 4 and 5 turbines in staggered arrangement in bi-directional flow with initial spacings of 4D longitudinal and 1.5D transverse; (b) Variation of array efficiency with iteration number, increased by 53%; (c) variation of individual turbine efficiency with iteration number; d) variation of array efficiency with maximum turbine movement in units of diameter.

References:

[1] Stallard,T.J., Feng,T. and Stansby, P.K. 2015 Experimental study of the mean wake of a tidal stream rotor in a shallow turbulent flow, J. Fluids and Structures, 54, 235-246

[2] Stansby,P.and Stallard,T. 2016 Fast optimisation of tidal stream turbine positions for power generation in small arrays with low blockage based on superposition of self-similar far-wake velocity deficit profiles, Renewable Energy 92, 366-375.

Wake characteristics of a scaled tidal rotor with monopile support structure for co-located wind and tidal farms

David Lande-Sudall*, Tim Stallard, Peter K. Stansby
School of Mechanical, Aerospace and Civil Engineering, University of Manchester, UK

Summary: A series of experiments have been conducted to characterise the influence of a monopile support structure, capable of supporting both wind and tidal stream turbines, on near-wake mixing and far-wake recovery. Comparison is drawn between wakes due to rotor only, support only and the combined rotor and support.

Introduction

Previous experiments [1] characterised the wake of a 1/70th scale, plastic rotor with minimal support structure. The near-wake was characterised by a nearly axisymmetric shear layer with width increasing linearly with downstream distance and transitioning to a far-wake which follows a two-dimensional, Gaussian self-similar form from approximately eight rotor diameters (D) downstream. Superposition of the far-wake of a single rotor has been shown to reasonably predict the wake of small arrays of the same turbine [2]. This approach has been developed to account for variable blockage downstream and optimisation of turbine positions for power generation [3] and used by [4] for estimating the energy yield from a site of co-located wind and tidal stream turbines. The smaller diameter of tidal stream turbines allows closer spacing than wind turbines. To minimise foundation number, tidal stream turbines may be installed on individual supporting structures or on the same support as a wind turbine. For tidal turbines on individual supports, there have been limited studies of the influence of the support on wake structure and consequent effects on loading, particularly when operating in arrays. For structures supporting both tidal and wind turbines, the support structure diameter may be relatively large compared to the diameter of the tidal turbine. A series of scaled experiments has been conducted to characterise the impact of such support structures on wake development.

Experimental Method

A 1/70th scale 3-bladed cobalt-nickel alloy rotor of diameter D = 270 mm was employed. The foil section and radial variation of chord twist and thickness is as used by [1] for rotors manufactured from glass fibre reinforced plastic. Mean inflow speed at the rotor, U_0 = 0.46 m/s with a depth-averaged turbulence intensity of 12%. The turbine was supported above water line by a small diameter tower (d_1=D/18) extending to mid-depth only. This tower is instrumented to measure axial thrust and a dynamometer ensures the rotor operates with constant torque.

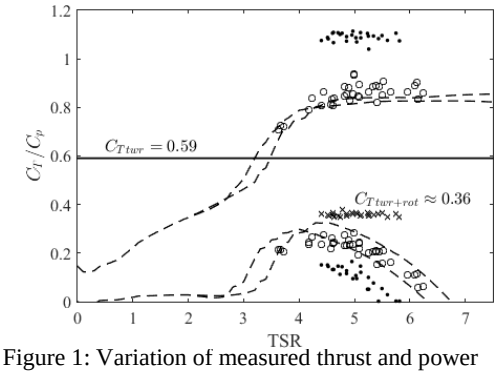

Figure 1: Variation of measured thrust and power coefficient for rotor-only with minimal support of diameter d_1=D/18 (o), for which measured thrust reduced by tower drag due to onset flow only, and with monopile of diameter d_2=D/3.5 (●) for which tower drag measured separately and shown weighted by swept-area for with (x) and without rotor (▬). Prediction by BEMT (---) based on two sets of lift and drag coefficients for this blade [1].

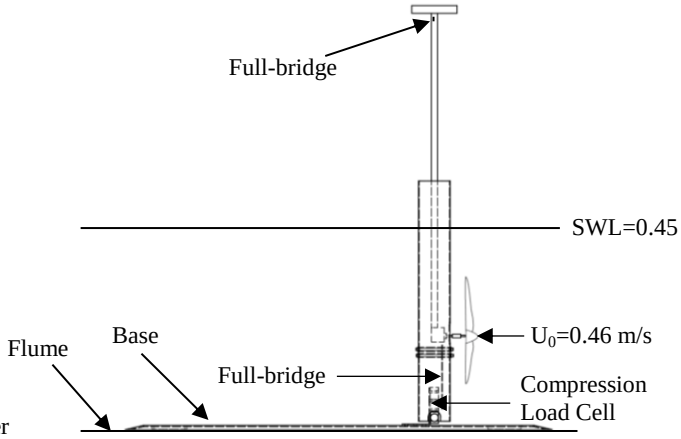

Figure 2: Experimental arrangement of scaled rotor and support structure representing monopile.

* Corresponding author.
Email address: david.lande-sudall@manchester.ac.uk

The time averaged thrust coefficient, C_T is slightly larger than the value predicted from blade element momentum theory (Figure 1), implying higher momentum extraction. In this comparison the BEMT prediction is with the Prandtl tip loss and Buhl high-induction factor correction and the effect of blockage (0.025 based on rotor swept area) is neglected. The rotor-only wake has been characterised for operation with tip speed ratio of 4.5, close to peak power coefficient, C_p of this rotor. The far wake velocity deficit is similar to that observed previously for a plastic rotor [1] although with lower velocity deficit over the range X< 2D. Loading and wake were also measured with a larger supporting structure of diameter $d_2 \approx D/3.5$, representing a full-scale diameter of approximately 5 m, typical of monopile supports to offshore wind turbines with rating of 3-5 MW [5]. Blockage for this arrangement is 0.032. The cylinder is bed mounted and instrumented (Figure 2) to resolve the line of action and overturning moment due to the distributed load on the tower. Measured thrust coefficient for the rotor in this configuration (Fig. 1) is 35% higher at TSR=4.5 while the tower drag is 40% lower than for the tower-only. As such the aggregate of rotor and tower drag remains the same as the aggregate of each in isolation.

Preliminary Results

At mid-depth, the velocity profile of the wake of the monopile alone exhibits a self-similar Gaussian form from X = 1D downstream (see Fig. 3), with the centreline deficit recovering to within 90% of the freestream velocity by 12D downstream. This contrasts with the wake due to the minimal support of the rotor-only system which has been shown to have decayed by 1.5D downstream [1]. At X=2D (Figure 4), the tower-only centreline deficit is 30% of the rotor-only deficit and 53% at X=8D. Preliminary analysis of the combined rotor-support wake appears to give a centreline deficit 12% greater than the rotor-only wake at X=2D (Fig. 4) and 21% greater by X=8D (Fig. 5). Superposition of the rotor-only and tower-only centreline velocity deficits at X=8D predict the combined wake to within 2% of the measured.

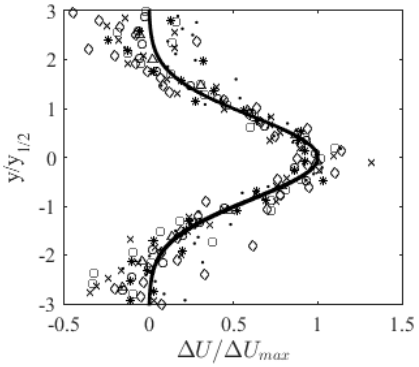

Figure 3: Support-only velocity deficits at X/D=1(Δ), 2(o), 3(□), 4(*), 6(.), 8(+) and 12 (◇).

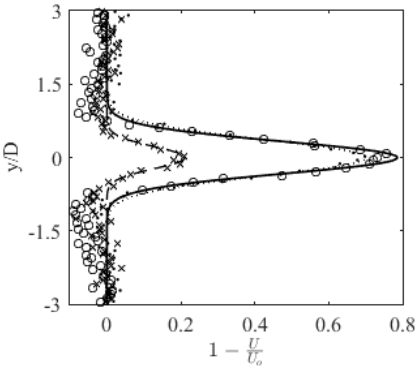

Figure 4: Wake velocity deficits at X/D=2 for tower-only (x---), rotor-only (•…) and combined (○▬).

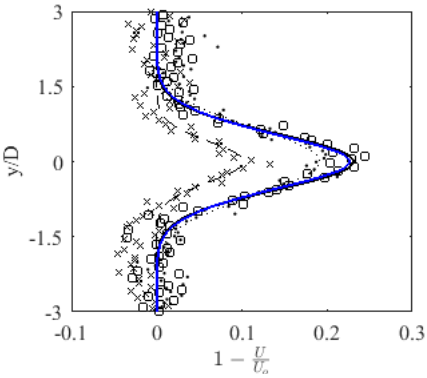

Figure 5: Wake velocity deficits at X/D=8 for tower-only (x---), rotor-only (•…) and combined (○▬) with superposition of rotor-only and tower-only (▬).

Conclusions

A scaled experimental study of a tidal stream rotor operating in a turbulent current with a support structure representing a wind turbine model have been conducted to assess the influence of a support structure on the wake of a tidal turbine in a turbulent channel. This study informs the analysis of loading and performance of co-located wind and tidal stream farms. Preliminary comparison of the wake of a rotor with a monopile of diameter representative for a typical wind turbine shows a centreline deficit 10-20% greater than for the rotor-only wake. Superposition of rotor and tower far-wakes predict the centreline velocity deficit to within 2% of the measured. Further analysis of the influence of support structure on the rotor wake and system loading will be presented.

References:

[1] Stallard,T., Feng,T. and Stansby, P.K. (2015) Experimental study of the mean wake of a tidal stream rotor in a shallow turbulent flow, *J. Fluids and Structures*, 54, 235-246. DOI: 10.1016/j.jfluidstructs.2014.10.017

[2] Olczak, A., Sudall, D., Stallard, T. and Stansby, P.K. Evaluation of RANS BEM and self-similar wake superposition for tidal stream turbine arrays. In: *Proc. 11th European Wave and Tidal Energy Conference*, 07B2-3.

[3] Stansby, P. and Stallard, T. (2016) Fast optimisation of tidal stream turbine positions for power generation in small arrays with low blockage based on superposition of self-similar far-wake velocity deficit profiles *Renewable Energy*, 92, 366-375. DOI: 10.1016/j.renene.2016.02.019

[4] Sudall, D., Stansby, P. and Stallard, T. (2015). Energy Yield for Collocated Offshore Wind and Tidal Stream Farms. In: *Proc. European Wind Energy Association Offshore Conference*, 268.

[5] E.ON (2012) Rampion: Draft ES – Section 2a Project Description (offshore)

Tidal Turbine Wake Analysis using Vessel- and Seabed-Mounted ADCPs

James McNaughton*
GE Renewable Energy, Bristol, UK

Summary: This work presents the analysis of a full-scale tidal turbine wake using seabed-mounted and vessel-mounted flow profilers. The wake is qualitatively assessed through analysis of these flow measurements paired with the performance data of the turbine.

Introduction

The wake of a tidal turbine is a significant consideration for farm design, with likely layouts wanting to ensure sufficient flow recovery whilst minimising wake-induced turbulence and reduce other costs such as cables. Another layout-impacting factor could be blockage effects which boast the potential to increase performance [1,2]. Significant effort has been made to understand wakes experimentally [3]. These provide essential datasets for numerical-model validation which will ultimately be used in array design.

GE Renewable Energy's (formally Tidal Generation Ltd) 18 m diameter (D) 1 MW turbine, DEEP-Gen IV, was deployed at the European Marine Energy Centre (EMEC) as part of the ETI ReDAPT project. This work outlines wake analysis using flow measurements and turbine performance data over the DEEP-Gen IV programme.

Methods

Flow measurements were carried out using Teledyne RDI Workhorse Sentinel Acoustic Doppler Current Profilers (ADCP) placed on the seabed or using a vessel-mounted (VM) survey. Several seabed-mounted (SM) measurement campaigns were performed between 2013 and 2015. Data is processed by separating by flood and ebb and correcting for time offsets. Poor quality flow data is then removed based on the pitch and roll of the sensor and the beams' error velocities. The velocity-deficit, U_D, is computed as:

$$U_D = 1 - \frac{U}{U_T}, \tag{1}$$

With U the measured velocity magnitude and U_T the turbine-related flow velocity. This turbine-related velocity is back-calculated via an efficiency curve, η_P, as a function of shore power, P, up to rated velocity and an efficiency-curve scaling factor, η_α, based on the blade-pitch angle, α. Hence:

$$U_T = \left(\frac{P}{\eta_P \eta_\alpha 0.5 \rho \pi R^2}\right)^{1/3} \tag{2}$$

Note that the turbine-controller data (i.e. power and pitch angle) is sampled at a higher frequency than the ADCPs and so is down sampled onto the flow-data time channels.

For the VMADCP, data is recorded continuously and sampled at 1 Hz. The spatial sampling is thus a function of the vessel speed and direction and resulted in data points at 2.1 m resolution along the vessel route. The velocity deficit is interpolated onto spatial grids in relation to the turbine with 6 m resolution and a 12 m radius of influence. This is to ensure sufficient data points to average over although some areas were not covered by the vessel route which leads to patches in the analysis. For the SMADCPs the data is reduced according to the power below rated and the pitch position at rated and then presented in terms of depth and turbine performance characteristics.

Results

Velocity deficit plots in the vertical plane, obtained from VMADCP measurements, are shown in Figure **1**. The flow is significantly affected by the turbine generating power resulting in a near wake of around 3D downstream. The far wake extends further downstream with the test not capturing an obvious end to the velocity deficit. The far-wake expansion appears 2-3D across after establishing.

The velocity deficit as a function of depth and the turbine performance (power and pitch) are shown in Figure 2. This is processed from 19 days of data from a SMADCP positioned 3.3D downstream of the turbine. There is a more substantial wake as rated power is approached followed by a decrease in the velocity deficit as blade pitching reduces the thrust acting on the flow.

* Corresponding author.
Email address: j.mcnaughton@live.co.uk

Conclusions

Seabed and vessel-mounted flow measurements have been used to assess the wake of a full-scale tidal turbine. Data is normalised using a turbine-related velocity; one issue associated with this is that the spatial variation of flow in the site is not accounted for. This could be addressed by performing measurements when the turbine is not generating or through the use of numerical models of this region.

The final presentation will discuss the data processing in more detail, provide more information of the wake in the stream wise and lateral planes, and analyse results from SMADCPs at different locations within the wake. A review of lessons learnt will be provided for wake analysis from an industry perspective.

Acknowledgements:

The author would like to thank: Brian Sellar (University of Edinburgh) for providing SMADCP data under ReDAPT; Tristan Thorne (Triscom Marine) for VMADCP measurements; Greg Pittam, James Harrison, Simon Harper and Roggie Sinclair (GE Renewable Energy) for useful discussions on analysis.

References:

[1] Nishino, T., & Willden, R. H. (2012). The efficiency of an array of tidal turbines partially blocking a wide channel. *Journal of Fluid Mechanics*, *708*, 596-606.

[2] Schluntz, J., & Willden, R. H. J. (2015). The effect of blockage on tidal turbine rotor design and performance. *Renewable Energy*, *81*, 432-441.

[3] Stallard, T., Collings, R., Feng, T., & Whelan, J. (2013). Interactions between tidal turbine wakes: experimental study of a group of three-bladed rotors. *Phil. Trans. R. Soc. A*, *371*, 20120159.

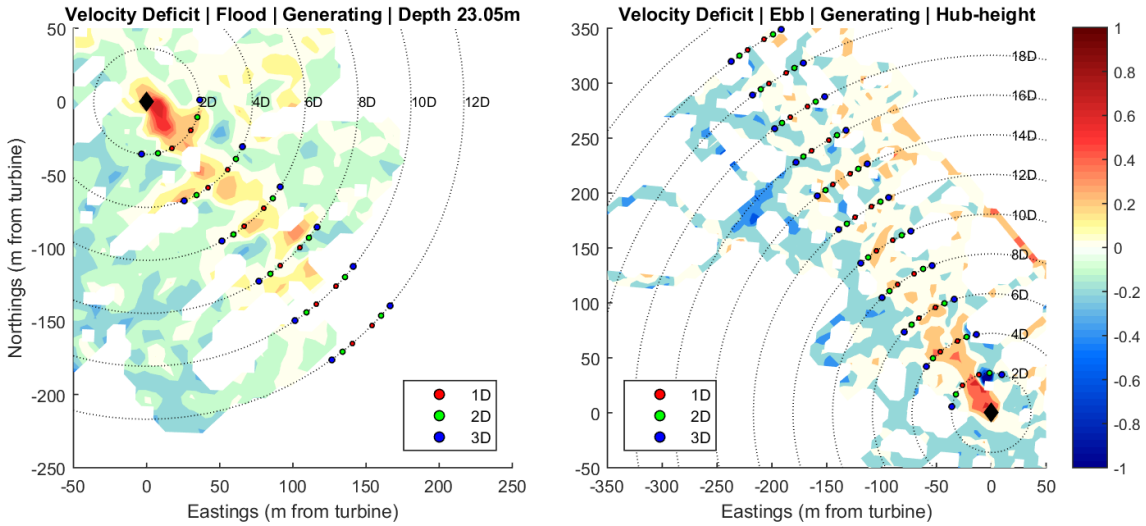

Figure 1 Velocity deficit for the flood (left) and ebb (right) directions on plane at hub-height in the water column. Coloured markers indicate lateral spacing from turbine centre line.

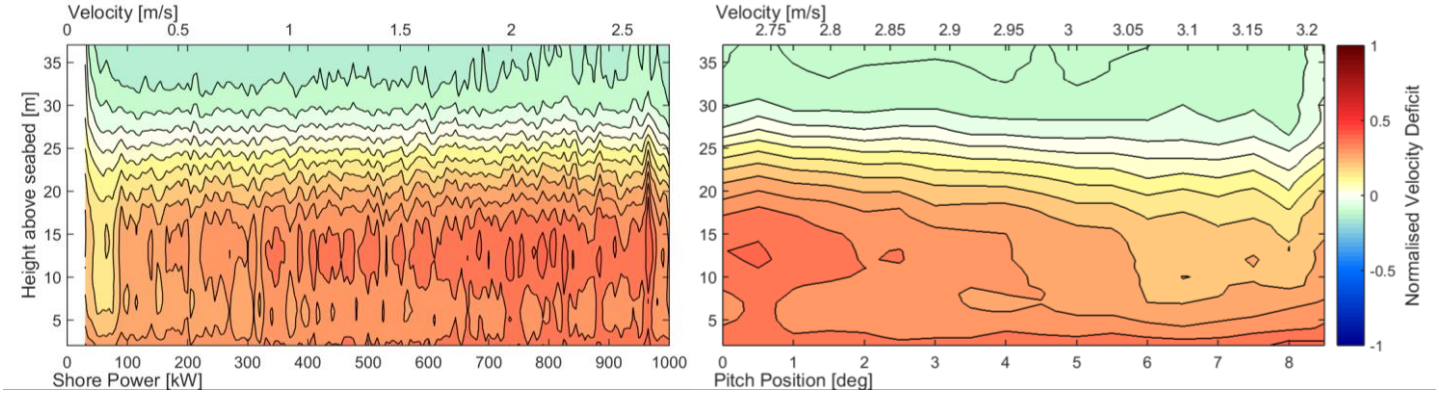

Figure 2 Velocity deficit shown as a function of depth and turbine power (left) and blade pitch position (right) for an ADCP in the wake of the turbine. Calculated turbine-related velocity is shown on top axis of both plots.

Impacts of Various Floating Platforms on FOWT System

Yuanchuan Liu and Qing Xiao*
Department of Naval Architecture, Ocean and Marine Engineering, University of Strathclyde, UK

Summary: Floating offshore wind turbine (FOWT) industry has been under rapid development in the past few years. Among various components in a FOWT system, the floating platform supporting the wind turbine and its tower plays a vital role on the performance of FOWT and system stability. In this paper, we studied two FOWTs which are supported by two commonly used platforms, i.e. a semi-submersible and a spar platform, under a combined wind-wave environmental condition. Using a Computational Fluid Dynamics (CFD) method, we intended to examine the influences of platforms on the performance of the floating system.

Introduction

As a clean and renewable energy source, wind energy has been more and more exploited during the past several decades. According to a report published by the European Wind Energy Association [1], by the end of 2014, the cumulative wind power capacity has reached 128.8 GW and can match 10.2% of Europe's electricity demand, which is a remarkable increase from 2.4% in 2000. In recent years, floating offshore wind turbines have been widely developed and tested. As one of the most important elements in a FOWT system, there are three different types of floating platforms, e.g. the Semi-submersible platform; the Spar platform and the Tension Leg Platform (TLP). While the application of these platforms is quite mature in the oil and gas industry, the knowledge of their impacts on the application in FOWT industry is limited. The significance of such study is therefore extremely important as the platform and its supported wind turbine constitute a fully coupled system.

In this study, two different types of FOWT, i.e. a semi-submersible and a spar platform, are investigated using a CFD method. To compare the dynamic responses of different floating systems and wind turbine performance, numerical modelling is carried out with a three-bladed wind turbine under a same wind-wave condition.

Numerical Methods

The present CFD tool is based on OpenFOAM with further development, where two-phase incompressible RANS equations are solved by Finite Volume Method (FVM). The interface between air and water is captured via a VOF method with a bounded compression technique. The pressure-velocity coupling is handled with the PIMPLE algorithm which combines the well-known PISO and SIMPLE algorithms. The code is integrated with a numerical wave tank module for wave generation and damping [2], as well as a mooring system analysis module to deal with offshore floating structures. The backward Euler scheme is used for temporal discretisation and a second-order upwind scheme is adopted for the convection terms.

Model

The models investigated in the present study are the Hywind spar FOWT [3] examined in the OC3 project (Offshore Code Comparison Collaboration) proposed by IEA (International Energy Agency) and the DeepCWind semi-submersible FOWT [4] involved in the OC4 project. The National Renewable Energy Laboratory (NREL) offshore 5-MW baseline wind turbine [5] is used for both models. Fig. 1 and Fig. 2 show the sketches for both models (see parameter details from references). Fig. 3 represents the typical mesh for an OC4-DeepCWind FOWT. The wave under consideration is a second-order Stokes wave with a wave height H of 7.58 m and a wave period T of 12.1 s. Only one wind speed is tested with a steady wind velocity V of 7.32 m/s. The turbine rotor rotates at a speed of 4.95 RPM with a collective blade pitch angle of 6.4 degrees.

Results

Fig. 4 demonstrates the difference between the aerodynamic thrust of the FOWT and that from a fixed wind turbine for the OC4 model. It is shown that, due to the movement of the floating system, the aerodynamic torque associated with a floating platform has a profound variance. The amplitudes indicated with red squares in Fig. 4 account for roughly 10% of the mean torque. In terms of the installation of wind turbine on the platform responses, we found that the mean surge of platform increases significantly from 0.87 m to 1.74 m and the mean pitch also shifts from near-zero to 0.4 degrees due to the aerodynamic thrust from the upper rotating turbine. Amplitudes of surge and pitch are not affected though and they are 2 m and 0.83 degrees respectively.

* Corresponding author.
Email address: qing.xiao@strath.ac.uk

Fig. 5 shows the comparison between the motion responses of the OC3-Spar FOWT and those from the OC4-Semi FOWT, including surge, heave and pitch degrees of freedom. Although the responses for the OC3-Spar FOWT have not converged to a quasi-steady state due to the limited computational time, it is already revealed that the spar-type FOWT seems to have better performance over the semi-type in the surge motion, reflected by smaller surge amplitude, probably due to its smaller water-plane area as compared to a semi-submersible platform. However, a much larger heave displacement is observed for a spar platform than a semi-submersible one as indicated in Fig. 5.

Conclusions

By investigating an OC4 Semi-submersible FOWT and an OC3 spar FOWT, it is revealed that a fully coupled modelling of FOWT is necessary in order to better predict the performance of wind turbine and estimate the dynamic response of floating platforms. Even under the same wind-wave condition, the influence of different platforms on the wind turbine performance may be different. The results obtained from this study would be helpful in selecting appropriate platform to be used in the future FOWT applications.

References:

[1] EWEA, *Aiming High: Rewarding Ambition in Wind Energy*, 2015.
[2] Shen Z., Cao H., Ye H. *et al.* (2013). Development of CFD Solver for Ship and Ocean Engineering Flows. In: *8th International OpenFOAM Workshop*, Jeju, Korea.
[3] Jonkman J., *Definition of the Floating System for Phase IV of OC3*, NREL/TP-500-47535, National Renewable Energy Laboratory, Golden, Colorado, USA, 2010.
[4] Robertson A., Jonkman J., Masciola M. *et al.*, *Definition of the semisubmersible floating system for phase II of OC4*, National Renewable Energy Laboratory, Golden, Colorado, USA, 2014.
[5] Jonkman J. M., Butterfield S., Musial W. *et al.*, *Definition of a 5-MW reference wind turbine for offshore system development*, NREL/TP-500-38060, National Renewable Energy Laboratory, Golden, Colorado, USA, 2009.

Fig. 1. OC3-Hywind [3]

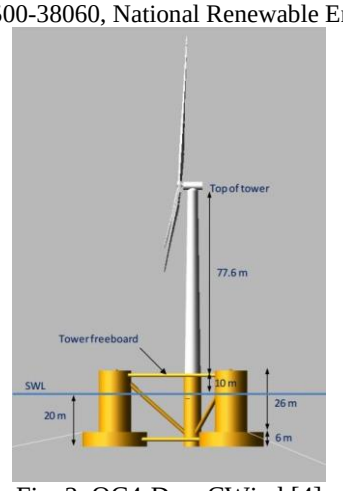

Fig. 2. OC4-DeepCWind [4]

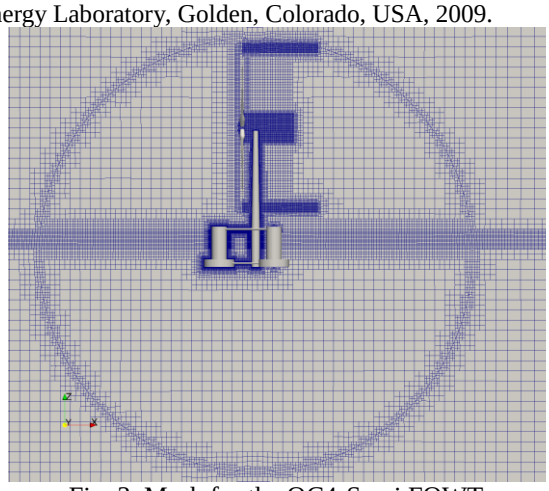

Fig. 3. Mesh for the OC4-Semi FOWT

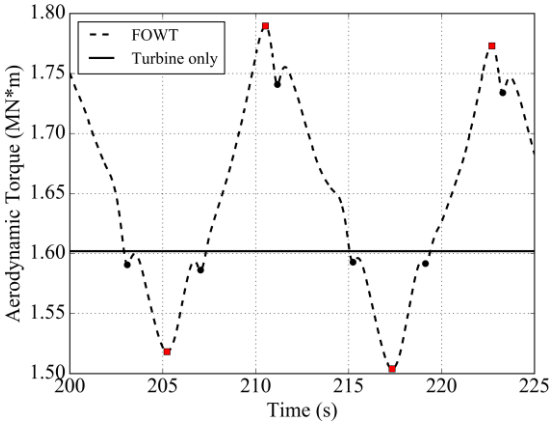

Fig. 4. Comparison of OC4 FOWT aerodynamic torque with data from fixed turbine simulation

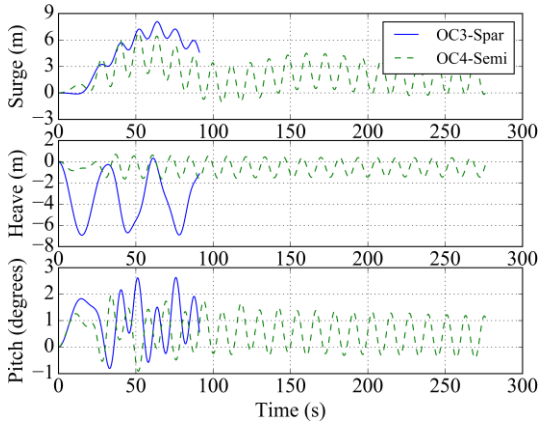

Fig. 5. Comparison of the motion response between OC3-Spar and OC4-Semi FOWT

RANS-VOF Modelling of Floating Tidal Stream Systems

Edward J. Ransley*, Scott A. Brown, Deborah M. Greaves
School of Marine Science and Engineering, Plymouth University, UK

Simon Hindley
Mojo Maritime Ltd, Falmouth, UK

Paul Weston
A&P Group Ltd., Falmouth, UK

Eamon Guerrini
Modular tide Generators Ltd., Woking, UK

Ralf Starzmann
Schottel Hydro GmbH, Spay/Rhein, Germany

Summary: A fully nonlinear coupled CFD approach has been developed to simulate the behaviour and power output of a floating tidal stream concept. The model includes RANS-VOF and rigid body solvers based on OpenFOAM®, a hybrid-catenary mooring system and a two-way-coupled, actuator-line model for a Schottel Instream Turbine with over-speed control. Simulations are performed in spring currents at the PTEC site with and without the 1-in-1 year wave present. Results show considerable complexities beyond periodic behaviour necessitating the use of models that include the complete coupled system and hydrodynamic conditions.

Introduction

Numerical models are now capable of providing the quantitative description required for engineering analysis. However, for structures such as floating tidal stream concepts, the complete system can rarely be included using existing functionality. To better understand the behaviour of these systems, a coupled CFD model, including a floating barge, hybrid-catenary mooring system and the influence of a submerged turbine, has been developed and tested at full-scale in waves and currents based on those at the Perpetuus Tidal Energy Centre (PTEC) site.

Method

The open-source software OpenFOAM® solves the fully nonlinear, incompressible, Reynolds-Averaged Navier-Stokes (RANS) equations for air and water using the finite volume method and a Volume of Fluid (VOF) treatment of the interface. The device motion is found using a rigid-body solver and new two-way coupled actuator-line model for the turbine. Wave and current, generation and absorption are achieved via the expression-based boundary conditions and 'relaxation zone' formulation of additional toolbox waves2Foam [1].

The 18x7x1.5m buoyant barge is based on existing plans with a 'moon-pool' to accommodate a 4m diameter turbine. The computational domain is 320x60x90m with a background mesh of cubic cells (side-length 1.67m) and local multi-level octree refinement at the free-surface, on the barge surface and around the turbine.

The Schottel Instream Turbine (SIT) is a lightweight, horizontal axis turbine rated at 62kW electrical power for flows ~3ms^{-1} with a cut-in speed of 1ms^{-1}. At rated power, an over-speed control strategy including blade flexure is used. To model all of these features, an axial induction factor, a, is assumed where

$$a = 1 - U_\infty / U_T \tag{1}$$

and the thrust on the turbine is

$$T = 2\rho A U_\infty^2 a(1-a) \tag{2}$$

where ρ is the water density, A is the turbine swept area and U_∞ and U_T are the far field and local flow velocity respectively. This leads to three operating regimes with a constant a at low speeds and an a that depends on U_∞ in the two over-speed regimes (max torque, max power). A series of polynomials have been fitted to existing turbine data to predict a, as well as the angular velocity of the turbine, from U_T in these over-speed conditions.

* Corresponding author.
Email address: edward.ransley@plymouth.ac.uk

During the simulations, the local velocity, U_T, is approximated as the ratio of the vector sum of the weighted velocities to the sum of the weights within a cylindrical region containing the turbine. To represent the turbine blades the weights are derived using Gaussian distributions running both axially and with angular distance from each of the blade centres (which rotate at run-time according to the calculated angular velocity).

The total thrust force is then applied as an additional force in the 6DoF rigid body solver for the barge's motion. The influence of the submerged SIT on the fluid flow has been included by applying an equal and opposite distributed body force field to the momentum equation with the same weighting as for U_T.

The mooring system consists of four 235m cables (85m synthetic line, 150m chain). The full nonlinear reaction force from each cable is found using tri-linear interpolation across a 'look-up table' derived manually using OrcaFlex®. These are then applied as four further additional forces in the 6DoF rigid body solver.

Spring peak surface flow rates at the ~57m deep PTEC site are ~2.5-2.9ms^{-1} [2]. The velocity profile has been approximated using the von Karman-Prandtl equation (U^* = 0.13, Z_0 = -2.24) [3]. The waves are based on a Weibull fit to the wave data from the south-west with a return period of 1 year (H = 6.1m, T = 9s) [1].

Results

Simulations were run in spring current conditions with and without the 1-in-1 year waves. The combined case has a return period of ~85 years making it typical of the design limit state of offshore structures. Fig. 1 shows the local flow velocity, U_T (a), the thrust (b), the electrical power generated (c) and the revolutions per second (d) during simulations including currents separately (red) and waves and currents combined (blue).

It can be seen that there is significant variation in power and thrust even in the current-only case. This is believed to be due to a combination of residual surge motion and the effect of rotating blades. Unsurprisingly, the variations in the combined case are considerably more dramatic. The turbine experiences oscillations between periods of power saturation and high thrust, when a crest passes and periods of reduced power output and low thrust, when a trough passes. The revolutions per second also show correspondingly large variations.

Conclusions

The power delivery and forces on a floating tidal stream turbine show considerable complexities beyond simple periodic behaviour. Complete, coupled models, such as the one proposed here, are therefore necessary to understand the behaviour and power delivery of floating tidal stream concepts in real offshore conditions.

Acknowledgements:

This work used the ARCHER UK National Supercomputing Service (http://www.archer.ac.uk) and has been funded as part of Innovate UK Project 102217 through the Energy Catalyst Early-stage Round 3.

References:

[1] Jacobsen, N., Fuhrman, D., and Fredsøe, J., 2012, "A wave generation toolbox for open-source CFD library: OpenFOAM®", *Int. J. Numer. Meth. Fluids*, 70, 1073-1088.

[2] Royal HaskoningDHV, 2014, "Chapter 7: Physical Processes", in "Perpetuus Tidal Energy Centre (PTEC), Environmental Statement", Royal HaskoningDHV, Amersfoort, Netherlands.

[3] Dyer, K. R., 1970, "Current Velocity Profiles in a Tidal Channel", *Geophys. J. R. astr. Soc.* 22, 153-161.

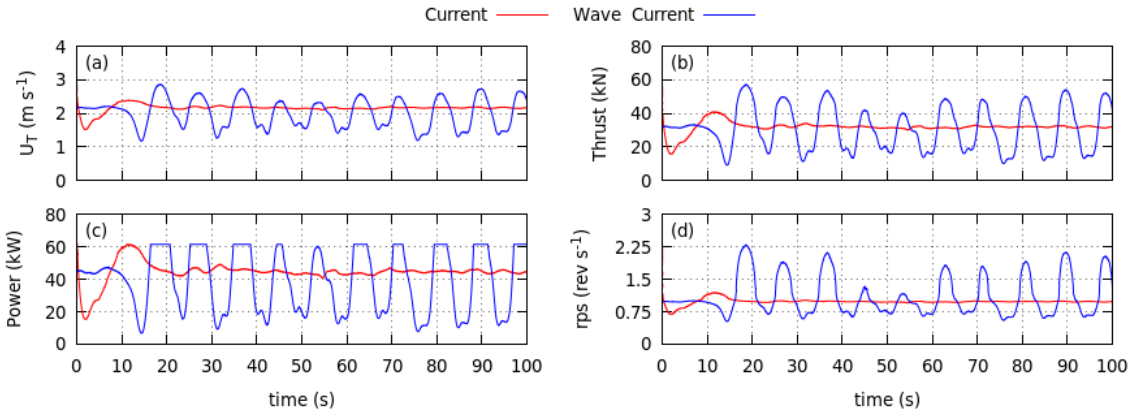

Fig. 1 Local flow velocity (a), thrust (b), electrical power (c) and the revolutions per second (d) from simulations including currents separately (red) and waves and currents combined (blue).

Evaluating Passive Structural Control of Tidal Turbines

Song Fu[#1], Cameron Johnstone[#2], Joe Clarke[#3]

Energy Systems Research Unit, Department of Mechanical and Aerospace Engineering, University of Strathclyde, Glasgow, UK, G1 1XJ

[1]*song.fu@strath.ac.uk*

[2]*cameron.johnstone@strath.ac.uk*

[3] *joe@esru.strath.ac.uk*

Summary: The abstract discusses the structural analysis of turbines, and proposes the use of a tuned mass damper system to control loads on the turbine.

INTRODUCTION

The environment tidal turbines operate within is considered dynamic due to turbulence and wave motion components encompassed within the bulk tidal flow. Considering wave-current coupled forces as excitations, the dynamic load experienced on a tidal turbine is a complicated physical problem which poses a challenge for engineers trying to design larger tidal turbine towers and other floating support structures. Different structural damping strategies have been implemented in the wind industry such as tuned mass dampers and some control technologies like generator torque control and blade pitch control are also developed to reduce the fatigue and structural loading.

The aim of this project is to design a tidal turbine station keeping system with a tuned mass damper in order to reduce fatigue and peak structural loading experienced by the turbine. This may result in a reduction of mass and costs associated with the structural support and station keeping system.

Unlike onshore and offshore wind turbines, tidal turbines are fully submersed in water, so the effect of added mass cannot be ignored. The tower is considered to be a vibrating rod in the water column in order to calculate the added mass and viscous damping [1]. A wind turbine with a tower-monopile supporting structure can be modelled as an inverted pendulum [2], as shown as a general representation of the system in Figure 1. The same model can be applied to tidal turbine with a tower-monopile supporting structure. The tower-monopile support structure for the Torr Head Tidal Array project is used as a case study for this investigation and relevant parameters are shown in Table 1. This is for a 1MW tidal turbine whose rotor diameter is about 20m.

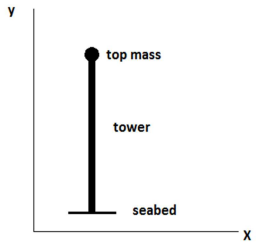

Figure 1. Structural model of a flexible wind (tidal) turbine [2].

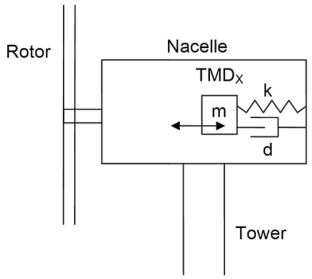

Figure 2. Schematic of TMDX in turbine nacelle[3]

Materials	Steel
Height of centre of nacelle	25m
Pile diameter	2.5 to 2.8 m
Structure weight	Dry weight of 100 to 120 tonnes.
Top mass	85 tonnes

Table 1. Tower-monopile support parameters.

In this project, the locations of the Tuned Mass Dampers (TMDs) are in the nacelle and TMD_X indicates that it oscillates horizontally in a fore-aft direction. A simple schematic of the TMD_X configuration is shown in Figure 2. Once the tower-monopile's natural frequencies have been derived, one can calculate the TMD properties [4].

Method

The algorithm used is based on dynamic analysis, and the tower-monopile dynamics can be modelled as forced response of a non-gyroscopic damped linear system, given by:

$$M\ddot{x} + D\dot{x} + Kx = F(t) \tag{1}$$

where x is the tower displacement and F is the applied force, which in this case is predominantly the rotor thrust, which can be calculated by Blade Element Momentum Theory in wave-current coupled conditions [5]. M is the total mass matrix with added mass correction, the damping matrix term D is corrected with a viscous damping factor which is generally small (<0.002 in this system) and K is the total stiffness matrix.

RESULT

The evaluation undertaken and results presented are for the system calculated with optimum TMD of the tower-monopile structure. Figure 3 shows the frequency domain analysis for the tower-monopile base bending moment in three different

conditions. Figure 4 show the time series result of a dramatic impact on tower-monopile system. Figure 5 shows the time series result of tower-monopile system under unsteady wave-current coupled forces.

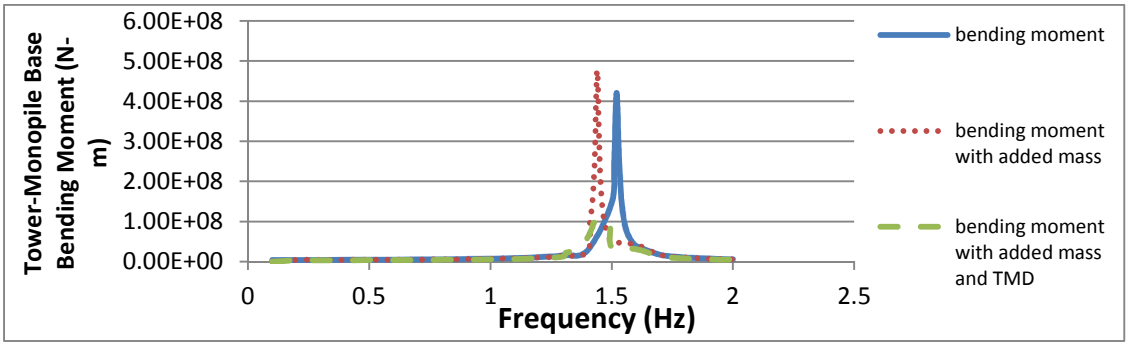

Figure 3. Frequency domain analysis of tower-monopile base.

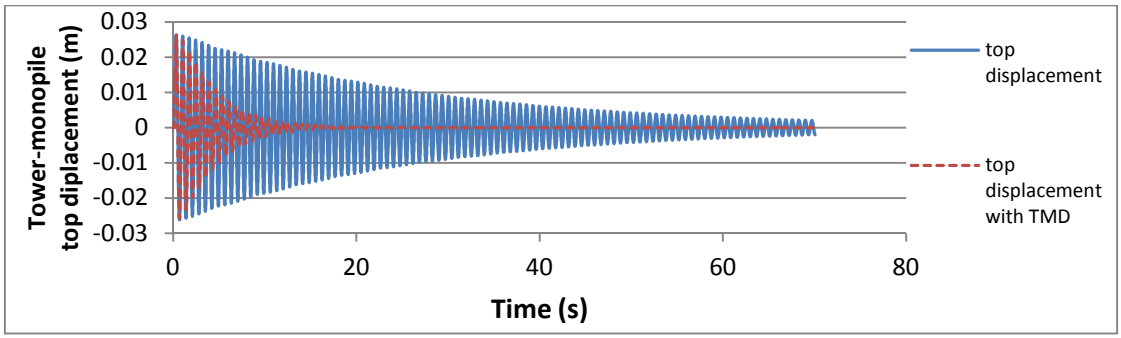

Figure 4. Tower-monopile top displacement.under a instant dramatic impact

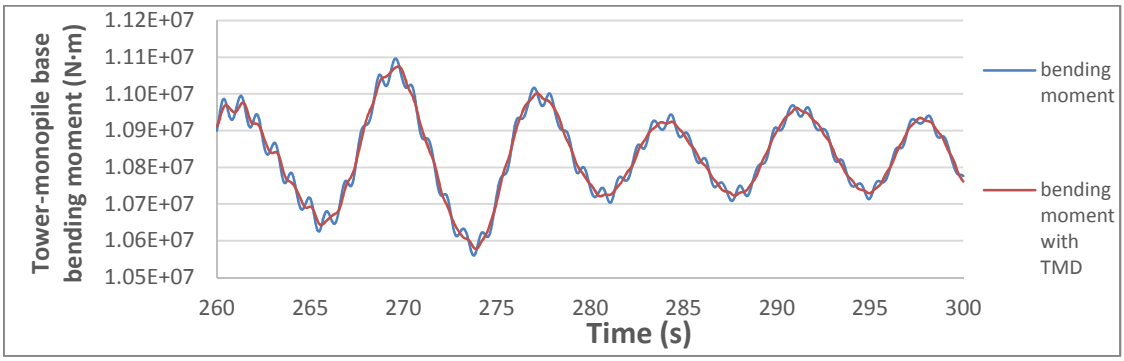

Figure 5. Tower-monopile fore-aft base bending moment.under unsteady wave-current coupled forces

CONCLUSION

This work has demonstrated, unlike offshore wind turbines, tidal turbine tower-monopile system in this project shows higher first natural frequencies due to the shorter length. Furthermore, the added mass correction will make natural frequencies of the structure slightly reduced; in most cases, the water viscous damping is very small and can be ignored. When TMD_x is implemented in the system, it has significant effects in resonance reduction and for-aft fatigue load-reduction under instant fluctuating impacts. However, compared with the fluctuating impact, TMD has an insignificant effect when unsteady wave-current coupled forces are applied on the structure.

References:

[1] M.W. Wambsganss, S.S. Chen, and J.A. Jendrzejczyk. (1976). Added Mass and Damping of a Vibrating Rod in Confined Viscous Fluids. *Journal of Applied Mechanics*, vol. 43, no. 2, pp. 325-329, 1976.

[2] J. V. der Temple. (2009). Ch 8. Offshore Turbines: Dynamics and Fatigue. *Offshore Wind Power*, Multi-Science Publishing Company.

[3] Matthew A. Lackner and Mario A. Rotea. (2011). Passive structural control of offshore wind turbines. *Wind Enery*, vol. 14, pp. 373-388, 2011.

[4] Yimaz, Onur Can. (2014). The Optimization of Offshore Wind Turbine. Master's thesis, University of Massachusetts, Amherst, 2014.

[5] Nevalainen, T.M and Johnstone, C.M and Grant, A.D. (2015). An Unsteady Blade Element Momentum Theory for Tidal Stream Turbines. In: *Proceedings of the 11th European Wave and Tidal Energy Conference*, Nantes, 2015.

Unsteady Tidal Turbine Blade Loading; an Analytical Approach

Gabriel Scarlett, Ignazio Maria Viola*
Institute for Energy Systems, School of Engineering, University of Edinburgh, UK

Summary: A model utilising linear 2D analytical theory is used to quantify the unsteady loading on tidal turbine blades due to the combined effects of waves and turbulence with shear and tower shadow. Initial results show that unsteady loads are mostly dominated by low frequency turbulence and waves, but if pitch control is employed loads are reduced by three orders of magnitude.

Introduction

The translation of a tidal turbine blade through waves, turbulence, shear and tower shadow introduces a time dependent angle of attack (α). For small harmonic oscillations in fully attached flow the solution to the unsteady lift coefficient C_L is given by Theodorsen as added mass and circulatory components [1]. The former accounts for flow acceleration effects, and the latter for circulation around the foil and shed vorticity in the wake introducing a time delay and amplitude reduction from the quasi-static loads. Loewy adapted the model for a rotor in hover to account for the effects of neighbouring and returning wakes on the unsteady loads [2]. Recent research has shown that attached unsteady loads may exceed steady loads by up to 15% [3], but has been confined to axial perturbations caused by waves and turbulence [3], or waves and yaw misalignment [4]. In order to further aid the design process a model is introduced which incorporates turbulent perturbations in all three coordinates, wave induced velocities in the axial (x), and vertical (z) directions, as well as the velocity deficit in x, and induced velocity in y, due to the presence of a tower structure.

Method

A three bladed 18 m diameter rotor located in a channel 45 m in depth and operating at the optimum tip speed ratio of 4.5, is considered [5]. Tests are carried out at the mid-section where the profile takes that of a NACA $63-439$, where the chord length is 1.45 m, and the pitch is 13.5°. The zero lift and static stall angles were determined using Xfoil [6]. Four inline waves were tested with frequencies $\boldsymbol{f_w} = (0.13, 0.18, 0.29, 0.67)$ Hz, respective heights $\boldsymbol{H_w} = (3.25,\ 1.75, 0.75, 0.25)$ m, and probability occurrences $\boldsymbol{P_w} = (\ 0.07, 5.83, 27.16, 7.14)$. These were selected from a MET office data set of measurements from the Pentland Firth [7]. Wave particle velocities are determined in the x, and z coordinates using Stokes second-order wave theory. Turbulence is simplified by assuming it comprises of four frequency constituents $\boldsymbol{f_t} = (0.01, 0.1, 1, 4)$ Hz, with amplitudes matched respectively to the following kinetic energies, measured in The Puget Sound [8], in x, y and z coordinates: $\boldsymbol{Ek_x} = (1.2\times10^{-1},\ 1.15\times10^{-2}, 1.4\times10^{-4}, 1.1\times10^{-4})$ m^2s^{-2}, $\boldsymbol{Ek_y} = (1.1\times10^{-2}, 1.8\times10^{-3}, 1.4\times10^{-4}, 1.4\times10^{-5})$ m^2s^{-2}, $\boldsymbol{Ek_z} = \boldsymbol{Ek_y}$. Turbulent intensities of 12%, 9% and 7% in the x, y, and z coordinates, respectively, were selected from a flow characterisation study carried out at The Sound of Islay [9]. The shear profile is assumed to agree with the 1/7th power law where the mean current at the hub is 2 ms^{-1} at a depth of 20 m. The velocity deficit in x, and induced velocity in y caused by the presence of a 2 m diameter tower, 5 m downstream of the rotor are determined using a potential flow model. For each test an α history is formed, as shown in Fig. 1, where time (t) is non-dimensioned by the rotational period (T_{rot}). The amplitude and peak frequency are then determined in order to form a harmonic angle of attack (α_h) signal, so as to be introduced into the theories of Theodorsen and Loewy to determine C_L (Fig. 2).

Results

The amplitude load response ΔC_L for each individual frequency component (f) non-dimensioned by the rotational frequency (f_{rot}), is shown in Fig. 3. These results are in qualitative agreement with ref. [10]. The greatest load fluctuations are caused by low frequency turbulence, associated with channel scale eddies greater than 100 m, and large amplitude waves. Figure 4 shows the effect of each wave combined with all other forcing frequencies (turbulence, shear, tower shadow). The lowest frequency wave leads to the largest combined ΔC_L. Figure 1 shows the α history for this case over 20 rotations, and Fig. 2 illustrates the resulting C_L. Under this operating condition dynamic stall does not occur because the stall angle, which is greater than 20°, is not exceeded. Clearly at lower current velocities and closer to the root, separation might occur. With higher frequency waves,

* Corresponding author.
Email address: I.M.Viola@ed.ac.uk

the dominating combined effect on ΔC_L is low frequency turbulence. Interestingly, if pitch control was to be adopted so as to filter every frequency up to twice f_{rot}, ΔC_L would decrease by three orders of magnitude.

Conclusions

The combination of low frequency turbulence and +3 m high waves lead to maximum ΔC_L. However, load fluctuations due to relatively large waves (~2 m), shear layer and tower shadow are negligible compared to those due to low frequency turbulence. Load fluctuations can be reduced by three orders of magnitude using pitch control at $2\times f_{rot}$. Further research is ongoing to determine the effects over a broader range of conditions as well as the effects of yaw misalignment, site specific shear, and flow separation.

Acknowledgements:

This work was supported by the Physical Sciences Research Council [grant number EP/M508032/1].

References:

[1] Theodorsen, T. (1935). "General theory of aerodynamic instability and the mechanism of flutter," NACA Technical Report No. 496.
[2] Loewy, R.G. (1957). "A two-dimensional approximation to the unsteady aerodynamics of rotary wings," J. Aeronaut. Sci, 24 (2): 81-92.
[3] Milne, I.A., Day, A.H. Sharma, R.N. and Flay, R.G.J. (2015). "Blade loading on tidal turbines for uniform unsteady flow", Renewable Energy, 77:338-350.
[4] McNae, D. M. (2013) "Unsteady hydrodynamics of tidal stream turbines". PhD thesis. Imperial College London.
[5] Gretton, G.J., and Ingram, D.M., (2011), "Development of a computational fluid dynamics model for a horizontal axis tidal current turbine", PerAWaT, MA1003, WG3 WP5 D1.
[6] Drela, M. (1989). "XFOIL: An analysis and design system for low Reynolds number airfoils". In Low Reynolds number aerodynamics (pp. 1-12).
[7] McCann, G. N., Hitchcock, S., and Lane, S. (2008). "Implications of site-specific conditions on the prediction of loading and power performance of a tidal stream device", In ICOE 2008, Brest.
[8] Thomson, J., Polagye, B., Durgesh, V., and Richmond, M. C. (2012). "Measurements of turbulence at two tidal energy sites in The Puget sound, WA". J., Oceanic Eng., 37(3), 363 - 374.
[9] Milne, I. A., Sharma, R.N., Flay, R. G. J., and Bickerton, S. (2011). "Characteristics of the onset flow turbulence at a tidal-stream power site", In EWTEC 2011.
[10] Sequeira, C.L. and Miller, R.J., 2014, September. "Unsteady gust response of tidal stream turbines. In IEEE/MTS OCEANS'14, St. John's.

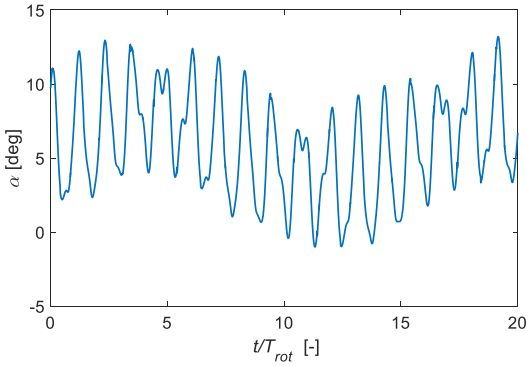

Fig. 1. Angle of attack fluctuations

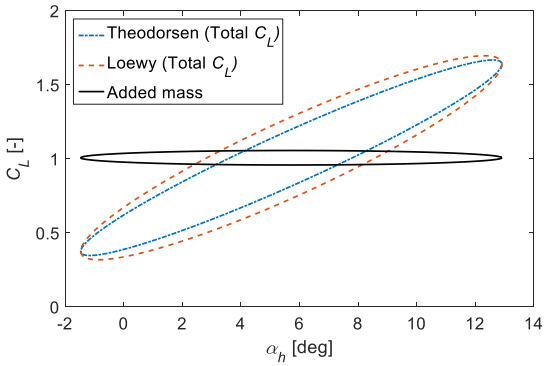

Fig. 2. Unsteady lift coefficient history

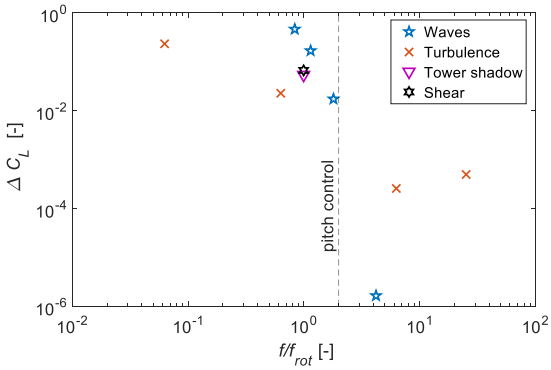

Fig. 3. Individual load effect

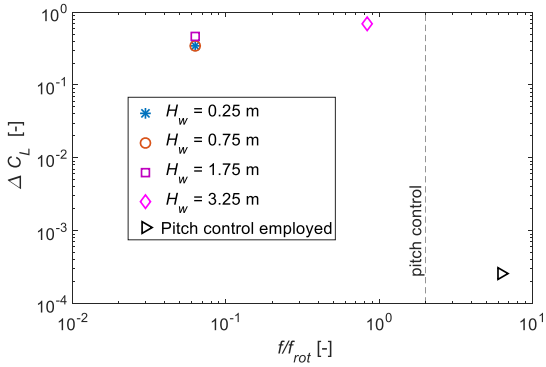

Fig. 4. Combined load response

Unsteady hydrodynamics of flexible submerged foils

Ignazio Maria Viola*, Susan Tully, Gabriel Scarlett
Institute for energy Systems, School of Engineering, University of Edinburgh, UK

Summary: The wave induced hydrodynamics of rigid and flexible foils are investigated by means of experimentation, including Particle Image Velocimetry (PIV), and analytically through Theodorsen's unsteady loading theory. High-amplitude high-frequency fluctuations were investigated in order to explore extreme flow fluctuations, which cannot be matched by a pitch control system, and to assess the limits of Theodorsen's linear approach. We found a strong non-linear interaction between the separated boundary layer and the trailing edge vortex, with circulation counter to the bounded case present. This resulted in low lift-to-drag ratio (i.e. low efficiency) and poor agreement between Theodorsen and experiments for the rigid foil. Conversely, the flexible foil was very promising: preventing large flow separation, it resulted in 25% higher lift-to-drag ratio, 30% lower flow fluctuations and reasonable agreement with Theodorsen's prediction.

Introduction

A submerged foil experiences wave-induced flow fluctuations resulting in periodic load variations. In the case of tidal turbine blades, peak load fluctuations can lead to dynamic failures while multiple load cycles can lead to fatigue failures. Therefore, it is critical that the nature of dynamic loading is fully understood; that accurate predictive tools are developed and that mitigating technologies are conceived. Unsteady loading on tidal turbines has been investigated measuring the thrust and torque at model-scale [1-3], and predictive tools based on the Morrison equation [1], Vortex Lattice Method [2], and Loewy's theory and Theodorsen's [4] have been developed. The latter theory is used in the state-of-the-art industry standard design tool Tidal Bladed Research. However, significant disagreement between numerical and experimental results have been reported [3]. While differences were thought to be due to flow separation and dynamic stall (which Theodorsen does not account for), flow measurements around the blades have never been performed to investigate these phenomena. In this paper we compare the loads measured experimentally on model-scale blades with those predicted by Theodorsen's theory. We then discuss the differences through the analysis of the flow field measured with PIV. The focus is on large-amplitude fluctuations in order to explore non-linear effects; and on high-frequencies (six per turbine revolution) which cannot be matched by a pitch control system. Most wind turbine flow-control techniques used to mitigate load fluctuations cannot be adopted by the tidal industry because they are incompatible with the harsh marine environment. For example, marine biofouling precludes the use of moving appendages and recessions. An emerging means for flow control, which could be employed by tidal turbines, is the use of flexible materials. Here we investigate blades with a flexible trailing edge.

Method

We 3D-printed a rigid and a flexible NACA 4415 foil, with a chord of 0.15 m extruded spanwise for 0.3 m. The Young's modulus of the flexible material was 0.97 MPa. We mounted the models between two splitter plates and immersed them at mid-depth in the University of Edinburgh's combined wave-current flume, which is 0.4 m wide and has a water depth of 0.45 m. We tested at a Reynolds number of 7.5×10^4. We generated opposing waves with Froude number 0.53, reduced frequency 1.9, steepness 0.04, depth/chord ratio 1.5 and relative depth 1.25 (see ref. [5] for further details). Lift and drag forces were measured with two independent load cells, PIV measurements were performed on the mid-span section at 7.5 Hz, and turbulence statics were measured via Laser Doppler Velocimetry at mid-depth, ten chords upstream of the model.

Results

The wave orbitals led to large-amplitude periodic variations of the flow speed ($U_{\mathrm{rel}} \in [0.76,1.22] \times U_{ref}$, where U_{ref} is the current velocity without waves) and of the angle of attack ($\alpha_{\mathrm{tot}} = 10° + \alpha$, where $\alpha \in [-13°, 13°]$). A phase delay of $\pi/2$ occurs between U_{rel} and α. The turbulence intensity was 3%. Figure 1 shows the anti-clockwise hysteresis loop of the lift force variation (divided by the dynamic pressure based on U_{rel}) versus α. When $\alpha = 0$ and is increasing (point A in fig. 1), U_{rel} is maximum and trailing edge separation occurs on both foils. This separation is associated with anti-clockwise circulation (a trailing edge vortex), which decreases the bound circulation around the foil and thus leads to a loss of lift (Δ Lift < 0). For the rigid model, in steady conditions, any further increase of α would lead to stall. However here α increases by 13° ($\alpha_{\mathrm{tot}} = 23°$)

* Corresponding author.
Email address: i.m.viola@ed.ac.uk

and only a mild boundary layer separation was observed on both foils. The deflection of the flexible trailing edge leads to a change in the orientation of the chord, defined as a line joining the leading and trailing edge of the foil. This results in a lower α oscillation ($\alpha \in [-4°, 4°]$) as compared to the rigid foil. The loss of momentum associated with the boundary layer separation is significantly reduced for the flexible model. When $\alpha = 0$ and is decreasing (point B in fig. 1), U_{rel} is minimum and boundary layer separation is clearly visible on the upper side of both foils. The α decrease prevents stall and the flow with low momentum slowly convects downstream along the foils. When the cycle restarts and α begins to increase again, the low momentum flow has reached the trailing edge and therefore strengthens the counter-rotating trailing edge vortex that begins to form. On the flexible foil, where less momentum is lost in the boundary layer, a much smaller trailing edge vortex is formed than on the rigid foil. This was further reflected in a 25% increased lift-to-drag ratio for the flexible model over the rigid model. The strong non-linear interaction between the separated boundary layer and the trailing edge vortex leads to a poor prediction using Theodorsen's theory for the rigid model. It should be noted that the effect of the shed circulation is opposite to that of the added mass (AM in fig. 1), which shows a clockwise hysteresis loop.

Conclusions

We found that wave-induced, large-amplitude, high-frequency flow fluctuations lead to periodic trailing edge separation (not dynamic stall). On a rigid model, this results in dynamic loads more than 20% higher than for current alone. Theodorsen's method, which is used in industry, may predict load fluctuations more than double that which was observed here. This highlights the need for advanced predictive tools. A flexible trailing edge can be used to mitigate load fluctuations by more than 30% and to increase efficiency by more than 25%, preventing large flow separation.

Acknowledgements: This work was supported by the Engineering and Physical Sciences Research Council [grant number EP/M508032/1].

References:

[1] Whelan, J. I. (2010) "A fluid dynamic study of free-surface proximity and inertia effects of tidal turbines" PhD thesis. Imperial College London.
[2] McNae, D. M. (2013) "Unsteady hydrodynamics of tidal stream turbines" PhD thesis. Imperial College London.
[3] Milne, I. A. (2014) "An experimental investigation of turbulence and unsteady loading on tidal turbines" PhD thesis. University of Auckland.
[4] Sequeira, C. L. (2014) "Hydrodynamics of Tidal Stream Turbines" University of Cambridge
[5] Tully S. and Viola I. M. (2016) "Reducing the wave induced loading of tidal turbine blades through the use of a flexible blade" ISROMAC, April 10-15, Honolulu

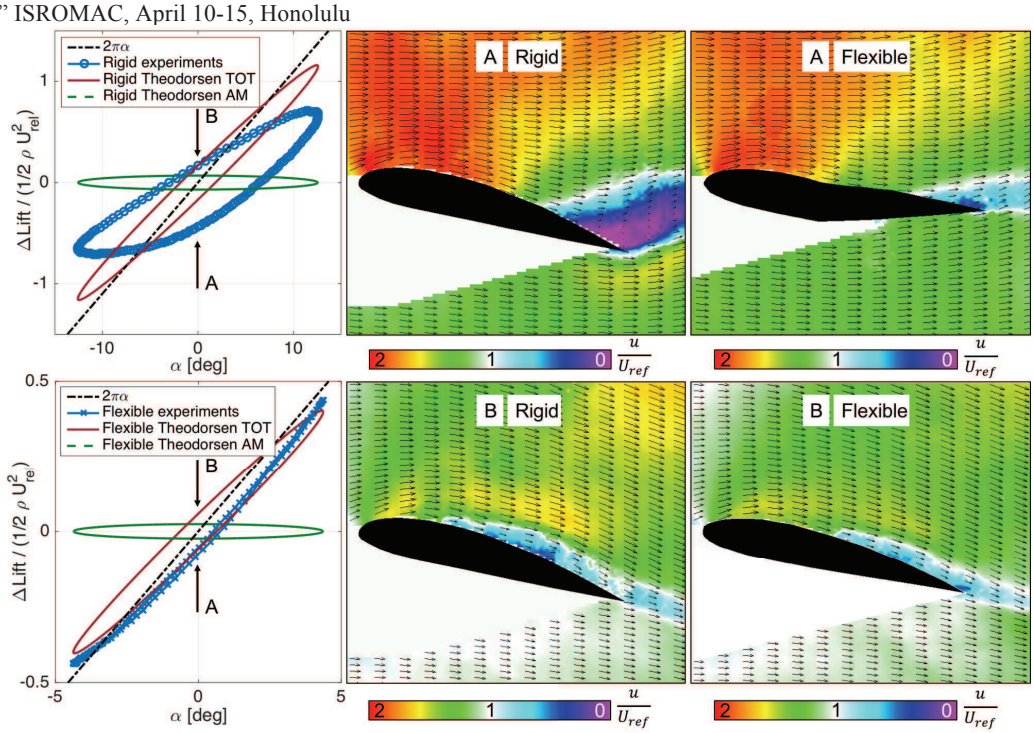

Fig. 1: Lift variations and flow fields for a rigid and a flexible model subjected to wave-induced large-amplitude high-frequency flow fluctuations.

Harvesting Energy from a Flexible Flapping Membrane in a Uniform Flow

Guangyu Shi and Qing Xiao*
Department of Naval Architecture, Ocean and Marine Engineering, University of Strathclyde, UK

Summary: The flapping dynamics and strain energy distribution of a flexible membrane immersed in a uniform flow is numerically studied. The system is controlled by two main parameters, i.e.the structure-fluid mass ratio (M^*) and the reduced flow velocity (U^*). Simulation results demonstrate that the membrane exhibits a periodic oscillation with one dominant frequency for a certain range of non-dimensional velocity. Within this range, flapping amplitude increases with U^*, and non-uniform strain energy distribution is generated along the membrane. In addition, the maximum available strain energy shows an upward trend with an increasing of U^*.

Introduction

With the increasing demand of clean and eco-friendly energy, flow-induced instabilities as one of the potential mechanisms to generate small amount of electric power from flows have received renewed attentions [1]. Such instabilities which originate from the competition between the fluid force and structure's rigidity are able to induce a self-sustained oscillation of a flexible body. A canonical example is a flexible membrane, or plate, immersed in a uniform flow, which has been extensively studied in both experimental and numerical ways due to its rich flapping dynamics [2].When the membrane is made of piezoelectric materials, the fluid energy, which is continuously pumped into the membrane, can be extracted and transferred into electricity. This novel power generator has attracted many researchers' interest. Some experiments and numerical simulations have been conducted to study its flapping dynamics and conversion efficiency [3-5]. In the present work, we simulated an energy-harvesting membrane immersed in a uniform flow by solving the *Navier-Stokes equations* and the structural motions were obtained using a modal analysis approach. We first validated the numerical method developed with experimental results, and then studied the variation of total strain energy at various reduced velocities.

Methods

The coupled fluid-structure interaction is solved using our in-house code on a HPC facility, where a parallel computing using MPI for the information exchange between different processors is used. The unsteady Navier-Stokes equations are solved on structured multi-block grids with a cell-centred Finite Volume Method. The convective flux is discretized using a central differencing scheme with artificial dissipation. Implicit backward-difference scheme of second-order accuracy and dual-time stepping algorithm are adopted to ensure a strongly coupled solution in the time-domain. The linear structural equations are solved using a modal analysis method and the structural modes are obtained by the classical Euler-Bernoulli beam theory.

Results

We first compared our simulation results with the experimental results of Chen et al [6]. Fig. 1 and Fig. 2 demonstrate the variations of dimensionless amplitude A^* and frequency f^* as a function of reduced velocity, respectively. The reduced velocity U^* under investigation covers a range from 7 to 9 with corresponding Reynolds number from 4.5×10^4 to 5.7×10^4. The experimental results shown in Fig. 1 indicate that as the reduced velocity U^*increases, more flow energy is harvested by the membrane, resulting in the increase of flapping amplitude, which is well captured by the present simulation. However, with further increase of U^*, the incoming flow tends to supress the membrane's vibration due to a stronger fluid-structure interaction. Our simulation fails to replicate this nonlinear feature due to the linear structural model we adopted. With regards to the flapping frequency plotted in Fig. 2, we found that within the present reduced velocity range, the membrane always exhibits a periodic motion associated with a second order structural dynamic mode. The instantaneous deformation of membrane at $U^*=9$ is illustrated in Fig. 3. A closer inspection of this figure reveals that the vortex is formed at the leading edge and grows as it travels along the membrane and further shed into the wake in the vicinity of trailing edge. This periodical vortex shedding, responsible for large deformation of the structure, further strengthens the fluid and structure interaction between the membrane and wake vortices. To estimate the available power generated by the vibration of elastic membrane, the mean square of strain energy is computed from the deformation of membrane, more precisely, the curvature radius and membrane thickness (Techet et al [1]). Fig. 4 shows the mean square strain energy distribution along the membrane at various reduced velocities.

*Corresponding author.
Email address: qing.xiao@strath.ac.uk

It can be readily observed that the mean strain distribution is highly non-uniform along the membrane's length, which is similar to earlier studies [1] [5]. The higher strain is available near the leading and central part of membrane while diminishes near the tail edge. This is mainly because the membrane is vibrating at its second order structural mode with no bending deformation near the tail of the membrane, which can also be clearly observed from Fig. 3. The instantaneous membrane strain energy at different reduced velocity is represented in Fig. 5. It is clear that the maximum available strain energy grows linearly with the increase of reduced velocity resulting from the formation of strong vortices and the increase of flapping amplitude.

Conclusions

The energy-harvesting features of a flexible membrane immersed in a uniform flow are numerically studied in this paper. The simulation reveals that the flapping amplitude of the membrane grows with the increase of U^* at the beginning, but showing a downward tendency as a further increase of U^*due to the suppression of incoming flow. On the contrary, an opposite variation is observed on the flapping frequency. The strain energy distribution along the membrane is non-uniform, presenting the peaks at the leading and central part of membrane. More strain energy can be harvested by increase incoming stream velocity.

References

[1] A. H. Techet, J. J. Allen, A. J. Smits(2002), Piezoelectric eels for energy harvesting in the ocean. In: *Proc. 12nd International Offshore and Polar Engineering Conference*, Kitakyushu, Japan,pp. 713-718.

[2] M. J. Shelley and J. Zhang (2011), Flapping and bending bodies interacting with fluid flows. *Annu. Rev. Fluid Mech.* 43, 449-465.

[3] L. Tang, M. P. Paidoussis, J. Jiang (2009). Cantilevered flexible plates in axial flow: Energy transfer and the concept of flutter-mill. *J. Sound Vib.***326**, 263-276.

[4] S. Michelin, O. Doare (2013). Energy harvesting efficiency of piezoelectric flags in axial flows.*J. Fluid Mech.***714**, 489-504.

[5] S. Shi, T. H. New, Y. Liu(2013). Flapping dynamics of a low aspect-ratio energy-harvesting membrane immersed in a square cylinder wake. *Exp. Thermal Fluid Sci.***46**, 151-161.

[6] M. Chen, L. Jia et al. (2014). Bifurcation and chaos of a flag in an inviscid flow.*J. Fluids Struct.***45**, 124-137.

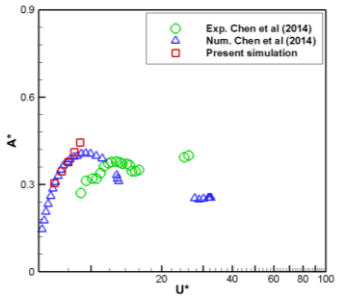

Figure 1. Dimensionless amplitude A^*vs. reduced velocity U^*

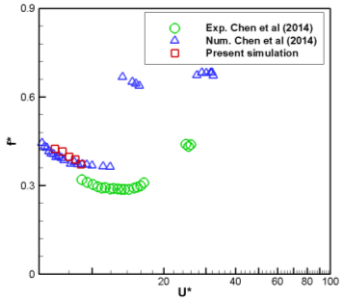

Figure 2. Dimensionless frequency f^* vs. reduced velocity U^*

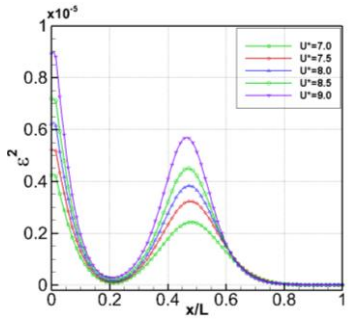

Figure 4. Square of strain over the membrane length at various U^*.

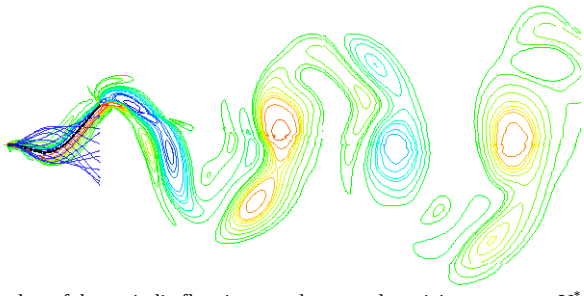

Figure 3. Snapshot of the periodic flapping membrane and vorticity contour at U^*=9.

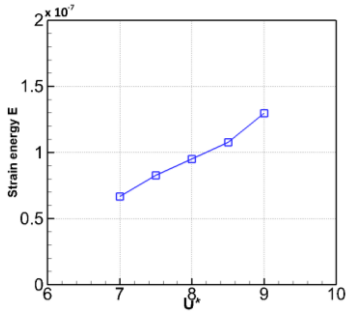

Figure 5. Strain energy E vs. reduced velocity U^*

Adjustable Camber for Extended Fatigue Life

Anna Young* and Judith Farman
Whittle Laboratory, University of Cambridge, UK

The lifespan of a tidal turbine is strongly affected by fatigue, and so reducing the response of the turbine to flow unsteadiness would enable a significant increase in turbine lifespan. One way of reducing the unsteady loads passed through the turbine is to fit control devices to the blades to reduce fluctuations in torque and/or thrust as a result of unsteady flow.

In terms of blade performance, the way to keep thrust constant in a fluctuating flow is to keep lift constant despite changes in incidence. This can be achieved by actively changing the camber of the blades, and one such method of doing this is to fit flaps towards the trailing edge of the blades.

A model scale turbine with flaps was tested at IFREMER under steady flow conditions and with waves. Figure 1 shows the steady performance of the turbine with the flaps in the neutral position and deployed towards the suction surface (reduced camber). It can be seen that there is a modest drop in power (small increase in drag), but a more substantial drop in thrust (large decrease in lift) as the blade is de-cambered.

To examine the potential for active load alleviation, surface waves were used to generate a periodic flow fluctuation and the flaps were operated sinusoidally such that they moved in and out of phase with the incoming waves. The results of this test are shown in Figure 2, where it can be seen that the thrust fluctuations are alternately damped and amplified by the flaps. The potential load reduction from a control system with flaps can be estimated from this figure.

Acknowledgements:
The authors would like to thank EPSRC SUPERGEN and the Maudslay Society for the funding that made this work possible. They are also grateful to IFREMER for help with testing, and to Ivor Day for technical assistance.

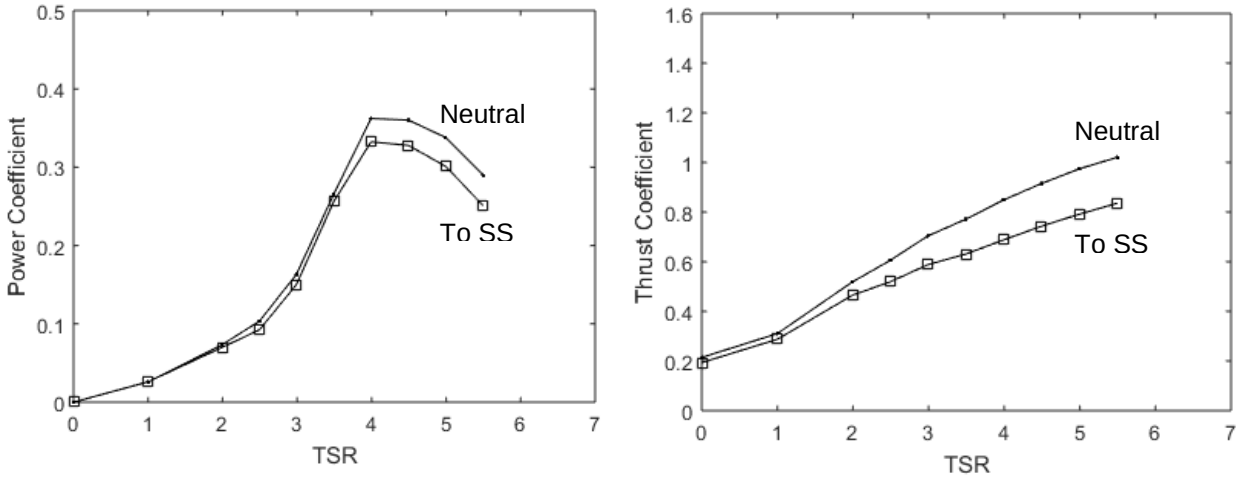

Figure 1: Effect of steady deployment of flaps on (a) power coefficient, and , (b) thrust coefficient.

* Corresponding author.
Email address: amy21@cam.ac.uk

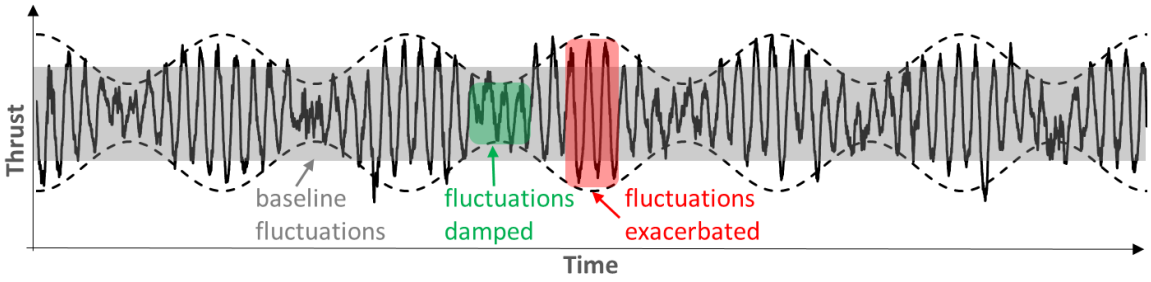

Figure 2: Fluctuations in thrust with flaps moving in and out of phase with incoming surface waves, showing potential for load alleviation.

Tidal Turbine Blade Design from a Fatigue Point of View

Vesna Jaksic
MaREI Centre - Environmental Research Institute (ERI), University College Cork, Ireland

Ciaran R. Kennedy, Sean B. Leen
Department of Mechanical Engineering, National University of Ireland, Galway

Conchúr M. Ó Brádaigh
Institute for Materials and Processes, University of Edinburgh, Scotland, UK

Summary: The structural design of tidal turbine blades is governed by the hydrodynamic shape of the aerofoil and extreme loading. The design of the aerofoil, chord and twist distribution along the blade, is generated so that the turbine has the optimum performance over the life time. Structural design gives the optimal layout of composite laminae such that the ultimate strength and buckling resistance requirements are satisfied while ensuring that certain fabrication criteria are satisfied. However, the structural design is using only static extreme loads while there is a lack of dynamic loads-based fatigue design of the tidal blades. In that regard the approaches for tidal turbine material fatigue life are studied.

Introduction

Tidal energy is a predictable renewable energy source and as such is gaining increased attention. However, the tidal force can vary over a small geographical space. Blade failures on a number of prototypes emphasise the need for design that will withstand the expected hydrodynamic loads. Glass fibre reinforced polymers (GFRP) such as epoxy or vinyl ester are traditionally used for tidal blades due to their properties of corrosion resistance, high strength and low cost. The polymers normally used in GFRP can absorb up to 5% water by weight when immersed for long periods and this can reduce the tensile strength of the material more than 25%. This paper gives the overview of the studies related to the degradation in tidal turbine blade life.

Moisture Resistance and Fatigue of GFRP Laminates

GFRP tend to absorb a small amount of water, typically less than 5% [1]. Epoxy matrices absorb less water than vinyl esters, but have superior mechanical properties. The water diffuses into the polymer matrix, changing its mechanical properties. The water will fill any small voids and attempt to dilute any unreacted constituents of the polymer, while the resulting osmotic pressure can cause damage to the laminate, i.e. stress corrosion cracking (SCC) of the fibres may occur. The multidirectional nature of laminates complicates the fatigue damage mechanisms. Matrix cracking parallel to the fibres or inter fibre failure (IFF) is first seen in the most off-axis plies under tensile loading. Most of the IFF cracking takes place in the first 25% of fatigue life and the significant drop in stiffness is complete with only a minor reduction in stiffness after this point. However, fatigue strength reductions do not follow the changes in static strength since the damage mechanisms are different in fatigue [2].

Modelling of GFRP fatigue life

Composites are a natural choice for turbine blades but there is little test data available on material behaviour under coupled environmental and cycling loading. An extensive review of modelling of fatigue in GFRP has divided the work among three broad approaches [3]. First is a testing approach where life predictions are based on test data of the exact or similar material, second is the phenomenological approach where predictions are based on the stiffness and residual strength behaviour, and thirdly a progressive damage approach where damage in the UD lamina is predicted and incremented until a final failure state is reached, thereby predicting fatigue life. The testing approach to fatigue life estimation is by far the most widely used [4]. The technique is constantly being refined to include effects like spectrum loading and complex constant life diagram (CLD) results [5]. Strength degrades during fatigue and an early model proposed that it degrades linearly per cycle in constant amplitude fatigue. Key problems with all residual strength methods are the large scatter in the residual strength test results and complexity of the degradation. Stiffness of GFRP laminates degrades in the range of 10 to 20% during fatigue cycling. The technique has been used to predict the life of particular wind blade laminates. These models have the advantage that they predict the stiffness degradation of the structure as it is damaged but a disadvantage is that they do not have an inherent failure point. The main drawback of the models discussed up to this point is their lack of flexibility in dealing with different laminate layups and/or loading patterns. Micromechanical approaches that predict the

response of the laminate based on damage mechanisms in the individual unidirectional (UD) plies offer a potential solution. The simplest approach is to degrade the matrix properties based on observed levels of cracking [6] and use classical laminate theory (CLT) to integrate the results. Others have considered two damage mechanisms, namely matrix cracking and interlaminar delamination [7]. Fracture mechanics approaches have been presented to predict matrix cracking behaviour and fibre failure. Energy approaches have been used to model delamination and stochastic methods have been used to enhance existing techniques. However, lot of work is ongoing to improve those predictive capabilities of test results and to reduce the amount of testing required to produce reliable fatigue life estimates.

Fatigue design methodology

The turbine blade fatigue design methodology is modular in nature, combined to facilitate the hydrodynamic and structural calculations required for preliminary design of a tidal turbine blade with respect to fatigue life. The first module in the design process algorithm is a tidal model, which predicts the tidal current speed at any time for specified pertinent local tidal velocities measured [8; 9]. The output from this tidal model forms a key input to a hydrodynamic model, which in turn computes the radial distributions of: local relative blade-fluid velocities, axial and tangential blade forces, optimum chord length, and pitch angle. The subsequent structural module, based on development of a finite element model of the blade, and driven by the output from the hydrodynamic model, is then employed to characterise the strain distribution in the turbine blade. The fatigue model accounts for each rotation of the blade explicitly and determines the maximum strain in the blade for each cycle. It then takes that maximum strain, compares them to an experimentally determined strain-life curve for the material and obtains a damage fraction for that cycle.

Conclusions

In order to fully utilise the tidal blade structural material fatigue life it is necessary to have information on its performance in marine environment for the full design life of marine renewable energy devices (10-20 years). To date, however, there are no reports available of experience with heavily loaded GFRP structures operating in this environment. In addition, the literature of fatigue test programs on the composite materials that will be used in marine renewable energy devices is limited. Consequently designers of these devices are forced to be quite conservative in their structural design, leading to increased cost. A comprehensive fatigue life model for composite blades, incorporating realistic hydrodynamic loadings, cyclically-varying blade stresses and wet composite material fatigue properties, will therefore be very valuable for tidal turbine designers.

Acknowledgements:

The Science Foundation Ireland SFI Advance award (14/ADV/RC3022); MARINCOMP Project reference: 612531, Grant agreement no.: FP7-612531, Funded under: FP7-People and Marine Research Energy Ireland (MaREI), Grant no. 12/RC/2305, a Science Foundation Ireland (SFI) supported project is gratefully acknowledged.

References:

[1] Baba, Nor Bahiyah, et al. (2015), Study on Mechanical and Physical Behaviour of Hybrid GFRP, *Advances in Materials Science and Engineering,* 2015, 7.

[2] Kennedy, Ciaran R, Brádaigh, Conchúr M Ó, and Leen, Sean B (2013), A multiaxial fatigue damage model for fibre reinforced polymer composites, *Composite Structures,* 106, 201-10.

[3] Degrieck, Joris and Van Paepegem, Wim (2001), Fatigue damage modeling of fibre-reinforced composite materials: Review, *Applied Mechanics Reviews,* 54 (4), 279-300.

[4] DNV GL – Energy (2014), Horizontal axis tidal turbines, *Renewables Certification – Wave and Tidal*, 284.

[5] Vassilopoulos, Anastasios P., Manshadi, Behzad D., and Keller, Thomas (2010), Influence of the constant life diagram formulation on the fatigue life prediction of composite materials, *International Journal of Fatigue,* 32 (4), 659-69.

[6] Duan, X. and Yao, W. X. (2002), Multi-directional stiffness degradation induced by matrix cracking in composite laminates, *International Journal of Fatigue,* 24 (2–4), 119-25.

[7] Talreja, RAMESH (2013), Continuum modeling of the development of intralaminar cracking in composite laminates, *ICF7, Houston (USA) 1989*.

[8] Grogan, DM, et al. (2013), Design of composite tidal turbine blades, *Renewable Energy,* 57, 151-62.

[9] Kennedy, Ciaran R, Leen, Sean B, and Brádaigh, Conchúr M Ó (2012), A preliminary design methodology for fatigue life prediction of polymer composites for tidal turbine blades, *Proceedings of the Institution of Mechanical Engineers, Part L: Journal of Materials Design and Applications*, 1464420712443330.

Performance and interaction of short fences of tidal turbines

Rohan Ramasamy, Richard H. J. Willden*
Department of Engineering Science, University of Oxford, UK

Summary: The paper uses numerical simulation of flows through actuator disk representations of tidal turbines to determine the performance limit for multiple arrays of disks arrayed in a single plane normal to the flow through a channel. Consistent with pervious research it is found that as the length of a single array of turbines is increased the limit of power extraction also increases. New results presented here show that it is possible to recover much of the power limit of a single fence by constructing the fence from shorter sub-arrays that are themselves spaced reasonably widely apart; several device diameters between each sub-array is possible without large performance decrement.

Introduction

The effects of flow blockage on the flow past a single tidal device are well established with significant performance uplift available; Garrett & Cummins [1]. The partial fence theory of Nishino & Willden [2] provides a model by which the upper limit of energy extraction can be estimated for a long but finite fence array of turbines partially spanning the width of a much wider flow channel. Adaptions of the model to incorporate free surface effects, Vogel et al. [3], and multiple rows of turbines, Draper & Nishino [4], have been made. The length of the tidal fence required to approximate the theory models has also been explored through numerical simulation, Nishino & Willden [5], as well as through experimental investigation, Cooke et al. [6]. It has been found that as the fence length increases the upper limit of energy extraction asymptotes to that of the infinitely long partial fence theory, and that for fences of length > 8 turbines the reduction in the power limit below that suggested by partial fence theory is in the region of 5%. Further work has been done to establish whether these higher limits of power extraction can be attained by rotors, as opposed to actuators, designed for such high blockage operation. The numerical simulations of Schluntz et al. [7] have shown using actuator line representations of fences of up to 8 turbines that turbines can be designed to achieve power levels in excess of those achievable using standard unblocked design techniques, with an 8 turbine fence achieving a power coefficient of 0.65 which is a significant uplift on unblocked rotor performance, although still less than the limit of power extraction suggested by actuator simulation of this fence length.

Whilst long, perhaps 8 turbine, closely spaced turbine fences may be desirable from a performance perspective they may be hard to achieve in practice unless the turbines are connected to a single support structure, and even then the costs involved in such an installation may be prohibitive, at least at this early industrial stage. We therefore explore the performance limit for shorter fences of 2 and 4 disks, and also the interactions between multiple arrays of 2 and 4 disks to determine whether the performance of a long array, 8 disks, can be recovered using multiple two-disk or four-disk sub-arrays.

Methods

The computations are performed in 3D in the CFD package Fluent, with the turbines presented as actuator disks. A typical structured mesh configuration at the rotor plane is shown in Fig. 1. The mesh is extruded in the streamwise direction and stretches from -30d upstream of the rotor plane to +60d downstream, where d is the rotor diameter. The water depth is 2d and we maintain a rigid lid so that the flow through the system is driven by a pressure drop from inlet to outlet. The overall width of the domain varies between configurations but is adjusted to maintain an overall global blockage of 0.0785. We make use of symmetry planes at mid-water depth and at the left hand side of the mesh shown so that the mesh shown represents an array of 8 porous disks; m=4 sub-arrays of n=2 disks each. Meshes are developed for various internal sub-array spacings, s/d, and for various spacings between sub-arrays, s_a/d. Although the near disk flow field is notionally steady, unsteady simulations are conducted to allow simulation of large unsteady mixing in the array far wake. Turbulence closure is provided through the RANS k-ω SST turbulence model.

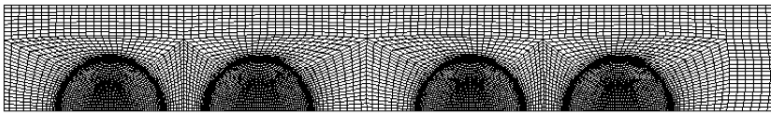

Fig. 1. Rotor plane mesh for an array of 8 disks; symmetry planes at left hand side and bottom.

* Corresponding author.
Email address: Richard.willden@eng.ox.ac.uk

Results

Consistent with pervious studies it is observed that for a single continuous fence the limit of power extraction is a function of intra-turbine spacing and fence length, and that the limit increases as the number of turbines increases; see Fig. 2. The horizontal dashed lines represent the power limit for single (m=1) fences of n=2, 4 and 8 disks with the power limit seen to increase by around 6% from the shortest to the longest fence considered. We further consider the case of multiple fences (m>1). Placing 2 two-turbine arrays (m=2, n=2) with the separation between the sub-arrays at 4d results in an uplift in performance above that for the optimal two turbine array (m=1, n=2), but to still less than the optimal achievable with 4 disks. Moving the 2 two-turbine arrays closer together results in an asymptotic approach to the power limit for a single four-turbine array. What is perhaps surprising is not that the 4 disk power limit is reached but that there is little performance decrement from separating the single 4 disk array into 2 two-turbine arrays that are themselves spaced considerably apart; at s/d=1 the performance decrement is less than 0.5%. Similar observations may be made for 8 disks split into 4 two-turbine arrays (m=4, n=2) and for 2 four-turbine arrays (m=2, n=4). The whole array performance can then be related to the array resistance, distribution of resistance across the array, array by-pass flows, between sub-array by-pass flows (see Fig. 2) and the cross-flow component of the velocity field.

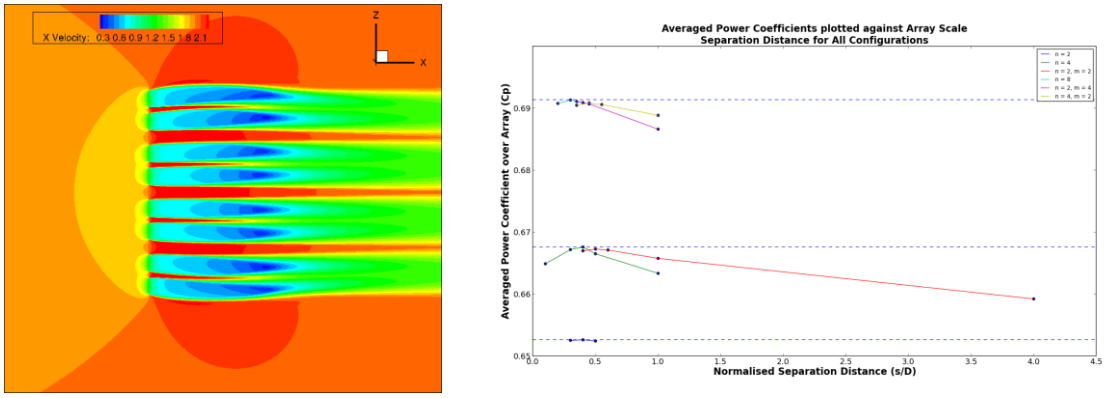

Fig. 2. Left: Streamwise velocity contours on the centre-plane of an array of m=4 sets of n=2 disk sub-arrays. Right: Upper limit of performance of m arrays of disks with n disks in each array.

Conclusions

We present simulation results for 1, 2 and 4 short fences of 2, 4 or 8 disks, with total disk number not exceeding 8, arrayed normal to the flow in a low global blockage flow-field. It is observed that even with significant separation between sub-arrays, which may be practical for investment, deployment and practical engineering purposes, it is possible to recover almost all of the power limit offered by a single homogeneous fence consisting of the same total number of disks.

References:

[1] Garrett, C. & Cummins, P. (2007). The efficiency of a turbine in a tidal channel. *J. Fluid Mech.* **588**, 243-251**.**

[2] Nishino, T. & Willden, R.H.J. (2012). The efficiency of an array of tidal turbines partially blocking a wide channel. *J. Fluid Mech.* **708**, 596-606.

[3] Vogel, C.R., Houlsby, G.T & Willden, R.H.J. (2016). Effect of free surface deformation on the extractable power of a finite width turbine array. *Renew Energy* **88**, 317-324.

[4] Draper, S. & Nishino, T. (2014). Centred and staggered arrangements of tidal turbines, Journal of Fluid Mechanics (739) 72-93

[5] Nishino, T. & R.H.J. Willden (2013). Two-scale dynamics of flow past a partial cross-stream array of tidal turbines, *J. Fluid Mech*. **730** 220-244.

[6] Cooke, S.C., Willden, R.H.J., Byrne, B., Stallard, T. & Olczak, A. (2015). Experimental investigation of tidal turbine partial array theory using porous discs. In Proc. 11th EWTEC Conference, Nantes, France.

[7] Schluntz, J., Vogel, C.R. & Willden, R.H.J. (2014). Blockage Enhanced Performance of Tidal Turbine Arrays. In Proc. 2nd AWTEC Conference, Tokyo, Japan.

Tidal turbine wake simulation using a high-order weakly-compressible Cartesian finite volume solver.

Baptiste Elie*, Guillaume Oger, Pierre-Emmanuel Guillerm, Bertrand Alessandrini
LHEEA Lab. (ECN/CNRS), Ecole Centrale Nantes, FRANCE

Summary: This paper presents the first validation steps of a tidal turbine farm simulation tool. The first part is dedicated to the presentation of the Navier-Stokes solver together with the actuator-disc tidal turbine model. Then, comparisons with experimental results from *Mycek et al.* [1] on a single turbine are presented and discussed. Finally, a discussion on the performances and limitations of this tool is provided.

Introduction

In order to rationalise the use of tidal energy resources, tidal turbines are planned to be set up as industrial farms on identified potential sites. In this configuration, machines interact with each other so that it is essential to correctly model the interactions in order to predict the global performance of a given farm. This is the reason why wake interaction effects have to be considered in complement with global performance analysis, which is generally conducted on single tidal-turbines. Regarding the fluid solver, a Navier-Stokes weakly-compressible explicit Cartesian finite volume solver is retained in this study. Its weakly-compressible feature allows a fully-explicit scheme, facilitating the integration of the solver in a massively parallel environment. Regarding the tidal turbine, an actuator disc model is adopted.

Methods

WCCH is a CFD software developed by the LHEEA Lab. of Ecole Centrale Nantes (ECN). This solver is a cell-centered Finite Volume formulation based on the compressible Navier-Stokes equations, within an explicit formalism [2]. In order to reduce the CPU time, the solver is built on a parallel framework based on a domain decomposition strategy (MPI library), including Adaptative Mesh Refinement (AMR). In the context of multiple tidal-turbine applications, the wake advection should be sufficiently accurate to predict correctly wake-wake and wake-turbine interactions, to allow eventually the optimization of a given farm. A preliminary work on the improvement of the order of the spatial interpolation scheme (WENO5 scheme [3]) has been performed in order to reduce the numerical diffusion. The HATT is modelled using the actuator-disc theory [4] together with an Immersed Boundary Method for the hub. The model we developed is not uniformly loaded and presents a radial and tangential distribution of the body forces characterized through a BEMT calculation process. This allows a better description of the tidal-turbine behavior and leads consequently to a better description of its impact on the surrounding flow. Finally, a LES method based on the Smagorinsky sub-grid scale model is adopted in this study.

Results

Comparisons are performed for one single tidal turbine in a turbulent axi-symetric flow. The turbine is placed in a cubic-shaped fluid domain of size 16D with 4D upstream to avoid interactions with the entrance area, and 12D downstream so as to observe the development of the wake. The spatial resolution in the refined zone corresponds to 60 cells in the turbine diameter, and a total of 1.8×10^6 cartesian cells are involved in the simulations. Thrust and power coefficients are in fairly good agreement with the experiments (C_P=0.42 and C_T=0.72). Figure 1 and 2 compare the averaged axial velocity and turbulence intensity rate fields obtained with our code with the reference case [1]. Results without presence of the hub are also included in Figure 2 for comparisons. A particularly good agreement is observed for the averaged axial velocity in the mid and far wake with and without the hub. From seven diameters downstream the tidal turbine, the averaged axial velocity results are in the margins of error of the experimental measurements (six diameters with the hub). The non-presence of the hub causes a top speed in the center of the machine along its rotation axis in the near and mid wake. Satisfactory results are obtained on the turbulence intensity rate between six and ten diameters downstream of the tidal turbine for all configurations. From x*=6 ($x^* = \frac{x}{D}$ and $y^* = \frac{y}{D}$), the turbulence intensity rate profile changes from a top hat shape to a bell shape. Note that this effect occurs more quickly in presence of the hub.

Conclusions

A validation was conducted with experimental results on a tidal turbine of 0.7 meter in diameter in the case of axi-symmetric low turbulent flows (3%). A comparison of the experimental and simulated wakes was conducted showing reasonably good agreement regarding the far wake where the inclusion of the hub does not have a significant impact. Further study will be needed to determine the importance of the hub in misaligned flows.

* Corresponding author.
Email address: baptiste.elie@ec-nantes.fr

Acknowledgements:

This study has been performed within the framework of a PhD funded by ANRT and ALSTOM Hydro France. Authors wish to thank them. The simulations were carried out in collaboration with the French computing center CRIHAN (project 2014005).

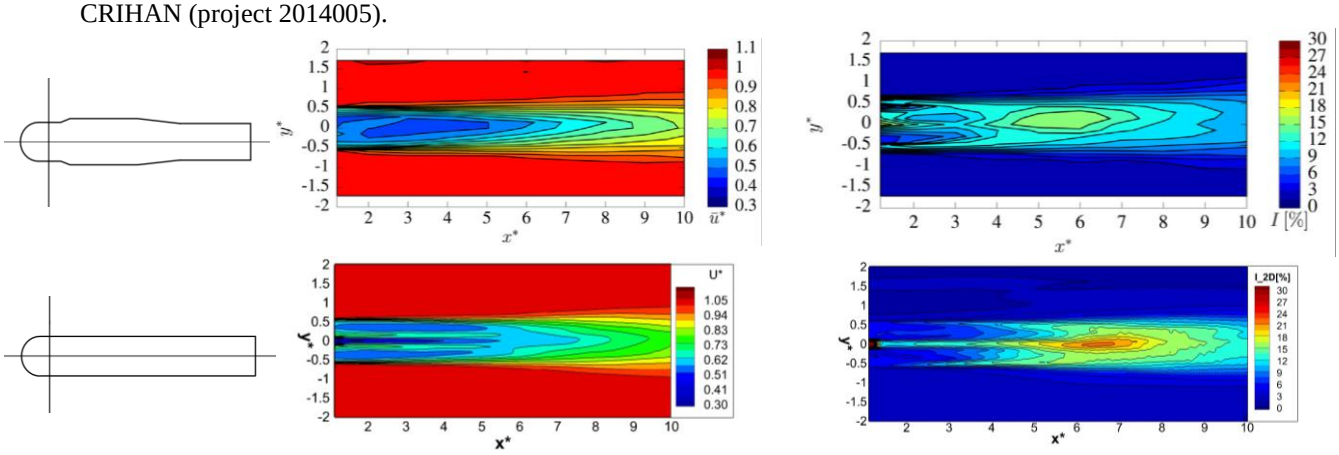

Fig. 1. Comparison of the averaged axial velocity fields and the averaged turbulence intensity fields in the wake for an ambiant turbulence intensity rate of 3% (up: results from [1], down: WCCH results).

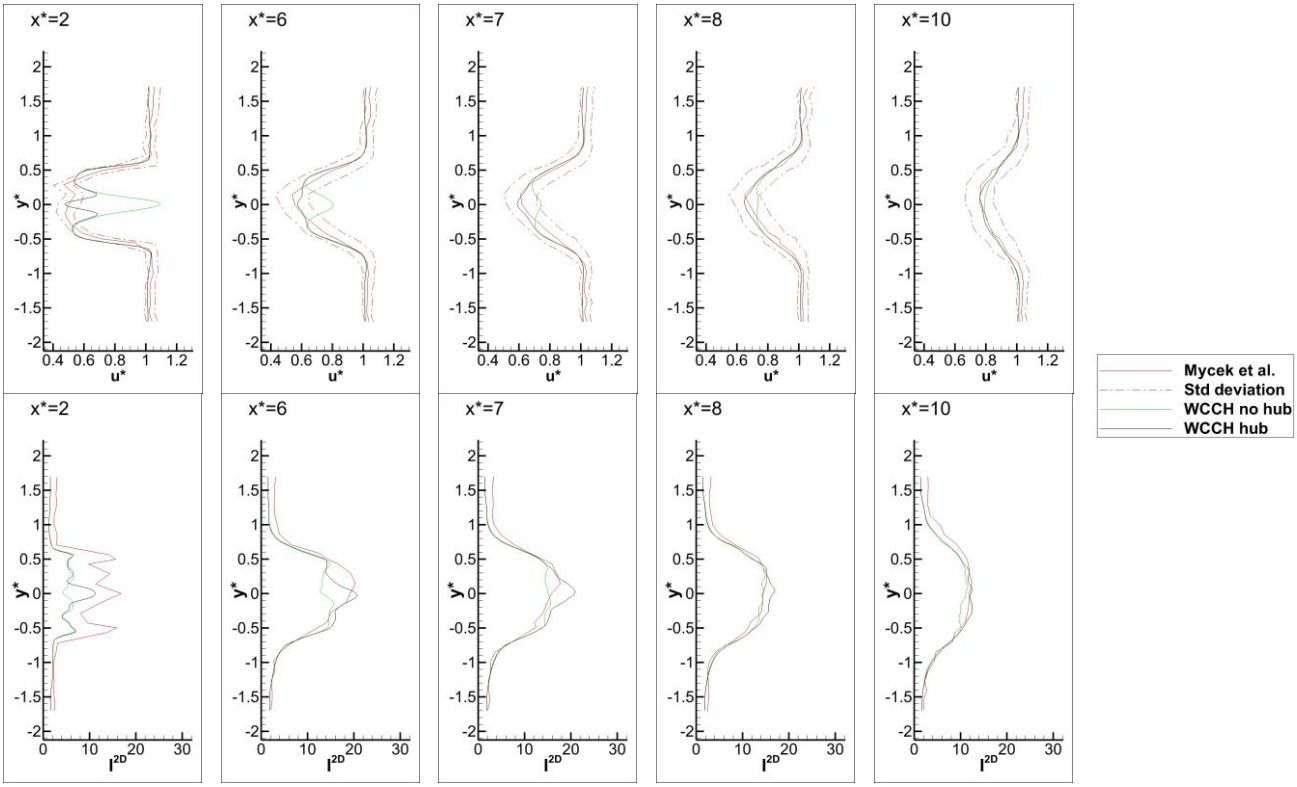

Fig. 2. . Influence of the hub on the averaged axial velocity profiles and the averaged turbulence intensity rate profiles in the wake for an ambient turbulent intensity rate of 3%.

References:

[1] Mycek, P., Gaurier, B., Germain, G., Pinon, G., Rivoalen, E. (2014). Experimental study of the turbulence intensity effects on marine current turbines behaviour. part i: One single turbine. *Renewable Energy*, 66:729-746.

[2] Bigay, P., Bardin, A., Oger, G., Le Touzé, D. (2014). A Cartesian explicit solver for complex hydrodynamic applications. *OMAE 2014, San Francisco, United States.*

[3] Titarev, V.A., Toro, E.F. (2004). Finite-volume WENO schemes for three-dimensional conservation laws. *Journal of Computational Physics*, 201(1):238-260.

[4] Myken, A., Sørensen, J. N. (1992). Unsteady actuator disc model for horizontal axis wind turbines. *Journal of Wind Engineering and Industrial Aerodynamics*, 39:139-149.

A comparison of synthetic turbulence generation methods

Michael Togneri*, Ian Masters
Marine Energy Research Group, College of Engineering, Swansea University, UK

Summary: We present a comparison of two methods used for generating turbulent velocity fields based on limited input data. The methods investigated are the synthetic eddy method (SEM) and the so-called Sandia method (named after Sandia National Laboratories where it was originally developed). We show that these methods produce turbulent velocity fields that are in some sense realistic insofar as they match measurements taken from observations of genuine turbulent flows. Finally, we compare the outputs of the two methods in terms of required computational resources and usefulness as boundary conditions for numerical models of tidal turbines.

Introduction

The purpose of these methods is to generate realistic velocity fields that can be used as inflow conditions for numerical models of tidal turbines (1), in particular models such as blade element momentum theory and vortex particle methods that do not model the complete fluid dynamics of the flow. Synthetic turbulence generation methods are particularly suitable for use in conjunction with models of this type, as their very point is to simulate turbine behaviour with reduced computational cost – if we require a computationally-expensive solution to the Navier-Stokes equations to generate physically-correct inflow conditions for our turbine models, we are defeating the purpose of the turbine models themselves. This does not mean, however, that our synthetic turbulent velocity fields cannot be used with more traditional CFD techniques; indeed, SEM was originally developed as a means of generating inflow conditions for LES/DES computations without requiring a precursor run.

Methods

Synthetic eddy method

SEM conceptualises turbulence as a collection of eddies that are carried by a mean flow, without affecting the mean flow themselves. Let us imagine a space for which we want to synthesise a turbulent velocity field. SEM populates this space with eddies positioned in a uniformly-random distribution, and then, based on specified statistical properties, assigns properties to the eddies such that the velocity field induced by their presence matches the specified statistics. For a space containing N eddies, we can specify the turbulent velocity at any point in space $\boldsymbol{x}$ by summing the contribution of all eddies as follows:

$$\boldsymbol{u}'(\boldsymbol{x}) = \frac{1}{\sqrt{N}} \sum_{k=1}^{N} \boldsymbol{a}^k \cdot f(\boldsymbol{x} - \boldsymbol{x}^k)$$

Here, $\boldsymbol{x}^k$ the position of the kth eddy and $\boldsymbol{a}^k$ its magnitude. f is a shape function that defines how the influence of an eddy is distributed over its vicinity. The dash denotes that we are dealing with the fluctuating turbulent component of velocity, and bold is used to indicate a vector quantity. If we are able to specify a Reynolds stress tensor R, with each element given by $R_{ij} = \langle u_i' u_j' \rangle$ (where angle brackets denote a time average), then it is possible to choose $\boldsymbol{a}^k$ and f such that the velocity field will match R in a statistical sense. The mathematics of this are covered in detail in, for instance, the work of Jarrin (1); in short, however, f must satisfy certain (not very stringent) normalisation conditions on its square integral, and $\boldsymbol{a}^k$ is obtained from linear combinations of the elements of the Cholesky decomposition of R with randomised sign.

Sandia method

The Sandia method (2) uses energy spectra and cross-spectra to generate time series of velocity at a collection of points. This method was originally developed as a means of generating synthetic turbulence flows for simulations of wind turbines, but is agnostic to the specific spectra used, so can easily be adapted to a tidal context. Note that some researchers report that marine turbulence is reasonably well-represented by standard atmospheric spectra (3), so it may in fact be possible to apply the method directly without modification.

* Corresponding author.
Email address: M.Togneri@swan.ac.uk

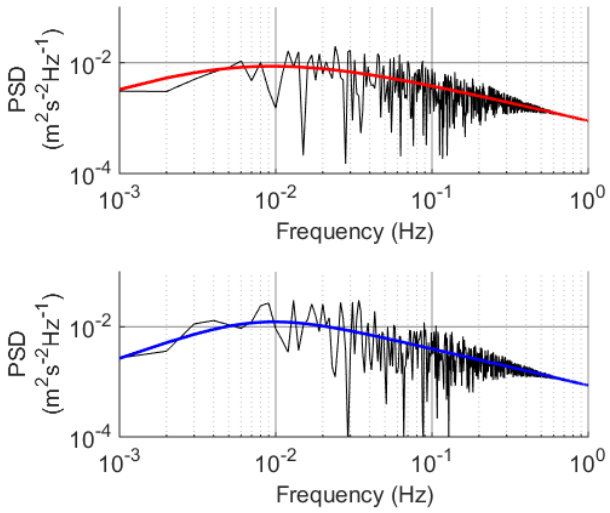

Figure 1: PSDs for von Kármán (blue) and Kaimal (red) spectra; black lines show synthetic spectra generated with Sandia method using the theoretical spectra as templates.

We begin the Sandia method by selecting the points for which we want to generate velocity series. For each of these points, we must have an energy spectrum; this may be from measurements or a standard model such as the von Kármán or Kaimal spectra (see fig. 1). In addition, we must also have cross-spectra for every pair of points; this is far more difficult to obtain, but Veers (2) suggests that we can straightforwardly generate a suitable selection of cross-spectra based on the single-point spectra and a coherence function that depends only on the separation between points.

By generating a set of vectors that randomise the phase of each frequency component, then linearly combining these phases according to a weighting that accounts for the relative correlatedness of the points (via the co-spectra), we can obtain a randomised time series for each point that retains the spectral qualities we originally specified. Note that introducing randomised phase means the Fourier problem is overspecified; this is overcome by recasting our one-sided spectrum as a two-sided spectrum, effectively increasing the frequency of the time series.

Results

We show that both methods produce suitable velocity fields, but that the Sandia method requires less computation time than SEM for comparable problems. We investigate the first-order properties of the velocity fields produced using these methods: in both cases it is second-order properties that are explicitly matched (Reynolds stresses for SEM, power spectra for the Sandia method, cf. fig. 1), so it is instructive to see what the result is in terms of actual turbulent velocity signals. Finally, we compare the outputs of each method in terms of the other i.e., the spectra of the velocity fields generated with SEM, and the Reynolds stress tensors of velocity fields generated with the Sandia method.

Acknowledgements:

The authors acknowledge the financial support of the Welsh Assembly Government and Higher Education Funding Council for Wales through the Sêr Cymru National Research Network for Low Carbon, Energy and Environment.

References

1. *Incorporating Turbulent Inflow Conditions in a Blade Element Momentum Model of Tidal Stream Turbines.* **M. Togneri, I. Masters and J. Orme.** Maui, USA : s.n., 2011.
2. **Jarrin, Nicolas.** Synthetic Inflow Boundary Conditions for the Numerical Simulation of Turbulence. Manchester : s.n., 2008.
3. **Veers, Paul S.** *Three-Dimensional Wind Simulation.* Albuquerque, USA : Sandia National Laboratories, 1988. SAND88-0152.
4. *The Role of Onset Turbulence on Tidal Turbine Blade Loads.* **I.A. Milne, R.N. Sharma, R.G.J. Flay and S. Bickerton.** Auckland, NZ : s.n., 2010.

Impact of the free surface proximity on the performance of a single Tidal Stream Turbine: A Vortex Filament Approach

Georgios Deskos[1], Johannes Spinneken
Department of Civil and Environmental Engineering, Imperial College London, UK

Matthew Piggott
Department of Earth Science and Engineering, Imperial College London, UK

Summary: In the present work, a single Horizontal Axis Tidal Turbine (HATT) is placed in an infinite width open-channel and is subject to a uniform free stream velocity. The Vortex Filament Method is used to model the turbine loading and the wake behind it while the free surface deformation is modelled using a panel method based on linear wave theory [1]. For the simulations presented here, an enhanced version of the mid-fidelity open source code CACTUS is used. Results for the power coefficient C_P are reported for a large number of Tip Speed Ratios λ and for two above turbine clearance scenarios. The extracted results are compared with experimental data [2] showing a good agreement for a broad range of λ.

Introduction

In recent years, a large number of CFD studies have been undertaken to model Horizontal Axis Tidal Turbines (HATTs). These range from full scale LES simulations [3] to more simplified models where an actuator disc is used to represent the turbine rotor and the flow field is solved using a RANS based approach along with a turbulence model [4]. An alternative approach to classic Eulerian-based numerical methodologies, is the Vortex filament method where Lagrangian material elements (vortex filaments) are used to model the vortical structures of the wake. The vortex filament method solves the unsteady Euler equations (viscosity is neglected) and in general exhibits a reduced computational cost compared to the respective Eulerian methods. The present model consists of a combination of a vortex filament method implementation for the wake and a panel method for the linearised free surface boundary conditions. The purpose of this study is to examine the impact of the free surface proximity on the extractable power and compare the results with existing experimental data [2]. The problem of the free surface proximity has been addressed in the past by [5] and more recently by [6] using experiments and theoretical models. Both studies concluded that the free surface has an impact on the performance of a single turbine or an array of turbines. For the purpose of this paper, an enhanced version of the mid-fidelity open source code CACTUS (Code for Axial and Cross-flow Turbine Simulation), developed originally at Sandia National Laboratories [7], is used.

Methods

For the vortex filament model, Prandtl's Lifting Line Theory [8] is used in order to generate the discrete vortices on the blades. The turbine blades are divided into small sections of approximately constant chord length c and thickness and for each section a bound vorticity Γ_b is computed by combining the Kutta-Joukowski condition with the lifting force coefficient C_L of an equivalent infinite span hydrofoil, $\Gamma_b = 0.5\ c\ C_L\ U_R$. For the wake, each filament is discretized using a lattice method [7], and the induced velocities at the lattice points are calculated by the Biot-Savart law. In this enhanced version of CACTUS, the vortex filaments are convected using a third order predictor-corrector scheme, which increases the accuracy of the computations at high tip speed ratios. For the free surface, the dynamic and kinematic boundary conditions are linearised and combined into the following equation,

$$U_\infty \frac{\partial^2 \varphi}{\partial x^2} + g \frac{\partial \varphi}{\partial y} = 0, \tag{2}$$

where φ is a velocity potential associated with the free surface, U_∞ is the free stream velocity and g is the gravitational acceleration. The free surface panels' strengths are computed by superimposing on U_∞ the vortex induced velocities from the wake. Finally, a free slip condition is applied on the panels of the horizontal bed.

[1] Corresponding author. *Email address*: g.deskos14@imperial.ac.uk

Results

The turbine geometry and setup are chosen in order to match the description of the experiments in [2]. Two above-tip clearance (distance between the turbine tip and the undisturbed free surface) scenarios are considered:

(1) a Large Clearance equal to 0.55D subject to a uniform free stream velocity 1.5 m/s and,

(2) a Small Clearance equal to 0.19D also subject to a uniform free stream velocity 1.5 m/s,

where D is the turbine diameter. On the left side of Figure 1, a comparison between the experimental and the obtained solution from CACTUS is presented. On the right side, the CACTUS solution for the free surface deformation η, normalised by the turbine diameter D is shown in a plan view for case (2) and $\lambda = 5$.

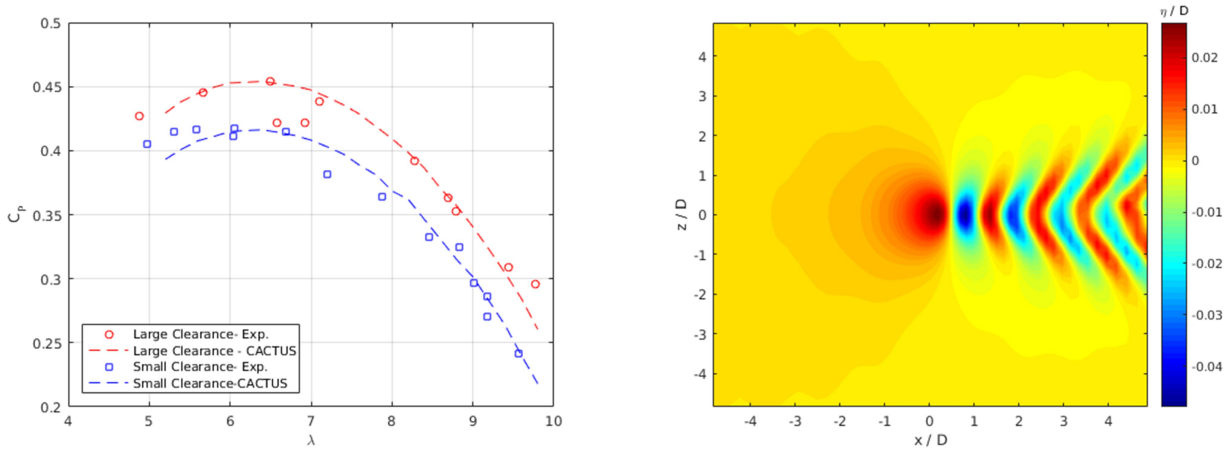

Figure 1. *Left*: Comparison between CACTUS and experimental data [2] for the turbine Power Coefficient C_P for cases (1) and (2). *Right*: A plan view of the free surface deformation η for case (2) normalized by the turbine diameter D.

Conclusions

The results of this analysis have demonstrated that the performance of a single turbine is reduced when the free surface is in close proximity and all other parameters are kept constant. The mid-fidelity model CACTUS was shown to yield accurate power coefficient estimates in excellent agreement with experimental data. Future effort will focus on the application of mid-fidelity approaches to (i) the loading of turbines, (ii) the importance of free surface modelling on the wake recovery (iii) the validation of such codes for a wide range of industry relevant scenarios and (iv) the application within array scale optimisation problems [9].

References:

[1] Newman, J. N., (1997). Marine Hydrodynamics, MIT Press

[2] Bahaj, A., Molland, A., Chaplin, J., Batten, W. (2007). Power and thrust measurements of marine current turbines under various hydrodynamic flow conditions in a cavitation tunnel and a towing tank. Renewable Energy, 32, 407-426.

[3] Afgan, I., McNaughton, J., Rolfo, S., Apsley, D. D, Stallard, T., Stansby, P. K. (2014). Turbulent flow and loading on a tidal stream turbine by LES and RANS. Int. J. of Heat and Fluid Flow, 2013, 43, 96-108.

[4] Batten, W. M. J., Harrison, M. E., Bahaj A. S. (2013). Accuracy of the actuator disc-rans approach for prediction the performance and wake of tidal turbines. Phil. Trans. of the Royal Soc. of Lond. A, 371.

[5] Whealan, J. L., Graham, J. M. R., Peiro, J. (2009). A free-surface and blockage correction for tidal turbines. J. Fluid Mech. **624**, 281-291.

[6] Vogel, C., Houlsby, G., Willden, R. (2016). Effect of free surface deformation on the extractable power of finite width turbine array. Renewable Energy, 88, 317-324.

[7] Murray, J. C., Barone, M. (2011). The development of CACTUS, a wind and marine turbine performance simulation code. 49th AIAA.

[8] Katz, J., Plotkin, A. (1991). Low Speed Aerodynamics, Cambridge University Press.

[9] Funke S.W., Farrell P.E., Piggott M. D. (2014). Tidal turbine array optimisation using the adjoint approach, Renewable Energy 63, 658-673

A BEMT model for a high solidity, hubless and ducted tidal stream turbine

Steven Allsop
Industrial Doctoral Centre for Offshore Renewable Energy (IDCORE), University of Edinburgh, UK
Christophe Peyrard
EDF R&D, Laboratoire Nationale d'Hydrauliques et Environnement (LNHE), France
Philipp R. Thies
College of Engineering, Mathematics and Physical Sciences, University of Exeter, UK

Summary: A Blade Element Momentum Theory (BEMT) model for 'conventional' 3 bladed designs of Tidal Stream Turbine (TST) is presented, with validations from scale model experiments carried out in a cavitation tunnel. Assumptions and limitations of the model are discussed in order to gauge potential use in assessing a high solidity, hubless and ducted TST design, which has been developed by OpenHydro. A number of adjustments to the model are considered, which are to be validated with fully blade resolved CFD studies and field data from a full scale device deployed at Paimpol-Bréhat, Brittany at the start of 2016 in collaboration with EDF.

Introduction

BEMT is a simple, fast processing and low computationally demanding method to predict the performance and thrust loading of a turbine. Commonly used in the wind industry, adaptation has more recently occurred in TST modelling, with academic and commercial models developed (e.g. [1] [2]). These are, however, limited to application with 'conventional' 3 bladed turbine designs, and unsuitable to assess high solidity, hubless and ducted designs. The objective of this study is to present a BEMT model developed for a 'conventional' TST, and discuss adjustments to assess an alternative configuration designed by OpenHydro in its latest generation 2MW device.

Methods

This study has developed a BEMT model, where the turbine is modelled as a frictionless, infinitely thin, semi-permeable actuator disc within a stream tube. Axial and tangential induction factors as well as flow angles of attack can be formulated based on the reduction in axial momentum on the flow as a result of the disc presence and the increase in tangential momentum due to the disc imparting rotation on the flow. The disc is split into a number of concentric annuli, where each section of the blade is taken as an independent 2D aerofoils and blade forces can be determined as a function of foil lift and drag coefficients. An iterative solver computes the angle of attack, induction factors and blade forces, and converges on a solution where equilibrium is achieved.

Correction factors have been applied including a Buhl factor for highly loaded conditions, and a Glauert factor to account for losses at the tip and hub. Inputs into the model include fluid properties, flow parameters and turbine geometry to replicate validation case conditions. Aerofoil coefficients are generated using a combined linear vorticity stream function panel method incorporating a viscous boundary layer. Du-Selig and Eggers models account for stall delay on a rotating foil, with post stall values attained using a Viterna extrapolation function.

To account for tunnel boundary layer effects a shear profile is applied to the inflow using a 1/7th power law, showing excellent agreement with flume data from a channel at EDF. Blockage corrections have been applied to the experimental coefficients and TSRs, to account for channel effects [3], converting results to 'equivalent open water' values for direct comparison with the model.

Results – Conventional Device

Coefficients of power (CP) and thrust (CT) curves for varying tip speed ratios (TSR) are shown in Figure 1.

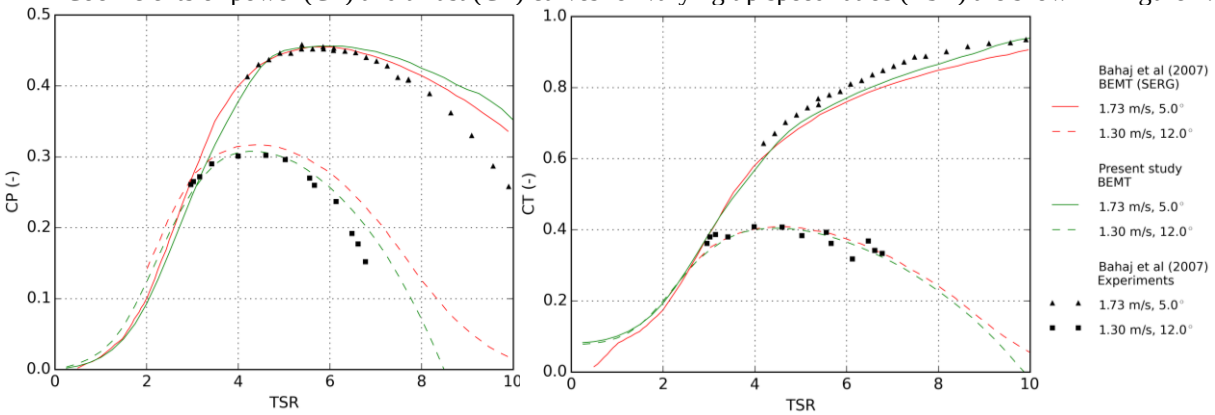

Figure 1 Power and thrust variation with TSR for a scale model TST from BEMT analyses and experimental data

Results from this study show good agreement with experimental data, and are consistent with another BEMT model [4]. At 1.73m/s flow, the models show an over prediction in power at high TSR, considered due to errors in large blockage factors applied to the experimental data [3].

Discussion – OpenHydro Device

Figure 2 shows the OpenHydro 2MW configuration to be analysed, with main differences including high solidity, open centre, hubless rotor and ducted flow. The following points discuss potential changes to the code to account for the new configuration, which are currently under investigation using CFD studies.

The one dimension flow assumptions neglect the radial flow that occurs due to the tendency of a fluid to flow around the blade tips from the pressure to the suction side or the rotor. This span wise flow reduces the hydrodynamic efficiency at the tip and hub, and can be approximated using an analytical solution proposed by Pandtl (Figure 3), taking the helical sheets as a succession of discs travelling at an average velocity of the wake and free stream. The new configuration sees blades reversed in orientation, with tips now facing towards the rotor centre, and the roots connected by the outer ring housed in the stator. A change in the formation of the vortex sheets requires a new tip/hub loss factor to be applied.

The modelling of an actuator disc in a stream tube predicts an unphysical reversal of flow in the wake at axial induction factors (a) greater than 0.5. This means that the increased thrust forces that occur at $a \geq 0.4$ (known as the highly loaded regime) are not predicted using this method. The Buhl correction factor is applied in this condition, a semi-empirical parabolic function based on Glauert's experiments with semi-permeable discs. For the 'conventional' design, highly loaded conditions are only seen at the near tip elements at high flow rates. As loading increases with decreasing disc permeability, high solidity designs will operate more in this regime (see Figure 4) and as a result will be have a higher sensitivity to experimental errors or inaccuracies.

The presence of a duct increases the inflow velocity at the rotor and restricts wake expansion, therefore impacting the assumptions of flow bounded by a stream tube. Combined Reynolds Average Navier Stokes (RANS) BEM models have been developed, able to represent the flow through the duct and open centred turbines [5]. In order to implement this into BEMT, a correction factor is considered based on similar blockage approximations of flow in a channel proposed by [6].

Fig. 2 OpenHydro latest generation 2MW device [7]

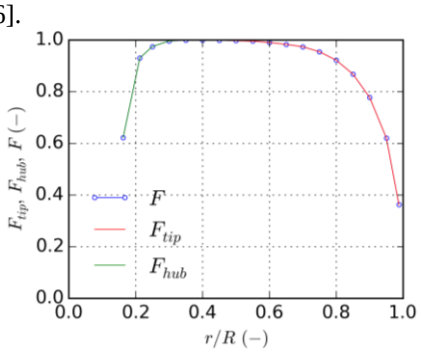

Fig. 3 Blade distribution of tip/hub loss factor for a conventional device at TSR 5

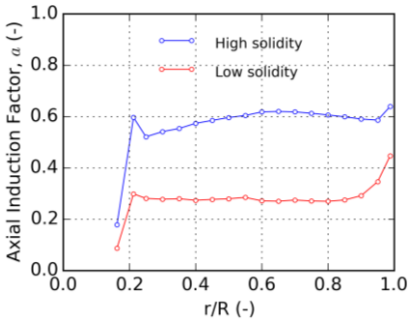

Fig. 4 Blade distribution of axial induction factor at TSR 5

Acknowledgements:

The Industrial Doctoral Centre for Offshore Renewable Energy (IDCORE) is funded by the Energy Technology partnership and the RCUK Energy Programme (Grant number EP/J500847/1).

References:

[1] I. Masters, J. C. Chapman, M. R. Willis and J. A. C. Orme, "A robust blade element theory model for tidal stream turbines including tip and hub loss corrections," *Marine Engineering & Technology*, vol. 10, no. 1, pp. 25-35, 2011.

[2] GL Garrad Hassan, "Tidal Bladed Theory Manual (V4.3)," 2012.

[3] A. S. Bahaj, A. F. Molland, J. R. Chaplin and W. M. J. Batten, "Power and thrust measurements of marine current turbines under various hydrodynamic flow conditions in a cavitation tunnel and a towing tank," *Renewable Energy*, vol. 32, pp. 407-426, 2007.

[4] A. S. Bahaj, W. M. J. Batten and G. McCann, "Experimental verifications of numerical predictions for the hydrodynamic performance of horizontal axis marine current turbines," *Renewable Energy*, vol. 32, pp. 2479-2490, 2007.

[5] C. S. K. Belloni, R. H. J. Willden and G. T. Houlsby, "Numerical analysis of open-centre, ducted turbines," in *Oxford Tidal Energy Workshop*, 2012.

[6] C. Garrett and P. Cummins, "The efficiency of a turbine in a tidal channel," *Fluid Mechanics*, vol. 588, pp. 243-251, 2007.

[7] "Image: SubSea World News," 2016. [Online]. Available: https://subseaworldnews.com/tag/openhydro.

Tidal turbine wake asymmetry due to wake-seabed interactions

Lada Murdoch[1]
CFD People Ltd.

Laura-Beth Jordan, Stuart J. McLelland, Stephen Simmons, Daniel Parsons
Department of Geography, Environment and Earth Sciences, University of Hull, UK

Rafael Ramirez-Mendoza, Laurent O. Amoudry
National Oceanography Centre, Liverpool, UK

Marco Vezza
School of Engineering, University of Glasgow, UK

Summary: A growing interest in the exploitation of tidal energy has been developing during the last two decades. The extraction of tidal energy by hydrokinetic turbines has progressed from theoretical considerations to field testing of full-scale devices within a few years. The present study is focused on the interactions between the wake of a model tidal turbine and the seabed with a particular emphasis on the wake asymmetry. The extent of the asymmetry of the wake close to the seabed is analysed by experimental investigations and numerical modelling.

Introduction

Given the interest driven by the need to tackle climate change, many studies of tidal energy extraction focused on the design and performance of the devices. A thorough understanding of the interactions of tidal turbines with the surrounding environment is, however, important for mitigation of possible changes of the seabed in the vicinity of tidal turbines. The interactions between the turbines and the flow have been studied in a number of laboratory experiments and numerical models. Overall, these investigations were either focused on particular processes or limited by the difficulty to measure specific variables. These limitations represented a disadvantage in the investigation of small-scale effects in the wake, which are crucial to understanding turbine-environment interactions. One feature rarely mentioned in previous studies is the asymmetry of the flow. The aim of this study is to show the importance of this asymmetry and how it affects local sediment transport.

Methods

Numerical modelling and a series of flume laboratory experiments have been used to study the wake of a model turbine, designed to match the performance of a community-sized three bladed horizontal-axis device. The modified Vorticity Transport Model [1] was used to analyse the turbine wake near the seabed. The experiments were conducted in the Total Environmental Simulator of the University of Hull by measuring flow characteristics using the Particle Image Velocimetry technique (PIV). The effects on the seabed were monitored using an Acoustic Ripple Profiler. Suspended sediment distribution was measured with an Acoustic Backscatter System.

Results

The numerical results indicate higher stream wise velocity in the left side of the numerical domain (in downstream view) than in the right side of about 0.25 m/s and shear stress also shows higher magnitudes in the left side. These results were confirmed in the experiments in the flume where flow characteristics were measured using the Particle Image Velocimetry technique (PIV). Recorded stream wise velocity remained without change in the near wake region up to a distance of approximately three turbine diameters downstream where the right side showed flow recovery while the left kept slow velocity in all the measured distance of more than five turbine diameters downstream. Turbulent kinetic energy from PIV measurements also showed higher magnitudes in the left side of the flume and about a distance of 2.75 times the turbine diameter. An asymmetric horse shoe shape in the near wake was the result of the scour due to the turbine and important deposition in the right side of the measured area with bed forms still present in the right side of the sediment bed. Figure 1 shows horizontal profiles of bed height, where cross wise location is indicated at the lower left corner on each plot. While at the

1 Corresponding author.
Email address: lada@cfdpeople.com

right side (in downstream view) bed forms were present, the sediment distribution on the left side was more uniform at the end of the experiments. The suspended sediment distribution also showed important crosswise variations.

Conclusions

Overall, the results of this study indicate a number of effects at both sides downstream of a single turbine in the flow and over a sediment bed. This has important implications when considering the installation of turbine arrays since the wake recovery will vary across the flow downstream of a single turbine due to the asymmetry of the wake. Moreover, related changes in sediment transport could affect the foundations and the efficiency of tidal turbine arrays. More studies are needed to characterize these asymmetric wake features and to include the asymmetry of tidal turbine wakes into hydrodynamic and morphology models in order to analyse the cumulative impact of turbine arrays on the marine environment.

Acknowledgements:

The numerical analysis was conducted during a PhD project at the university of Glasgow. The experimental investigations were supported by the INSTRON project as a part of the SUPERGEN Marine Challenge funded by the EPSRC. The authors would like to thank Prof. Richard Brown and Brendan Murphy for their contributions to this work.

References:

[1] Vybulkova L., Vezza, M. and Brown, R (2015). Simulating the Wake Down-stream of a Horizontal-axis Tidal Turbine Using the Modified Vorticity Transport Model. In: *IEEE Journal of Oceanic Engineering*, Vol PP, Issue 99, pp. 1-6.

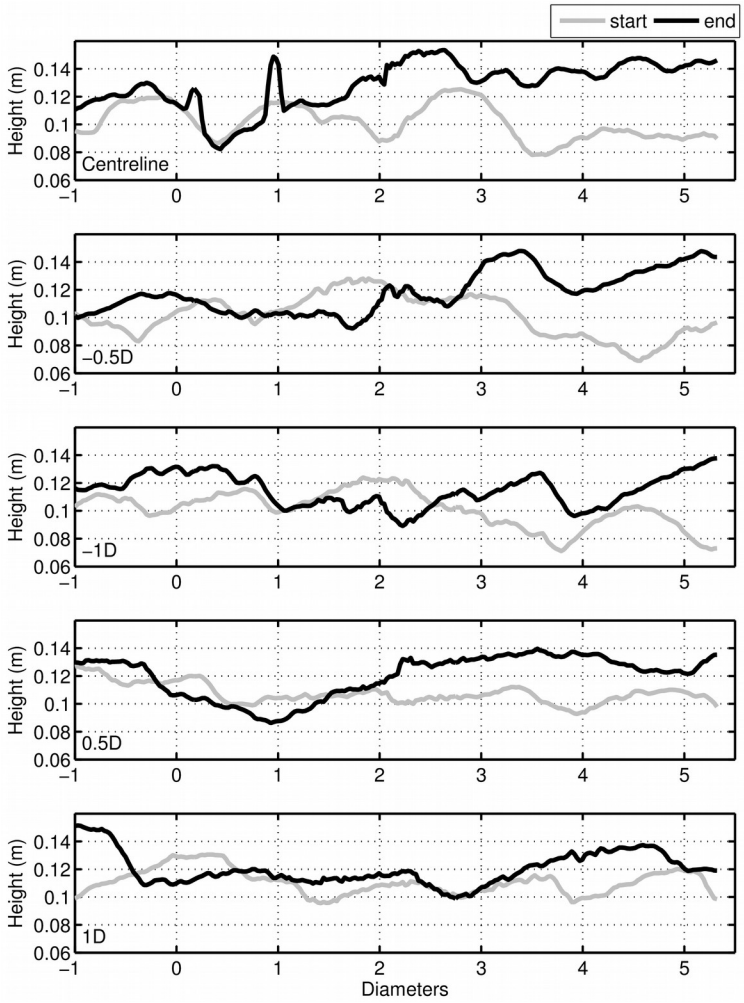

Fig. 1. Stream-wise horizontal profiles of bed height at varying distances from the centreline measured with the Acoustic Ripple Profiler: bed topography at the beginning of the experiments (in grey) and at the end of the experiments (in black). The flow direction was from left to right and the rotor was located at 0 diameters.

Experimental study of the boundary conditions on an undulating membrane tidal energy converter

Martin Träsch[1,2,3], Astrid Déporte[1], Sylvain Delacroix[1], Gregory Germain[2], Jean-Baptiste Drevet[1]

[1] *Eel Energy SAS. 60 rue Fokelstone, 62200 Boulogne s/ Mer. Email : mtrasch@eel-energy.fr*
[2] *IFREMER, 150 Quai Gambetta, 62200 Boulogne sur Mer*
[3] *ADEME. 20 avenue du Grésillé, 49004 Angers*

Summary: An experimental model at 1/20th scale has been developed to study the behaviour of an undulating membrane tidal energy converter. This abstract presents the experimental set-up and the comparison results of three membrane hanging devices. Each configuration induces a different membrane behaviour in terms of trajectory, motion amplitude and frequency. Critical velocity and efficiency are also presented, leading to the choice of an elastic spring with stops at ±15° as the best device to hold the membrane.

a) 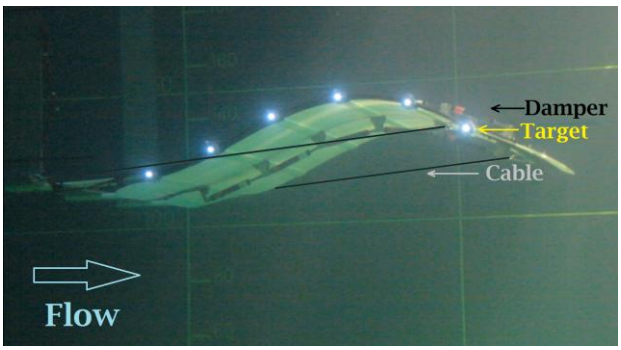

b) 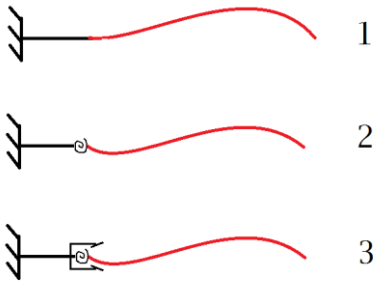

Figure 1.a – Photography of the 1/20th experimental model in the Ifremer wave and current flume tank
Figure 1.b – Schematic of tested hanging configurations: (1) clamped; (2) rotational spring; (3) rotational spring with stops at 15°. Arms are drawn in black and membrane in red

Introduction

An experimental model has been developed to study the Eel Energy undulating membrane tidal energy converter[1]. Indeed, fluid-structure interactions between a flexible plate and an axial flow result in undulating motions that can be used to harvest energy[2]. Knowing that the dynamic behavior of the membrane is linked to the imposed boundary conditions, we compare the effect of three kinds of hanging devices.

Methods

A 1/20th scale prototype has been tested in the Ifremer flume tank[1]. It is made of a 0.8m x 0.8m polyacetal membrane with carbon/epoxy bars to stiffen it in the transverse direction. The membrane is pre-stressed by cables that buckle it in streamwise direction before being submitted to axial flow. The buckling cables are about 0.95 times the length of the membrane. The experimental model used here is assembled with 12 adjustable linear dampers above and below the central line (Fig. 1.a). They are activated by the membrane undulations to simulate the power take off system. Above a critical flow speed, self-sustained oscillations are generated: the membrane undulates and dissipates energy through the dampers. The dampers have a non-linear damping behavior with respect to velocity. The dampers are characterized beforehand with a linear device which controls velocity and measures the damping force. The force response is segmented between several polynomial interpolations, depending on the velocity value and the acceleration sign. Combining both undulating motion data and dampers characterization enables to estimate the dissipated power.

Instrumentation is composed of a six-component load cell and a motion tracking system. Six targets are used, separated by 0.2L (L being the length of the membrane) in order to characterize the behavior of the system in terms of motion amplitude and frequency in function of the imposed boundary conditions.

Three different hanging conditions were experimented, in a range of fluid velocity from 0 to 1.2 m/s:

- Clamped-clamped arms (Fig. 1.b.1),
- Arms clamped to the frame and linked with an elastic spring to the membrane (Fig. 1.b.2),
- Clamped-elastic spring with stops at ±15° angle (Fig. 1.b.3).

Results

Figure 2 presents results showing the influence of boundary conditions on the behaviour of the undulating membrane. Results are given from critical flow speed (between 0.7 and 0.8 m/s) to 1.2 m/s. Parameters used here are dimensionless frequency (f*=f.L/U), amplitude (a*=A/L) and dissipated power coefficient ($p^*=2.P/(\rho.L.A.U^3)$), where f is the frequency of undulations, U is the upstream flow speed, A the maximal amplitude (of the most downstream target), P the dissipated power and ρ the water density. The use of a rotational link decreases the frequency and critical velocity in comparison with a clamped membrane. It also increases amplitude when not used with stops.

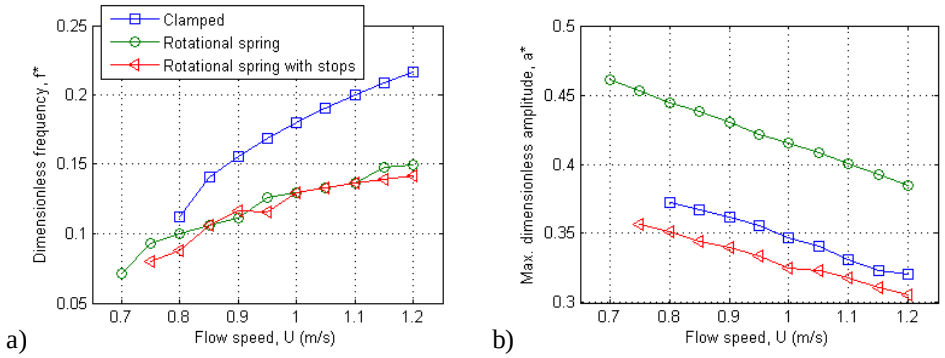

a) b)

Figure 2 – Influence of boundary conditions on dimensionless frequency (a) and maximum amplitude (b).

The estimation of dissipated power is displayed in Figure 3. The damping is the same for all dampers. Figure 3 clearly shows a better efficiency for the third hanging device: elastic spring with stops. The stops have a real importance because they induce a better distribution of the deformation along the membrane. The values of rotational spring stiffness and stops position can still be optimized. Dissipated power coefficient also has variations according to the flow speed, with a maximum of p*=0.27 for U=0.95m/s, which might be linked with a resonance phenomenon.

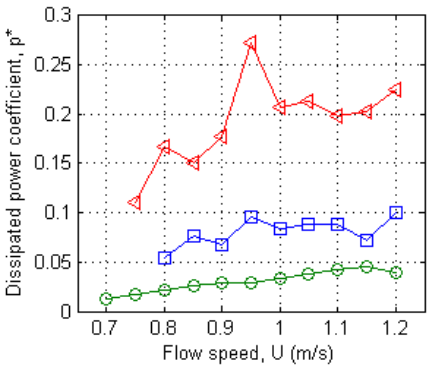

Figure 3 – Estimation of dissipated power coefficient

Conclusions

These results enable to valid the experimental model and show its utility to optimize the system. We were able to select a better hanging condition for the prototype. The power take off system is to be optimized, its setting is not precise.

Acknowledgements:

This work was supported by the French Environment and Energy Management Agency (ADEME) and Eel Energy SAS.

References:

[1] Déporte, A. et al. (2015). Three complementary approaches for the development of a flexible membrane tidal energy converter : analytical, experimental and numerical. Proc. *EWTEC 2015*. France.

[2] Michelin, S, Doaré, O. (2013). Energy harvesting efficiency of piezoelectric flags in axial flows. *J. Fluid Mech.* **714**, 489-504.

[3] Eloy, C., Souilliez, C., Schouveiler, L. (2007). Flutter of a rectangular plate. *J. Fluids Struct.*, **23**, 904-919.

Unsteady Load Relief of an Axial Flow Tidal Turbine in Sheared Flow by Individual Pitch Control

Jianxin Hu*, Richard H. J. Willden
Department of Engineering Science, University of Oxford, UK

Summary: The vertical shear of the velocity profile together with other once per revolution and high frequency events result in unsteady loading that will cause increased fatigue damage and structural vibrations, directly impacting the operating life of the turbine. Blade cyclically pitch control offers a potential method to adapt the blade to the changes in flow velocity around the azimuth to effect load relief in sheared flow. In the present study blade resolved CFD simulations are carried out of a three bladed axial flow tidal turbine model to investigate the reductions in unsteady blade load that can be achieved with Individual Pitch Control (IPC).

Introduction

Past research has investigated the impact of the harsh environment on the performance of axial flow tidal turbines [1-3], with observation that blade passage through the turbulent sheared current can lead to significant unsteady blade loading. Larsen et al. [4] demonstrated that IPC can be employed for efficient load reduction in wind turbines. However studies on pitch control methods for tidal turbines are limited, despite tidal turbines operating in a more severely sheared environment. Hence, we here study IPC for tidal turbines and develop control methods based on correcting fluctuations to the relative flow angle experienced by axial flow tidal turbines in sheared flow with objective to reduce the unsteady blade loading.

Methods

Three-dimensional fully blade resolved simulations are conducted in the CFD package OpenFOAM. The rotor geometry is a full-scale turbine prototype from TGL (Fig. 1) with diameter, D, of 18m. The rectangular simulation domain is of size 9D (stream-wise) × 2D (depth) × 4D (width), with an area blockage ratio, B, of 0.0982, discretized with hybrid hexahedral and tetrahedral cells (approximately 5.2×10^6 cells in total), and blocked into five subdomains to enable the sliding mesh with four pairs of Arbitrary Mesh Interfaces (AMI) such that each blade can rotate about its own axis, and the rotor can itself rotate through a fixed outer domain. A self-sustaining sheared flow profile (U=1.85-2.25m/s across rotor swept area) is applied at the upstream boundary, based on an assumed vertical linear shear stress profile, as derived for planar open channel flow following Schlichting [5]. Turbulence closure is provided through the RANS k-ω SST turbulence model.

In the absence of pitch control, the blade root twist, β, is constant with azimuth and hence changes in the relative flow angle, $\phi=\alpha+\beta$, between relative approach flow and rotor plane, due to changes in the inflow velocity with depth result in changes to the blade angle of attack, α, with azimuth. An IPC control method is designed accordingly by taking account of the cyclical pitch angle, β_{IPC}, required to achieve a stable relative flow angle, $\phi_{IPC}=\phi-\beta_{IPC}=\alpha+\beta$, hence achieving an azimuthally stable angle of attack, α, as shown in Fig. 2.

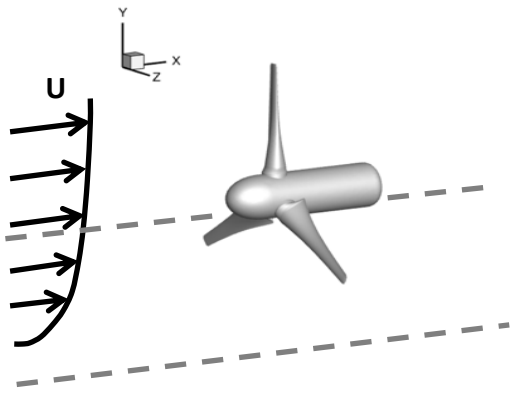

Fig. 1. Schematic of the turbine in sheared flow.

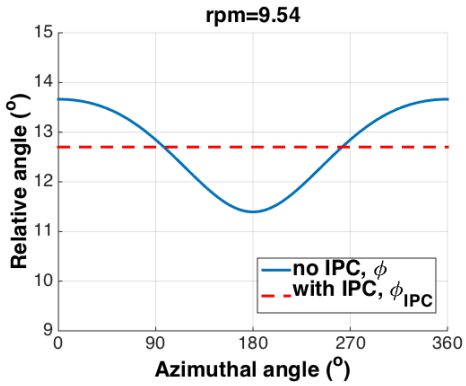

Fig. 2. Relative angle profiles with/without IPC.

* Corresponding author.
Email address: jianxin.hu@eng.ox.ac.uk

Results

We consider a test case of a rotor at a rotational speed of 9.54 rpm (tip-speed-ratio 4.5) with prescribed cyclical IPC. Fig. 3 presents the thrust and torque coefficient histories on a single blade and the whole rotor, whilst the blade load envelope and azimuthal thrust load variation are shown in Fig. 4. It is found that the fluctuating thrust load on a single blade is more sensitive to the change of the cyclic pitch angle than the torque. Near azimuthally uniform thrust loading is achieved through the proposed IPC strategy, whilst the fluctuating torque load, and rotor mean thrust and torque remain largely unaffected. Turbine tilt and yaw moments are also reduced through IPC. Analytic blade element analysis confirms that unsteady thrust should be more significantly affected by IPC than fluctuating torque.

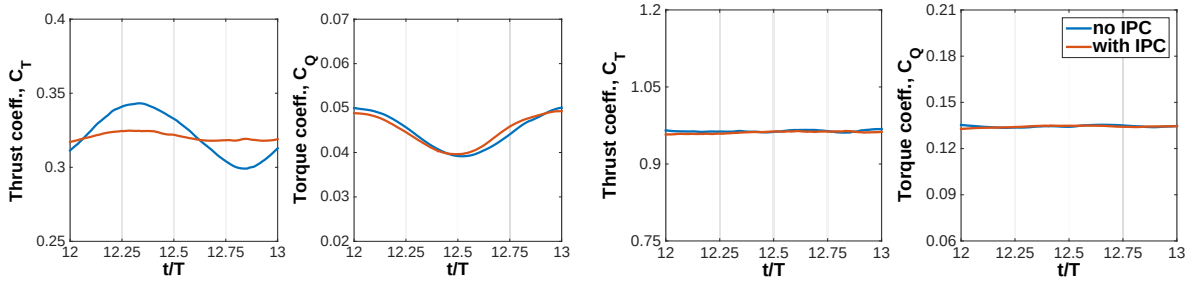

(a) (b)

Fig. 3. Load history of thrust coefficient and torque coefficient, on (a) single blade and (b) whole rotor.

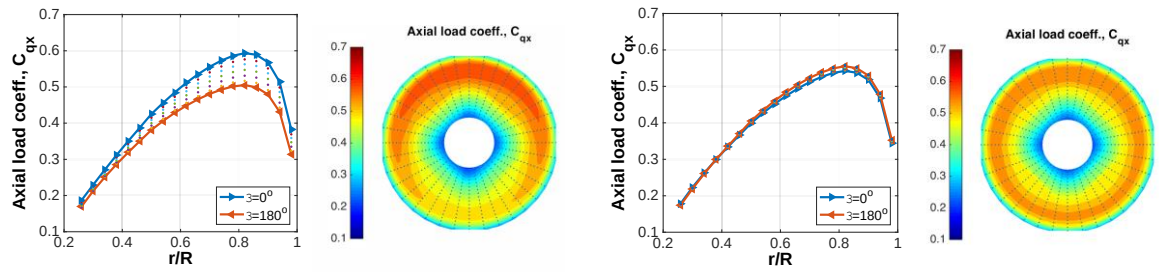

(a) (b)

Fig. 4. Axial loading envelopes and azimuthal distributions for a single blade (a) without IPC and (b) with IPC.

Conclusions

The results show that Individual Pitch Control based on correcting the relative flow angle to maintain a constant angle of attack can be very effective at reducing once per revolution fluctuating thrust forces whilst not impacting rotor performance.

Acknowledgements:

The authors wish to acknowledge the Advanced Research Computing services at the University of Oxford, and EPSRC who have supported this work through the marine challenge programme and RAP access to Archer.

References:

[1] Baltrop, N., Varyani, K. S., Grant, A., Clelland, D., Pham, X. P. (2007), Investigation into wave-current interactions in marine current turbines, *Proceedings of the Institution of Mechanical Engineers, Part A: Journal of Power and Energy*, **221 (2)**, 233-242.

[2] Batten, W. M. J., Bahaj, A. S., Molland, A. F., Chaplin, J.R. (2008), The prediction of the hydrodynamic performance of marine current turbines, *Renewable Energy*, **33**, 1085-1096.

[3] Fleming, C. F. (2014), *Tidal turbine performance in the offshore environment*, University of Oxford, DPhil thesis.

[4] Larsen, T. J., Madsen, H. A., Thomsen, K. (2005), Active load reduction using indi- vidual pitch, based on local blade flow measurements, *Wind Energy*, **8**, 67-80.

[5] Schlichting, H. (2000). *Boundary Layer Theory*, the 8th edition, Springer-Verlag.

Large-Eddy Simulation of tidal turbines using the immersed boundary method

Pablo Ouro[1], Thorsten Stoesser
Hydro-Environmental Research Centre, School of Engineering, Cardiff University, UK

Summary: Detailed knowledge of the hydrodynamics of tidal turbines and the fluid-structure interaction is essential for their design in particular because of the harsh and highly turbulent environment they operate in. Reliable numerical predictions of the performance of tidal turbines demand advanced numerical models. The method of Large-Eddy Simulation (LES) offers great accuracy in terms of predicting the turbulence of tidal streams however stable numerical schemes for the calculation of the complex fluid-structure interaction (FSI) are needed. The immersed boundary method has the potential to become an adequate FSI scheme for the simulation of tidal turbines which avoids expensive re-meshing processes compared to body fitted methods. The validation of an immersed boundary method based large-eddy simulation solver for vertical and horizontal axis tidal turbines is going to be presented. Comparisons of predicted power coefficient curves with experimental data show good accuracy of the method.

Introduction

The interest in tidal stream energy has been growing for the last years mainly because of two facts: (1) tidal streams are highly predictable and thus the energy that can be extracted from these streams through tidal turbines can be predicted until the end of their lifetime; and (2) the density of water is approximately 800 times greater than the air's density and hence tidal turbines are relatively small in comparison to their wind turbine counterpart. An obvious disadvantage of tidal stream energy is the harsh and challenging environment in which the turbines are operating in being constantly subjected to strong intermittent fluid forces which calls into question their survivability or implies very high operation and maintenance costs. The prediction of highly turbulent tidal streams, in which tidal turbines operate, require numerical models with high accuracy able to resolve the complex fluid-structure interaction between the turbine's rotor and the fluid flow. LES results into an adequate method for these flows as it can resolve the large scale flow structures though some modifications are required to be able to represent the turbine. The Immersed Boundary (IB) method appears to be a suitable approach to simulate moving bodies and thus tidal turbines. The objective of this study is to refine and validate an IB method based LES solver for the accurate prediction of vertical and horizontal axis tidal turbines.

Methods

The simulations will be performed using the in-house code Hydro3D that solves the fluid flow with the spatially filtered Navier-Stokes equations through finite differences with staggered storage of the velocity components on a Cartesian grid. The WALE sub-grid scale model is used in the current simulations. For the representation of the bodies the direct forcing Immersed Boundary (IB) method developed by Uhlmann [1] has been refined and adapted to tidal turbine simulations. A detailed description of this scheme applied to Vertical Axis Tidal Turbines can be found in Ouro et al. [2] and Ouro and Stoesser [3].

Results

In this study the numerical method has been employed to predict the performance of two generic turbine types, a three-bladed vertical axis tidal turbine and a three-bladed horizontal axis tidal turbine for which accurate experimental data is available for comparisons allowing assessment of the accuracy of the method.

Vertical Axis Tidal Turbine (VATT)
Experimental and numerical RANS results of a 3-bladed VATT were presented by Maitre et al. [4] and used for comparison with the present model. The turbine blades are cambered NACA 0018 and 5 different TSRs values [1.0-3.0] are used for the comparison ranging from the dynamic stall domination region up to the inertial forces domination region. In Fig. 1 the power coefficient (*Cp*) values obtained with the present approach for the different TSRs are shown and compared with experimental and RANS results. The 2D RANS model from Maitre et al. [4] overestimates the experimental power coefficient in particular for high TSRs while the present immersed boundary method LES solver improves this prediction with values closer to the experiments. As Fig. 2

[1] Corresponding author. *Email address*: OuroBarbaP@cardiff.ac.uk

demonstrates, the flow around the 3-bladed VATT is clearly three-dimensional, and it is shown that the vortical structures generated and shed from the blades have a significant impact on the power generation.

Horizontal Axis Tidal Turbine (HATT)

A 3-bladed HATT prototype developed by Tidal Stream Ltd. has been experimentally tested in the hydraulic flume at the School of Engineering at Cardiff University. The solver is employed to simulate the HATT and to predict the performance of this turbine under the same flow conditions. The power coefficient at different values of the TSR are investigated. LES results shows a good agreement with the experiments within a small error range, with an especially good agreement for the peak *Cp* value at TSR=3.
Further details of the tidal turbine simulations will be presented at the workshop.

Conclusions

An immersed boundary method has been adapted to a large-eddy simulation method with the goal to predict accurately the performance of vertical and horizontal axis tidal turbines. The method has been validated through comparisons with experimental data for both HATT and VATT with an overall good agreement is found.
Further comparison of the VATT LES results against RANS model results showed the relevance of the turbulence closure to represent accurately the fluid-structure and also highlighted the turbulent three-dimensional nature of the flow around these turbines.

Acknowledgements:

This work has been funded by the EPSRC, grant number 1355269. The authors would like to thank to the Advanced Research Computing @ Cardiff (ARCCA) Division at Cardiff University and HPC Wales for providing the HPC resources used for the presented research.

References:

[1] Uhlmann, M. (2005). An immersed boundary method with direct forcing for the simulation of particulate flows. *J. Comput. Phys.* **10**, 252-271.
[2] Ouro, P, Stoesser, T., McSherry, R. (2015). Large-Eddy Simulation of a Vertical Axis Tidal Turbine using an Immersed Boundary Method, In: CFD for Wind and Tidal Offshore Turbines, Springer International Publishing, Chapter 5, pp 49-58.
[3] Ouro, P., Stoesser, T. (2016). An immersed boundary-based large-eddy simulation approach to predict the performance of vertical axis tidal turbines. *Submitted to Applied Mathematical Modelling.*
[4] Maitre, T., Amet, E., Pellone, C. (2013). Modeling of the flow in a Darrieus water turbine: Wall grid refinement analysis and comparison with experiments. *Renewable Energy*. **51**, 497-512.

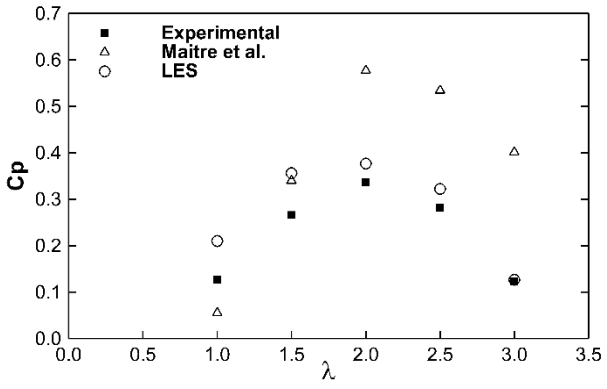

Figure 1 Power coefficient (C_P) versus TSR (λ) results for the VATT analysis.

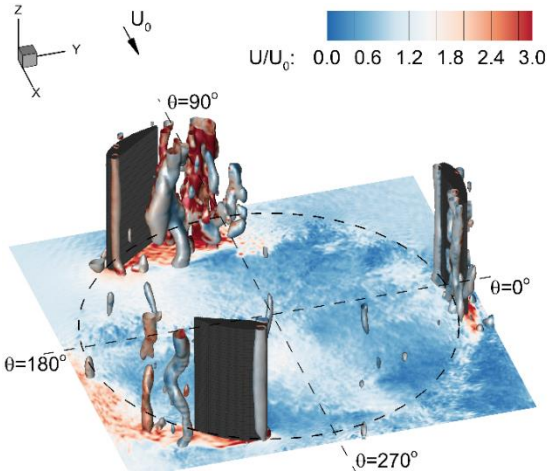

Figure 2 Iso-surfaces of Q-criterion=20 from [3] for the VATT case rotating at TSR=2.5.

Oxford Tidal Energy Workshop 2016 - Participants

Goward Brown, Alice	Bangor University
Lewis, Matt	Bangor University
Neill, Simon	Bangor University
Robins, Peter	Bangor University
Stephan, Bernd	Bangor University
Deng, Sheng	Cardiff University
Ebdon, Timothy	Cardiff University
He, Jianhao	Cardiff University
Hernández-Madrigal, Tattiana	Cardiff University
Ouro, Pablo	Cardiff University
Priegue, Luis	Cardiff University
Murdoch, Lada	CFD People, Ltd
Nishino, Taka	Cranfield University
Elie, Baptiste	École Centrale Nantes
Gunn, Kester	E.On
Stock-Williams, Clym	E.On
McNaughton, James	GE Renewable Energy
Waldman, Simon	Herriot Watt University
Trasch, Martin	IFREMER
Deskos, Georgios	Imperial College, London
Brown, Scott	Plymouth University
Ransley, Edward	Plymouth University
Shuker, Robert	Shuker & Sons
Edmunds, Matthew	Swansea University
Lake, Thomas	Swansea University
Masters, Ian	Swansea University
Togneri, Michael	Swansea University
Jaksic, Vesna	University College, Cork
Farman, Judith	University of Cambridge
Sjodahl, Amanda	University of Cambridge
Young, Anna	University of Cambridge
Allsop, Steve	University of Edinburgh
Bonar, Paul	University of Edinburgh
Crossley, George (GH)	University of Edinburgh
Kreitmair, Monika	University of Edinburgh
Maria Viola, Ignazio	University of Edinburgh
Noble, Donald	University of Edinburgh

Payne, Gregory	University of Edinburgh
Perez Ortiz, Alberto	University of Edinburgh
Scarlett, Gabriel	University of Edinburgh
Shah, Sunny	University of Edinburgh
Sutherland, Duncan	University of Edinburgh
Hardwick, Jonathan	University of Exeter
Bruce, Esther	University of Hull
Hachmann, Christoph	University of Manchester
Stallard, Timothy	University of Manchester
Stansby, Peter	University of Manchester
Lande-Sudall, David	University of Manchester
Adcock, Thomas	University of Oxford
Byrne, Byron	University of Oxford
Cooke, Susannah	University of Oxford
Gao, Chanshu	University of Oxford
Houlsby, Guy	University of Oxford
Hu, Jianxin	University of Oxford
Hunter, William	University of Oxford
McAdam, Ross	University of Oxford
Muchala, Subhash	University of Oxford
Sarkar, Dripta	University of Oxford
Santo, Harrif	University of Oxford
Schnabl, Andrea	University of Oxford
Vogel, Christopher	University of Oxford
Wang, Tuo	University of Oxford
Willden, Richard	University of Oxford
Wimshurst, Aidan	University of Oxford
Sun, Zhe	University of Southampton
Fu, Song	University of Strathclyde
Liu, Yuanchuan	University of Strathclyde
Shi, Guangyu	University of Strathclyde
Xiao, Qing	University of Strathclyde